Pt-Nanoparticles Encapsulated in Hollow Porous Carbon: Photocatalytic Synthesis, Structural Characterizations and Catalytic Activities

By

YUN HAU NG

March 2009

Pt-Nanoparticles Encapsulated in Hollow Porous Carbon: Photocatalytic Synthesis, Structural Characterizations and Catalytic Activities

A dissertation submitted to

The Graduate School of Engineering Science

Osaka University

in partial fulfillment of the requirements for the degree of

Doctor of Philosophy in Science

By

YUN HAU NG

March 2009

Contents

Abstract

Alcohols and olefins are interesting starting materials in the production of many fine chemicals and pharmaceuticals. Traditional synthesis routes to useful products from these chemicals often include oxidation or hydrogenation steps, which are generally performed using stoichiometric quantities of oxidants or reductants such as permanganate, chromic acid and sodium borohydride, creating a toxic waste stream. Using supported platinum as the heterogeneous catalysts, oxidation (hydrogenation) of various alcohols (olefins) can be performed with air or oxygen (hydrogen), which is a much cleaner process. However, many of these supported platinum catalysts suffer from catalyst leaching, particles growth, chemical poisoning or other deactivation mechanisms during reactions, which lead to decrease in the catalytic activity.

The work described in this thesis aims to design and develop an efficient carbon-based platinum nanocatalyst with unique structure using a novel synthetic method. To achieve this goal, we employed titanium dioxide (TiO_2), which acted as photocatalyst and template simultaneously, to prepare a hollow porous carbon encapsulating platinum nanoparticles (*n*Pt@*h*C). The highly active electrons (e^-) and positive holes (h^+) generated in TiO_2 upon ultraviolet light irradiation were utilized to reduce $PtCl_6^{2-}$ and oxidize phenol, respectively, to generate platinum-loaded TiO_2 covered by a layer of phenolic polymer. Subsequent calcination of this composite in vacuum to convert surface phenolic polymer into carbon components followed by removal of TiO_2 core particles by chemical etching yielded the *n*Pt@*h*C. Using combination of various characterization tools such as thermogravimetry, spectroscopy, chromatography, microscopy and porosity analyses, mechanism of the synthetic reaction and physical properties of *n*Pt@*h*C were identified.

Control of the carbon structures (morphology, density and porosity) was accomplished by optimizing the irradiation duration. The correlation of carbon structures and their catalytic performance in hydrogenation of olefins was examined. Tomography analysis using a TEM technique revealed the location of platinum particles in *n*Pt@*h*C. It was clearly observed that platinum particles were embedded inside the porous carbon shell and were physically separated from each other by the carbon matrix. As a result of this unique location, the platinum particles were frozen in the carbon, the possible movements were minimized, and hence, sintering and leaching of these platinum particles were effectively inhibited.

*n*Pt@*h*C-catalyzed oxidation of various alcohols with oxygen as oxidant was also investigated. From the mechanistic study in this work, the oxidation was found to take place *via* a dehydrogenation mechanism followed by the oxidation of the adsorbed hydrogen atoms with adsorbed oxygen. Several deactivation modes of platinum in alcohol oxidation have been identified previously in literature. They include formation of carbonaceous deposits, over-oxidation of platinum, metal particle-growth, metal leaching and chemical poisoning. It has been found that chemical poisoning was the major cause of platinum deactivation under current experimental conditions. The usual method employed to overcome the chemical poisoning is to introduce a secondary hazardous heavy metal such Pb and Bi. In this work, our catalyst directly suppresses the chemical poisoning without the incorporation with other metal promoter. *n*Pt@*h*C was found to be far more durable in oxidation of alcohols under oxygen atmosphere compared to other commercially available platinum catalyst.

CHAPTER 1

General Introduction

1.1 Research Background

1.1.1 Heterogeneous Metal Catalysis

Catalysis is an important field of knowledge that bridges chemistry, chemical engineering, materials science, biology and other disciplines of science. However, what is catalysis?

The first scientific description of catalytic phenomenon was given around 1835 by J. Berzelius.[1] He described catalysts as substances with ability to awaken affinities, which are asleep at a particular temperature, by their mere presence and not by their intrinsic properties. A few decades later in 1895, the modern definition of "catalysis" was introduced by W. Ostwald, whose works in catalysis, chemical equilibrium and reaction rates were recognized with a Nobel Prize in chemistry.[2] Oswald defined catalyst as a material that accelerates reaction rate and it itself remains unchanged after the reaction.

The application of a catalyst is one of the most fascinating and significant concepts in science and the world, and is one of the few words that have carried over broadly outside scientific language. Besides being employed in the production of wine, beer and cheese, toward the end of the nineteenth century, catalysts rapidly became important in a variety of industrial applications. The synthesis of indigo dye became a commercial possibility in 1897 when mercury was accidentally found to catalyze the reaction by which indigo was produced. Catalysis also made possible the commercial production of ammonia from its elements (the Haber-Bosch process),[3] of nitric acid from ammonia (the Ostwald process)[4] and of sulfuric acid from sulfur oxides (the contact process).[5] In twentieth century, several major catalysts were discovered in the field of chemical industry, for examples, titanium compounds for the production of polymers of 1-alkenes (Ziegler-Natta catalyst),[6] Pd complex catalyst for the oxidation of ethylene to acetaldehyde by oxygen in water (Wacker process)[7] and for C-C coupling reaction (Suzuki-Miyaura coupling process)[8] and many others. Industrial

production of chemicals has heavily relied on catalysts, and catalysis becomes more and more important in one's daily life.

In a chemistry context, a catalyst works by forming chemical bonds with reactant, generating intermediates that react more readily to give products than the reactants would alone, and finally giving back the catalyst. It also provides subtle control of chemical conversions, increasing the rate of a desired reaction but not the rates of undesired side reactions, so called *selectivity* of a catalyst. Unfortunately, each chemical process has its specific needs, including catalyst, and there is no one universal catalyst that suits all reactions. For example, Pd catalyzes the oxidation of ethane to vinyl acetate,[9] whereas Ag is used to obtain ethene oxide.[10] Another important aspect in catalysis, stability, is referred to how long a catalyst maintains its activity or selectivity during operation. Certainly, an ideal catalyst should be infinitely stable, as it is not consumed in the reaction and remain unchanged after the chemical process. However, catalysts in reality undergo changes causing loss of activity and/or selectivity, and must be replaced or reactivate (at intervals ranging from seconds to years).

Generally, catalysts could be categorized into two main groups by the states of them in use: homogeneous and heterogeneous catalysts. Homogeneous catalysts are used in the same phase as that of reactants, in most cases as dissolved catalysts in liquid reaction mixtures. Good examples of homogeneous catalysts are acid, base and metal complex which show high catalytic activity and selectivity in many industrial applications such as in syntheses of fine chemicals including asymmetric and pharmaceutical compounds. However, there are always pros and cons. Despite excellent activity and selectivity, homogeneous catalysts are difficult, if not impossible, to recover and reuse. This leads to a significant waste of valuable catalyst especially when an expensive noble metal is the case. Besides, use of strong acid/base in large

scale in industry is detrimental to the environment. It has become obvious that the practice of industrial chemistry has, apart from the desired products, some serious drawbacks, i.e., the environmental costs that directly related to human health. In recognition of the environmental effects of the chemical industry, many laws have been enacted and implemented throughout the world to force/encourage the industries to redesign the reaction process to eliminate/reduce the use of harmful substance and the generation of toxic waste. In this respect, heterogeneous catalysis emerges as the very competitive candidate in the development of environmentally benign processes.

In heterogeneous catalysis, the phase of the reactants and of the catalyst is different, in contrast to homogeneous catalysis, making the surface of the catalyst, which is the interface between catalyst and reactants, of great importance. Most catalysts used in heterogeneous catalysis are solids, usually consist of metal (or metal oxide or metal sulfide) particles. The big advantages of heterogeneous catalysis in comparison to homogeneous catalysis lie in the ease of separation of the reaction products from the catalyst (simple precipitation or centrifugation) and the possibility to operate in water medium or other less harmful solvents like ethanol.

The role of the surface of the heterogeneous catalyst is to provide an energetically favorable pathway for the chemical reaction. Typical surface processes involved in heterogeneous catalysis are shown in Figure 1. The first step is adsorption of the reactants, followed by activation and reaction at the surface of the catalyst, and the sequence is completed by desorption of the reaction products. Reactants not only adsorb as complete molecules but also dissociate into atoms or fragments of molecules that adsorb on the surface. During a chemical reaction, the bonding of the adsorbates to the surface of the catalyst is rather strong and is called chemisorption, in contrast to physisorption where adsorbates are

weakly bonded. The amount and the form, in which the chemical reactants are adsorbed and activated towards specific chemical products (selectivity), and the conversion rate of the reactants (activity) are dependent on the surface properties of the catalyst.

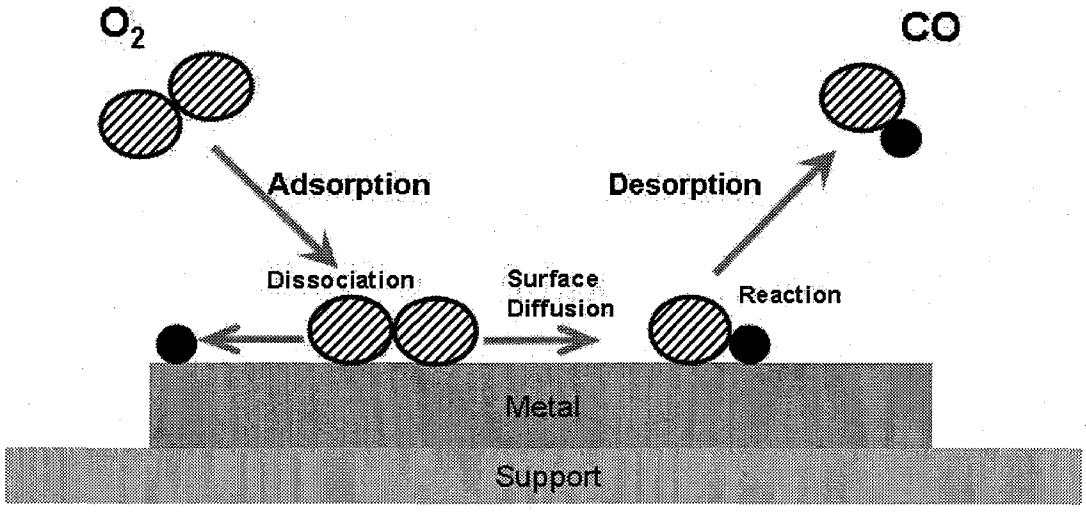

Figure 1. Schematic illustration of typical surface processes involved in heterogeneous catalysis.

Various kinds of heterogeneous metal catalysts are designed by means of a large variety of preparation methods. Even using the same metals, the catalytic activity and physicochemical properties of the catalysts obtained are strongly dependent on the combination of various aspects, e.g., metals and supports. Most of the efficient heterogeneous metal catalysts are dispersed on a support. The importance of support for metal particles is described in the next section.

1.1.2 Supported Metal Catalysts

The development of nanometer-sized metal particles has attracted considerable attention in the fields of fundamental science and also industrial applications. For example, they can serve as a model system to experimentally probe the effects of quantum confinement on electronic, magnetic, and other related properties.[11] Besides, they are also widely employed in photography,[12] catalysis,[13] biological labeling,[14] photonics,[15] optoelectronics,[16] information storage,[17] surface-enhanced spectroscopy,[18] sensing,[19] cancer therapy,[20] and formulation of magnetic fluids.[21]

In catalysis, their excellent ability is attributed to their large surface area and size-dependent properties different from bulk metals.[22] The conventional strategy to utilize these metal nanoparticles is to finely disperse them in an organic or aqueous solution, with or without the presence of certain protective agent to suppress the aggregation or coalescence.[23] In past decades, some important reactions, such as hydrogenation,[24] oxidation,[25] and C-C coupling[26] have been proved to work well in these suspension systems. However, due to the limited resources of many types of metals, difficulty in catalyst recovery and also their instability (tendency toward aggregation), this method encountered limited rooms for further development.

To prevent this problem, general strategy is to deposit the catalytically active components (in this case is therefore metal, metal oxides or metal sulfides) in a low concentration, and in a highly dispersed state, on a porous support material. Today, supported metal catalysts have emerged as an important group of heterogeneous catalysts. The transition metals, especially the group VIII metals (Fe, Co, Ni, Ru, Rh, Pd, Os, Ir, and Pt) and the group Ib metals (Cu, Ag, Au), are of greatest importance. They can catalyze oxidation, (de)hydrogenation, hydrogenolysis, aromatization, and isomerization reactions in a very mild condition

(sometimes even under atmospheric pressure and using water as solvent).[27] This turns out to serve well the contemporary global issue to create a sustainable development while preserving the environment.

Porous Metallic Oxides as Supports

In general, high catalytic activity is achieved by dispersing fine metal particles on the support to provide a large metal surface area per unit weight used. Therefore, porous materials with a large surface area (typically 100–2000 m^2 g^{-1}) having anchoring sites for the metal particles are the favorable candidates. With these properties, a support could reduce the possibility of sintering of metal particles. Sintering reduces the dispersion and therefore decreases the catalytic activity. The support further provides the mechanical strength of the catalyst.

Popular support materials are group of metallic oxides, such as silica (SiO_2), alumina (Al_2O_3) and zeolites (hydrated aluminosilicate). They are abundant, inexpensive, mechanically strong and thermally stable. Moreover, their structure could be carefully manipulated by various techniques and could be shaped into macroscopic dimensions. Besides, zeolite, for example HZSM-5, originally possesses acidic sites in its framework, providing the adequate ion-exchange anchoring sites for various alkali and alkaline earth metals. The acidic/basic nature of these metal oxides is also favorable in certain catalytic reactions. Extensive investigation on understanding the fundamental properties of these materials has been performed.[28]

Though applications of these metal oxides as support materials receive high recognition in certain reactions, their natural non-inertness is not always welcome. For example, an acidic support may not perform in a basic medium and *vice versa.* Also owing to their rich surface

hydroxyl groups, they are readily hydrophilic. As great numbers of catalytic reactions involve organic substances, a hydrophobic support with surface inertness which could be employed in both pH regions is therefore highly anticipated. This explains the rise of carbon as the alternative excellent support.

Carbon as Support

Carbon materials have been used for a long time in heterogeneous catalysis, because they satisfy most of the desirable properties required for a suitable support: inertness; stability under acidic, basic and other rigorous conditions; adequate mechanical properties; appropriate physical form for most reactors; high surface area; porosity and chemical nature.[29] The *Catalytic Reaction Guide* published by Johnson Matthey, one of the world's leading suppliers of catalysts, includes a list of 69 important organic reactions catalyzed by precious metals, nine of which use carbon as the only support material.[30]

However, the potential of carbon as catalyst support has not yet been fully exploited, though there is a considerable volume of literature devoted to this field in the last 30 years.[31] This large volume of research is mainly due to the fact that carbon has some characteristics that are very valuable and not attainable with any other support, although it is also true that carbon supports cannot be used in hydrogenation reactions > 700 K or in the presence of oxygen > 500 K, because they may be gasified to yield methane and carbon dioxide respectively.

In general, carbon materials of choice for most carbon-supported catalysts are graphite, carbon black, activated carbon, carbon fibers, carbon-covered alumina, glassy carbon, pyrolytic carbon, polymer-derived carbon, fullerenes, nanotubes and very recently, nanospheres.[32] These mentioned carbons normally have a porous structure consisting of

micropores or meso-/macropores or both, and usually are accompanied with a relatively small amount of chemically bonded heteroatoms (mainly oxygen and hydrogen). Content of other matters and structure of the carbons depend on the precursors and on its treatment (e.g. pyrolysis condition). Porous structures of carbon facilitate the flow of gases and the diffusion of reactants to the metal (active phase), improving the dissipation of reaction heat while retarding the sintering of the metal particles and increasing the poison resistance. Although most of the adsorption takes place in the micropores of porous carbon, meso- and macropores play very important roles in any adsorption process because they serve as a passage for the adsorbate to the micropores. It is then possible to understand the importance of the appropriate control of the treatment process to obtained carbons for specific applications since, within given limits, such control permits the tailoring of the porosity.[33]

Bifunctional TiO_2 as Both Photocatalyst and Support

Because of their resistance to photocorrosion, wide band-gap metal oxides have found greatest utility in heterogeneous photocatalysis. The most commonly studied photocatalysts are TiO_2, ZnO, and CdS. Due to its excellent photocatalytic activity and photostability, TiO_2 has become the benchmark photocatalyst against which photocatalytic activity is measured. Of the three crystalline forms of TiO_2 (anatase, rutile, and brookite), anatase is most commonly used. Upon photoexcitation of TiO_2 suspended in either aqueous or nonaqueous solutions or in gaseous mixtures, charge separation to generate electrons (e^-) and positive holes (h^+) occurs. This conversion often accomplishes either a specific, selective oxidation or a complete oxidative degradation of an organic substrate present. OH radicals generated from molecular oxygen are often assumed to serve as the oxidizing agent although details about the mode of its involvement have not been unambiguously demonstrated. Owing to the strong

oxidizing ability of that photogenerated h^+, TiO_2 has therefore been extensively employed in decomposition (oxidation) of organic pollutants.[34]

The deposition of noble metal on TiO_2 has been shown to be useful in improving the efficiency of photoredox transformation. For example, metallic platinum can be deposited on TiO_2 powder by photocatalytic reduction of an aqueous suspension containing chloroplatinic acid, sodium chloroplatinate, hexahydroxyplatinic acid, or platinum dinitroadiammine.[35] Formation of small Pt particles on TiO_2 surfaces results from platinum's property to act as an electron acceptor,[36] producing a metal loading while the TiO_2 surface remains accessible to photons and adsorbates. Other noble metals (Au, Pd, Rh and Ag) can be comparably deposited using the same photodeposition method, often leading to similar photoactivity effects. The loading level was important in governing the net effect of metallation, with heavy loading of metal normally inducing faster electron-hole recombination. At low Pt loading (0.1 -1 wt %) of the TiO_2 surface, enhancement of photoactivity probably results from an optimal attraction of free electrons of TiO_2 by Pt crystallites. In H_2 evolution from alcohols, the Pt crystallites are believed to assist the formation and desorption of H_2 molecules.[37] Also, faster electron exchange occurs between Pt and TiO_2 leading to modification of the catalytic properties of the TiO_2 semiconductor.

Besides working as an efficient photocatalyst, metal-loaded TiO_2 has also been employed in various catalytic processes. By using the TiO_2 support, it assists in tuning the selectivity of certain reactions. Pd supported on ZrO_2 catalyzes CO hydrogenation to yield methanol while Pd supported on TiO_2 was found to favor methane formation. [38] TiO_2-supported V_2O_5 works more effectively compare to V_2O_5 supported on silica and alumina in the reduction of NO_x by ammonia due to the resistance of TiO_2 toward sulfation. [39] Other than Pt, Rh and Pd, Ru/TiO_2 is also reported to have activity in hydrogenation of methyl oleate. [40] Au supported

on TiO_2 is found to chemoselectively hydrogenise nitro compounds and also oxidize CO at low temperature.[41] These instances clearly show that TiO_2 particles effectively function as support in many ordinary catalytic reactions other than in photocatalysis. Metal-loaded TiO_2 could be prepared either by using conventional impregnation/reduction method or photodeposition.

While organic pollutants are decomposed photocatalytically by the h^+, photoreduction of metal ions to metal particles consumes the e^- on TiO_2. However, simultaneous use of the reduction and oxidation abilities of TiO_2 in synthesizing nanocomposites (catalyst) has not yet reported. The possibility to extent the usage of TiO_2 in preparation of carbon-metal nanocatalyst is explored in this thesis and will be elaborated in detail in the following chapters.

General Methods for Preparation of Metal Catalyst

Nowadays much attention is paid to the chemistry of preparing catalysts to obtain the structure and properties of supported metal catalysts that result in an optimum catalytic performance. One of the successful preparation methods is to distribute the active metallic phase over the surface of the support in a highly dispersed form to maximize the activity per weight of active compound (and to minimize the costs associated). Although it is possible to deposit a metal directly from the vapor phase onto the support, the industrially important preparation methods are multistep processes consisting of distribution, calcination, activation and template removal steps (see Table 1.1).[42] The choice of precursor and the conditions of the distribution, calcination, activation and template removal determine the basic properties and structure of the catalysts such as the metal-support interaction, particle sizes etc.

Table 1.1 Preparation procedures of supported metal catalysts.

Preparation Steps	Description
Distribution of metal precursor over the support	-Impregnation -Ion exchange -(co)Precipitation -Photodeposition -Physisorption or chemisorption of organometallic cluster compounds
Rinsing and drying	-Removal of excessive and unreacted metal precursor and solvent
Calcination	-Oxidation of catalyst -Transformation of metal precursor to metal oxide -Transformation of carbon precursor to carbon (in vacuum) -Anchoring of metal oxide
Template Removal (Optional)	-Remove any hard, soft or self-assembly template
Activation	-Transformation of the metal precursor/ metal oxide into the active metallic phase by reduction in the gas or liquid phase

1.1.3 Carbon Supported Platinum Nanocatalyst in Oxidation of Alcohols

The catalytic oxidation of alcohols in liquid phase to provide an access to aldehydes, ketones and carboxylic acid has received considerable attention over the years. It is a very important transformation in the field of fine chemicals and pharmaceutical intermediates. Using carbon supported platinum or palladium as the catalyst, the oxidation of many alcohols can be performed selectively, with air or oxygen as the oxidant, and with water as medium. Moreover, the impact of platinum catalyzed oxidation processes on the environment is far lower than that of traditional oxidation processes using stoichiometric quantities of toxic oxidants such as permanganate, chromic acid and hypochlorite. Most of these stoichiometric oxidants are often used in halogenated organic solvents, and produce large amounts of

hazardous or toxic waste. Disposal of the metal wastes or isolation of the products is a serious drawback for economical and environmental benefits.

To improve the selectivity and stability of the Pt catalyst, addition of a promoter (an inactive metal), such as bismuth, lead, or tin[43] is the common method. However, leaching of these promoters (usually heavy metals) creates another problem. In later part of this thesis, I will present our strategy to improve the stability of Pt during reaction without introduction of promoters. In general, the oxidation could be performed under mild condition: 20-90 °C, atmospheric pressure, and pH 7-10 (though most literatures reported alcohol oxidation in basic medium). The reaction proceeds via an oxygen assisted dehydrogenation mechanism as suggested by Mallat and Baiker.[44]

A major bottleneck for commercial operation of platinum catalyzed alcohol oxidation is catalyst deactivation. Mallat and Baiker dedicated a large part of their review on platinum metals catalyzed alcohol oxidations to the mechanisms involved in catalyst deactivation: catalyst over-oxidation and catalyst poisoning. The reaction is generally assumed to take place on reduced (zero-valent) platinum sites. On exposure to oxygen, the platinum surface is oxidized, resulting in the formation of an inactive surface platinum oxide. This is also referred to as over-oxidation, oxygen dermasorption and sub-surface oxygen formation. It is most likely to occur in the absence of oxygen mass transfer limitation. However, the catalyst activity can be restored by in situ reduction of the catalyst by alcohols in the absence of oxygen, as was observed for 2-propanol.[45]

The deactivation may also occur through the blockage of catalytic sites by strongly adsorbing by-products or feed impurities as well. This is referred as the catalyst poisoning. Good example is adsorption of carboxylic acids on the surface of platinum at low pH, which prevents the reactant from reaching the catalytic site. This can be avoided by working at pH

>7 or by removing the product immediately.[46]

Under extreme conditions, irreversible types of deactivation may occur. Particle migration and growth has been observed under aqueous hydrogen at pH 13 and 90 °C.[47] Under prolonged oxidative conditions and in the presence of strong chelating agents, small platinum particles may dissolve and redeposit, leading to particle growth (Ostwald ripening) and a smaller active platinum surface.[48]

1.2 Research Objectives

The objectives of this research are:

(1) To synthesize porous carbon-supported platinum nanocomposites with novel hollow structure (*n*Pt@*h*C).

(2) To study the possible extension of TiO_2 application in the preparation of the *n*M@*h*C nanocatalyst (where M = noble metal).

(3) To investigate the physical and catalytic properties of the *n*Pt@*h*C nanocatalyst.

(4) To facilitate modification of physical properties of *n*Pt@*h*C nanocatalyst: carbon porosity, surface morphology and sintering resistance of platinum nanoparticles.

(5) To investigate the mechanism of oxidation of alcohols on platinum catalyst, and

(6) To study the suppression of deactivation using the *n*Pt@*h*C catalyst and to compare the properties with those of commercially available platinum catalysts.

1.3 Scope and Outline of the Thesis

This thesis brings together the information concerning the synthesis, characterizations, modification and catalytic application of hollow porous carbon-encapsulated platinum nanocatalyst (*n*Pt@*h*C). The outline of each chapter is as follows:

Chapter 1

History of the development of catalysis is reviewed with the focus on heterogeneous metal catalysis. Backgrounds and various aspects of supported metal catalysis are presented. By choosing platinum as the matter of this study, an important platinum catalyzed reaction, i.e. oxidation of alcohols, is introduced. Potential and problems encountered in this reaction is discussed in a broad sense. On the basis of such understanding, the objectives of this work are explained and the contents are outlined.

Chapter 2

In this chapter, by using a simple and unique method, we fabricate a carbon-metal catalyst composite. Through the photocatalytic reaction of TiO_2 nanoparticles in deaerated aqueous media, the composite is made of Pt nanoparticles incorporated in microporous hollow carbon nanospheres (*n*Pt@*h*C),. In this method, TiO_2 nanoparticles not only act as molds of hollow carbon but also induce simultaneous deposition of Pt nanoparticles and phenolic polymers by photocatalytic reduction and oxidation of a platinum(IV) precursor and phenol, respectively. Although photodeposition of metal nanoparticles on photocatalytic materials is a well-known phenomenon[49] and has been applied to make composites of metal nanoparticle-semiconductor nanoparticles in some studies,[50] this is the first description of the synthesis of nanocomposites using both reduction and oxidation abilities of photocatalysis. Comprehensive characterizations of *n*Pt@*h*C are carried out and general understanding of *n*Pt@*h*C is achieved. In addition, as an example of the use of *n*Pt@*h*C, we also show its efficient catalytic functions for liquid-phase hydrogenation of olefins.

Chapter 3

The study on *n*Pt@*h*C is investigated with the focus on the control of structural characteristics of the carbon. In this chapter, we investigate in detail the effect of photoirradiation time on structural characteristics of the phenolic polymer covered on the TiO_2 surface and thus-derived *n*Pt@*h*Cs composite. The structural aspects that are being investigated include carbon density, porosity and morphology. The correlation of these structures of *n*Pt@*h*Cs with their catalytic functions for hydrogenation of olefins is also examined.

Chapter 4

Despite successful preparation of *n*Pt@*h*C with novel structure as described in previous chapters, numerous structural features of thus-obtained composites still not fully clarified at that stage, for instance, behavior of Pt nanoparticles. In Chapter 4, therefore, we paid attention to their structures, focusing on the location of Pt nanoparticles in *n*Pt@*h*C using an electron tomography technique and the properties resulted from this unique position. Resistibility of these Pt nanoparticles to sintering, leading to minimization of loss of catalytic activity for hydrogenation reactions upon heat treatment of the *n*Pt@*h*C composite is observed and discussed.

Chapter 5

Due to the specific properties of the *n*Pt@*h*C nanostructure, it is proved to work as an active and reusable catalyst for hydrogenation of various olefins as discussed in previous chapters. We therefore decided to investigate the catalytic activity of *n*Pt@*h*C for alcohol oxidation, an important reaction in fine chemicals and pharmaceutical industries. Application

of *n*Pt@*h*C in aerobic oxidation in water of various alcohols is studied. Mechanism of oxidation of benzyl alcohol using Pt catalyst is examined. Over-oxidation of platinum, which is a deactivation mode that observed in most reported platinum catalyst, is greatly suppressed in our system.

Chapter 6

General conclusions of this thesis are given in this chapter. Several recommendations to readers/ prospective researchers for further research on this particular subject are shared.

1.4 References

[1] a) J. J. Berzelius, *Jahresberichte* **1835**, *15*, 237. b) A. Trofast, *Proceedings of Swedish Symposium of Catalysis* **1981**, 9.

[2] a) W. Ostwald, *J. Phys. Chem.* **1894**, *15*, 705. b) W. Ostwald, *Nature* **1902**, *65*, 522.

[3] R. Schlogl, *Angew. Chem. Int. Edn Engl.* **2003**, *42*, 2004.

[4] a) P. L. Charles, *Ind. Eng. Chem.* **1919**, *11*, 541. b) E. C. C. Baly, H. M. Duncan, *J. Chem. Soc. Trans.* **1922**, *121*, 1008.

[5] A. O. Jaeger, *Ind. Eng. Chem.* **1929**, *21*, 627.

[6] a) D. Singh, R. P. Merrill, *Macromolecules* **1971**, *4*, 599. b) E. R. Evitt, R. G. Bergmann, *J. Am. Chem. Soc.* **1979**, *101*, 3973. c) A. L. McKnight, R. M. Waymouth, *Chem. Rev.* **1998**, *98*, 2587.

[7] a) J. K. Stille, R. Divakaruni, *J. Am. Chem. Soc.* **1978**, *100*, 1303. b) E. Van Der Heide, J. A. M. Ammerlaan, A. W. Gerrisen, J. J. F. Scholten, *J. Mol. Catal.* **1989**, *55*, 320.

[8] a) N. Miyaura, A. Suzuki, *Chem. Rev.* **1995**, *95*, 2457. b) A. Suzuki, *J. Organomet. Chem.* **1999**, *576*, 147.

[9] M. Neurock, *J. Catal.* **2003**, *216*, 73.

[10] J. Couves, M. Atkins, M. Hague, B. H. Sakakini, K. C. Waugh, *Catal. Lett.* **2005**, *99*, 45.

[11] a) W. P. Halperin, *Rev. Mod. Phys.* **1986**, *58*, 533. b) A. C. Templeton, W. P. Wuelfing, R. W. Murray, *Acc. Chem. Res.* **2000**, *33*, 27. c) M. A. El-Sayed, *Acc. Chem. Res.* **2001**, *34*, 257.

[12] D. M. K. Lam, B. W. Rossiter, *Sci. Am.* **1991**, *265*, 80.

[13] L. N. Lewis, *Chem. Rev.* **1993**, *93*, 2693.

[14] S. R. Nicewarner-Pena, R. G. Freeman, B. D. Reiss, L. He, D. J. Pena, I. D. Walton, R. Cromer, C. D. Keating, M. J. Natan, *Science* **2001**, *294*, 137.

[15] S. A. Maier, M. L. Brongersma, P. G. Kik, S. Meltzer, A. A. G. Requicha, H. A. Atwater, *Adv. Mater.* **2001**, *13*, 1501.

[16] P. V. Kamat, *J. Phys. Chem. B* **2002**, *106*, 7729.

[17] a) H. Ditlbacher, J. R. Krenn, B. Lamprecht, A. Leitner, F. R. Aussenegg, *Opt. Lett.* **2000**, *25*, 563. b) C. B. Murray, S. Sun, H. Doyle, T. Betley, *Mater. Res. Soc. Bull.* **2001**, *26*, 985. c) J. W. M. Chon, C. Bullen, P. Zijlstra, M. Gu, *Adv. Funct. Mater.* **2007**, *17*, 875.

[18] a) S. Nie, S. R. Emory, *Science* **1997**, *275*, 1102. b) L. A. Dick, A. D. McFarland, C. L. Haynes, R. P. Van Duyne, *J. Phys. Chem. B* **2002**, *106*, 853. c) K. Kneipp, H. Kneipp, I. Itzkan, R. R. Dasari, M. S. Feld, *J. Phys. –Condes. Matter.* **2002**, **14**, 597.

[19] a) G. Raschke, S. Kowarik, T. Franzl, C. Sonnichsen, T. A. Klar, J. Feldmann, A. Nichtl, K. Kurzinger, *Nano Lett.* **2003**, *3*, 935. b) J. Yguerabide, E. E. Yguerabide, *Anal. Biochem.* **1998**, *262*, 157.

[20] P. K. Jain, I. H. El-Sayed, M. A. El-Sayed, *Nano Today* **2007**, *2*, 18.

[21] M. P. Pileni, *Adv. Funct. Mater.* **2001**, *11*, 323.

[22] a) S. Panigrahi, S. Basu, S. Praharaj, S. Pande, S. Jana, A. Pal, S. K. Ghosh, T. Pal, *J.*

Phys. Chem. C **2007**, *111*, 4596. b) T. Schalow, B. Brandt, D. E. Starr, M. Laurin, S. K. Shaikhutdinov, S. Schauermann, J. Libudaz, H. J. Freund, *Phys. Chem. Chem. Phys.* **2007**, *9*, 1347. c) K. L. Kelly, E. Coronado, L. L. Zhao, G. C. Schatz, *J. Phys. Chem. B* **2003**, *107*, 668. d) M. Haruta, M. Date, *Appl. Catal. A – Gen.* **2001**, *222*, 427.

[23] a) G. Schmid, *Chem. Rev.* **1992**, *92*, 1709. b) H. Hirai, *J. Macromol. Sci. Chem. A* **1986**, *13*, 633. c) N. Toshima, T. Yonezawa, *New. J. Chem.* **1998**, *22*, 1179.

[24] a) J. L. Pellegatta, C. Blandy, V. Colliere, R. Choukroun, B. Haudret, P. Cheng, K. Philippot, *J. Mol. Catal. A: Chem.* **2002**, *178*, 55. b) F. Lu, J. Liu, J. Xu, *Adv. Synth. Catal.* **2006**, *348*, 857.

[25] a) Y. Shiraishi, N. Toshima, *J. Mol. Catal. A: Chem.* **1999**, *141*, 187. b) A. Gniewek, A. M. Trzeciak, J. J. Ziolkowski, L. Kepinski, J. Wrzyszcz, W. Tylus, *J. Catal.* **2005**, *229*, 332.

[26] a) Y. Li, M. A. El-Sayed, *J. Phys. Chem. B* **2001**, *105*, 8938. b) R. Narayanan, M. A. El-Sayed, *J. Phys. Chem. B* **2004**, *108*, 8572.

[27] a) M. M. Schubert, S. Hackenberg, A. C. Van Veen, M. Muhler, V. Plzak, R. J. Behm, *J. Catal.* **2001**, *197*, 113. b) X. D. Mu, J. Q. Meng, Z. C. Li, Y. Kou, *J. Am. Chem. Soc.* **2005**, *127*, 9694. c) T. Kurosaka, H. Maruyama, I. Naribayashi, Y. Sasaki, *Catal. Commun.* **2008**, *9*, 1360. d) R. J. Davis, E. G. Derouane, *Nature* **1991**, *349*, 313. e) A. Bernas, N. Kumar, P. Maki-Arvela, N. V. Kulkova, B. Holmbom, T. Salmi, D. Y. Murzin, *Appl. Catal. A: Gen* **2003**, *245*, 257.

[28] a) M. Guisnet, P. Magnoux, *Appl. Catal.* **1989**, *54*, 1. b) P. B. Venuto, *Microporous Mater.* **1994**, *4*, 756. c) M. Iwamoto, H. Yahiro, K. Tanda, N. Mizuno, Y. Mine, S. Kagawa, *J. Phys. Chem.* **1991**, *95*, 3727. d) P. Feng, X. Bu, G. D. Stucky, *Nature* **1997**, *388*, 735.

[29] a) F. Rodriguez-Reinoso, *Porosity in Carbon: Characterization and Applications, Edward Arnold, London*, **1995**, 253. b) L. R. Radovic, F. Rodriguez-Reinoso, *Chemistry and Physics of Carbon, Marcel Dekker, New York*, **1997**, 243.

[30] L. R. Radovic, C. Sudhakar, *Introduction to Carbon Technologies, Secretariado de Publicaciones, Alicante, Spain*, **1997**, 107.

[31] a) H. C. Brown, K. Sivasankaran, *J. Am. Chem. Soc.* **1962**, *84*, 2828. b) M. Kaminsky, K. J. Yoon, G. L. Geoffroy, M. A. Vannice, *J. Catal.* **1985**, *91*, 338. a) J. S. Noh, J. A. Schwarz, *J. Catal.* **1991**, *127*, 22. a) E. J. M. Hensen, H. J. A. Brans, G. M. H. J. Lardinois, V. H. J. De Beer, J. A. R. Van Veen, R. A. Van Santen, *J. Catal.* **2000**, *192*, 98. a) F. Sen, G. Gokagac, *J. Phys. Chem. C* **2007**, *111*, 1467.

[32] a) C. A. Bessel, K. Laubernds, N. M. Rodriguez, R. T. K. Baker, *J. Phys. Chem. B* **2001**, *105*, 1115. b) F. Coloma, A. Sepulveda-Escribano, J. L. G. Fierro, F. Rodriguez-Reinoso, *Langmuir* **1994**, *13*, 750. c) A. Fortuny, J. Font, A. Fabregat, *Appl. Catal. B: Environ.* **1998**, *19*, 165. d) F. Li, J. Huang, J. Zou, P. Pan, G. Yuan, *Appl. Catal. A: Gen.* **2003**, *251*, 295. e) K. P. De Jong, J. W. Geus, *Catal. Rev. – Sci. Eng.* **2000**, *42*, 481. f) B. Coq, J. M. Planeix, V. Brotons, *Appl. Catal. A: Gen.* **1998**, *173*, 175. g) W. Li, C. Liang, W. Zhou, J. Qiu, Z. Zhou, G. Sun, Q. Xin, *J. Phys. Chem. B* **2003**, *107*, 6292. h) S. Ikeda, S. Ishino, T. Harada, N. Okamoto, T. Sakata, H. Mori, S. Kuwabata, T. Torimoto, M. Matsumura, *Angew. Chem. Int. Ed.* **2006**, *45*, 7063.

[33] a) P. Delhaes, *Carbon* **2002**, *40*, 641. b) S. B. Yoon, G. S. Chai, S. K. Kang, J. S. Yu, K. P. Gierszal, M. Jaroniec, *J. Am. Chem. Soc.* **2005**, *127*, 4288. c) S. Lei, J. Miyamoto, T. Ohba, H. Kanoh, K. Kaneko, *J. Phys. Chem. C* **2007**, *111*, 2459.

[34] a) R. A. Torres, J. I. Nieto, E. Combet, C. Petrier, C. Pulgarin, *Appl. Catal. B: Environ.* **2008**, *80*, 168. b) W. Zhao, W. Ma, C. Chen, J. Zhao, Z. Shuai, *J. Am. Chem. Soc.* **2004**,

126, 4782. c) T. Torimoto, S. Ito, S. Kuwabata, H. Yoneyama, *Environ. Sci. Technol.* **1996**, *30*, 1275.

[35] J. –M. Herrmann, J. Disdier, P. Pichat, *J. Phys. Chem.* **1986**, *90*, 6028.

[36] N. Jaffrezic-Renault, P. Pichat, A. Foissy, R. Mercier, *J. Phys. Chem.* **1986**, *90*, 2733.

[37] a) B. Ohtani, Y. Ogawa, S. I. Nishimoto, *J. Phys. Chem. B* **1997**, *101*, 3746. b) B. Kraeutler, A. J. Bard, *J. Am. Chem. Soc.* **1978**, *100*, 4317.

[38] W. –J. She, M. Okumura, Y. Matsumura, M. Haruta, *Appl. Catal. A: Gen.* **2001**, *213*, 225.

[39] G. Busca, L. Lietti, G. Ramis, F. Berti, *Appl. Catal. B: Environ.* **1998**, *18*, 1.

[40] S. A. da S. Corradini, G. G. Lenzi, M. K. Lenzi, C. M. F. Soares, O. A. A. Santos, *J. Non-Cryst. Solids* **2008**, *354*, 4855.

[41] a) A. Corma, P. Serna, *Science* **2006**, *313*, 332. b) M. Comotti, W. C. Li, B. Spliethoff, F. Schuth, *J. Am. Chem. Soc.* **2006**, *128*, 917.

[42] a) K. Foger, *Catalysis, Science and Technology*, *Springer-Verlag*, *Berlin* **1984**, *6*, 227. b) J. W. Geus, J. A. R. Van Veen, *Catalysis, An Intergrated Approach to Homogeneous, Heterogeneous and Industrial Catalysis*, *Elsevier*, *Amsterdam* **1993**, 335.

[43] a) H. H. C. M. Pinxt, B. F. M. Kuster, G. B. Marin, *Appl. Catal. A: Gen.* **2000**, *191*, 45. b) T. Mallat, Z. Bodnar, P. Hug, A. Baiker, *J. Catal.* **1995**, *153*, 131. c) C. Keresszegi, T. Mallat, J. Grunwaldt, A. Baiker, *J. Catal.* **2004**, *225*. 138.

[44] T. Mallat, A. Baiker, *Catal. Today* **1994**, *19*, 247.

[45] J. W. Nicoletti, G. M. Whitesides, *J. Phys. Chem.* **1989**, *93*, 759.

[46] A. Abbadi, H. van Bekkum, *J. Mol. Catal. A: Chem.* **1995**, *97*, 111.

[47] J. H. Vleeming, B. F. M. Kuster, G. B. Marin, F. Oudet, P. Courtine, *J. Catal.* **1997**, *166*, 148.

[48] Y. Schuurman, B. F. M. Kuster, K. van der Wiele, G. B. Marin, *Appl. Catal. A: Gen* **1992**, *89*, 47.

[49] a) A. J. Bard, *J. Photochem.* **1979**, *10*, 59. b) S. –i. Nishimoto, B. Ohtani, H. Kajiwara, T. Kagiya, *J. Chem. Soc. Faraday Trans. 1* **1983**, *79*, 2685.

[50] a) P. D. Cozzoli, R. Comparelli, E. Fenizza, M. L. Curri, A. Agostiano, D. Laub, *J. Am. Chem. Soc.* **2004**, *126*, 3868. b) S. C. Chan, M. A. Barteau, *Langmuir* **2005**, *21*, 5588.

CHAPTER 2

TiO_2 Photocatalytic Synthesis of Hollow Porous Carbon Encapsulating Platinum Nanoparticles (*n*Pt@*h*C)

2.1 Introduction

Carbon materials with ordered mesoporous and/or well-defined hollow nanostructures are promising candidates for adsorbates, optical devices, nanoreactors, electrochemical supercapacitors, and storage materials.[1-4] These nanostructured carbons are commonly fabricated by templating procedures using silica-based molds, which involve coverage or filling with carbon sources onto the surfaces of the molds followed by carbonization under inert conditions and subsequent removal of the molds by chemical etching. To date, various carbon sources have been employed to control the level of graphitization of carbon networks for adjusting conductivity, stability, and porosity in order to satisfy conditions for desired applications as well as to simplify the preparation procedure.[2,4]

These nanostructured carbons also exhibit potential abilities as efficient catalysts and electrocatalysts for various reactions when they are used in combination with metal nanoparticles, i.e., carbon-metal nanocomposites.[1c,3b,3d,4b] Although some studies have reported high catalytic functions of such composites,[1c,3d] effective control of metal size and dispersion in such composites as catalysts is yet to be established. On the other hand, when carbon-metal catalyst composites are fabricated by the reported methods, additional workup procedures, such as pretreatment of the silica molds with metal particles and post loading of them on thus-obtained carbon materials, are indispensable. Therefore, a more convenient approach for preparation of such composites is appreciated.

Here, we report a simple and unique method for obtaining a carbon-metal catalyst composite, i.e., Pt nanoparticles incorporated in microporous hollow carbon nanospheres (*n*Pt@*h*C), through the photocatalytic reaction of TiO_2 nanoparticles in deaerated aqueous media. In this method, TiO_2 nanoparticles not only act as molds of hollow carbon but also induce simultaneous deposition of Pt nanoparticles and phenolic polymers by photocatalytic

reduction and oxidation of a platinum(IV) precursor and phenol, respectively. Although photodeposition of metal nanoparticles on photocatalytic materials is a well-known phenomenon[5] and has been applied to make composites of metal nanoparticle-semiconductor nanoparticles in some studies,[6] this is the first report of the synthesis of nanocomposites using both reduction and oxidation abilities of photocatalysis. In addition, as an example of the use of *n*Pt@*h*C, we also show its efficient catalytic functions for liquid-phase hydrogenation of olefins.

2.2 Experimental

Preparation Procedures: Five hundred mg of TiO_2 (Ishihara Sangyo ST-21, 50 m^2g^{-1}) was dispersed in an aqueous solution (400 cm^3) containing phenol (200 mg, 2.1 mmol) and a small portion of hexachloroplatinic acid (H_2PtCl_6, 7.7 μmol, corresponding to 0.3 wt% for TiO_2) with a magnetic stirrer. The suspension was then evacuated several times in a Pyrex inner-irradiation-type vessel connected to a closed gas circulation and evacuation system to ensure complete air removal, followed by photoirradiation for 2.5 h with a high-pressure Hg lamp (450 W) through a Pyrex water jacket (cutoff < 290 nm) to keep the reactor temperature constant at 293 K under a reduced pressure of Ar (30 kPa). The evolved hydrogen was monitored by a Shimadzu GC-8A gas chromatograph equipped with a thermal conductivity detector (TCD) and a MS-5A column. After irradiation for 2.5 h, the resulting brownish phenolic polymer-coated powders were retrieved by filtration, washed with distilled water (ca. 2000 cm^3) to remove excessive unreacted phenol, and subjected to carbonization at 973 K for 6 h in vacuum. Dissolution of TiO_2 in thus-obtained powder with 50% hydrofluoric acid (10 cm^3) for 24 h followed by washing three times with acetone (20 cm^3) yielded *n*Pt@*h*C. In

order to obtain *n*Pt@*h*C samples containing different amounts of Pt nanoparticles, the above-described procedures were carried out with changes in the amount of H_2PtCl_6 (2.6 μmol and 25.7 μmol, corresponding to 0.1 wt% and 1.0 wt% for TiO_2, respectively). In a separate experiment, the reaction solution after the initial 10 min of photoirradiation was analyzed by using a Shimadzu GCMS-QP2010 GC-MS.

Characterization: TEM images and SAED patterns were obtained by using a Hitachi H-9000 TEM. Surface and pore analyses were carried out using a Quantachrome AUTOSORB-1 automated gas sorption system employing N_2 as the adsorbate after pretreatment of the sample at 473 K for 2 h. FT-IR spectra were obtained on a Nicolet 470 FT-IR spectrometer equipped with an MCT detector using KBr discs dispersed with the samples. Quantitative analysis of Pt amount was carried out by using a Perkin-Elmer OPTIMA 3000-XL ICP emission spectrometer. For the ICP analysis, *n*Pt@*h*C samples were immersed in aqua regia for 2 h to dissolve the Pt particles. The undissolved carbon particles were filtered by a Millipore syringe-driven membrane filter. The clear solution was then diluted to an appropriate concentration before elemental analysis. Raman spectra were obtained on a JASCO NRS-3100 Laser Raman Spectrophotometer.

Catalytic Hydrogenation of Olefins: Catalytic reactions were conducted in a stainless-steel autoclave equipped with a glass reactor (50 cm^3). Typically, 1.4 mg of *n*Pt@*h*C, 10 cm^3 of acetone and 5 mmol of 1-hexene, 2-hexene, or cyclohexene were put into the glass vessel under N_2. Reactions were started by purging pressurized H_2 at 210 KPa (in absolute pressure) under 348 K with stirring (1200 rpm). Catalytic activities were evaluated by the conversion of substrates using a Shimadzu GC 2010 gas chromatograph equipped with a flame ionization detector and a TC-FFAP capillary column. In order to confirm the reusability, hydrogenation of cyclohexene was carried out by using the recovered *n*Pt@*h*C sample. After the first run, the

sample was collected by centrifugation at 3500 rpm for 10 min, followed by 3 times washing with acetone. Then the reaction was done by the same procedures described above. Note that all of these procedures were operated in the same glass tube; therefore, the loss of *n*Pt@*h*C was negligible.

2.3 Results and Discussion

Bifunctional TiO_2 as Photocatalyst and Template

Photoirradiation was performed in an air-free closed gas circulation system with a Pyrex reaction cell. The TiO_2 photocatalyst used was commercial anatase TiO_2 powder supplied by Ishihara Sangyo (ST-21). A suspension containing the TiO_2 powder, phenol and a small portion of hexachloroplatinic acid (H_2PtCl_6, containing Pt atoms corresponding to 0.3 wt.% for TiO_2) was photoirradiated under Ar (30 kPa) with a high-pressure Hg lamp through a Pyrex water jacket (cutoff < 290 nm, so that light of wavelength > 290 nm reached the suspension). Upon photoirradiation to the suspension, monotonic liberation of H_2 was observed, while prolonged irradiation gradually reduced the rate of H_2 liberation (Figure 1a). Such H_2 liberation has commonly occurred in a deaerated aqueous suspension of TiO_2 in the presence of H_2PtCl_6 and organic compounds such as methanol and propan-2-ol.[7] Previous studies have proved that the predominant redox reactions by photogenerated e^- and h^+ in these systems are reduction of H_2O into H_2 on in situ deposited Pt metal by the reduction of H_2PtCl_6 and oxidation of alcohols into corresponding aldehyde or ketone, respectively.[7b, 7c] Thus, we suppose that similar photocatalytic reactions occurred in the present system. In practice, by analyzing the reaction solution after the initial 10 min of photoirradiation using gas chromatography-mass spectroscopy (GC-MS) analysis, we confirmed that products in the

solution mainly consisted of hydroquinone, resorcinol, biphenol, and phenoxyphenol, which are typical compounds produced by oxidation of phenol.

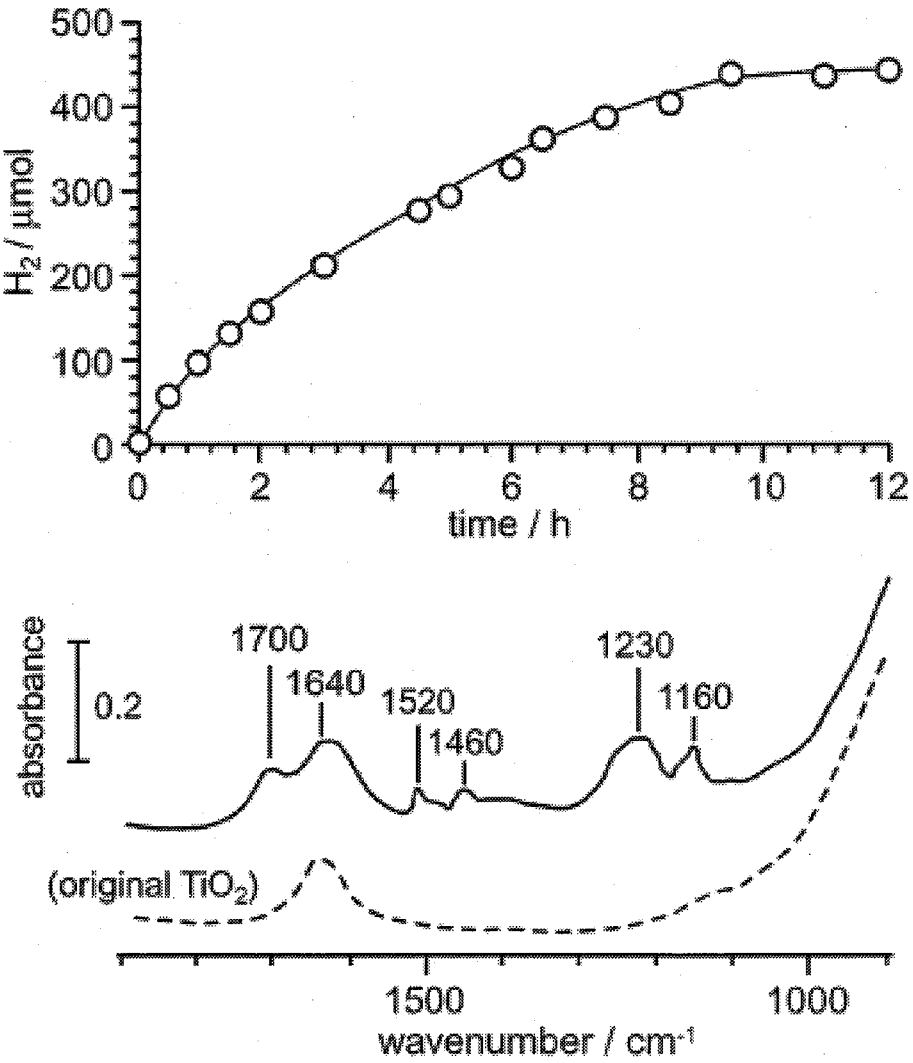

Figure 1. a) Time course of H_2 liberation over TiO_2 from an aqueous solution containing phenol and H_2PtCl_6. b) Fourier transform infrared (FTIR) spectra of TiO_2 particles: solid line, a sample recovered after 2.5 h photoirradiation; dashed lined, original TiO_2.

With gradual decrease in the rate of H_2 liberation as shown in Figure 1a, TiO_2 particles became brownish in color, implying deposition of organic components on the TiO_2 surface. To identify these organic species, FT-IR analysis of the brown-colored TiO_2 particles recovered after 2.5-h photoirradiation was conducted (Figure 1b). In addition to the OH bending band of adsorbed H_2O at 1640 cm^{-1}, which is seen in the spectrum of original TiO_2, several adsorption bands are observed in the thus-obtained TiO_2 sample. Absorption bands centered at 1160 and 1230 cm^{-1} indicate C-O-C symmetric and C-OH stretching vibrations, respectively. The presence of benzene ring is verified by absorption bands at 1460 and 1520 cm^{-1} of aromatic C-C stretching vibrations. Since these absorption bands are typical of polyphenol and/or phenolic resin,[8] we can confirm that the surface covered organic components are the result of the polymerization of phenol. In addition, there is another appreciable band at 1700 cm^{-1}. This band is probably attributable to the C=O stretching band of ester groups probably generated via coupling between phenol and dicarboxylic acid derivatives as a result of oxidative ring-opening reaction of the benzene ring.

Owing to the high oxidation potential of photogenerated h^+ in TiO_2, various chemical reactions can take place on the TiO_2 surface, and this makes it difficult to determine the exact chemical reaction in the photoirradiated suspension.[9] Based on the results of GC-MS measurements and FT-IR analysis described above, however, major oxidation pathways are likely to be similar to those of electrolysis to generate organic tars on the electrode surface through the polymerization of phenol,[10] shown schematically in Figure 2. During the first step, phenol is oxidized to form phenoxy-radicals, which can be further oxidized to dihydroxylic benzenes[11] or can react to produce dimeric compounds. Since the coupled phenol units, e.g., biphenol, have a lower oxidation potential than that of phenol[10] they are readily oxidized to radicals and can undergo coupling reactions resulting in the formation of

polymer chains. The resulting cross-linking polymer chains deposit and cover the TiO_2 surface because of their insolubility in aqueous media.

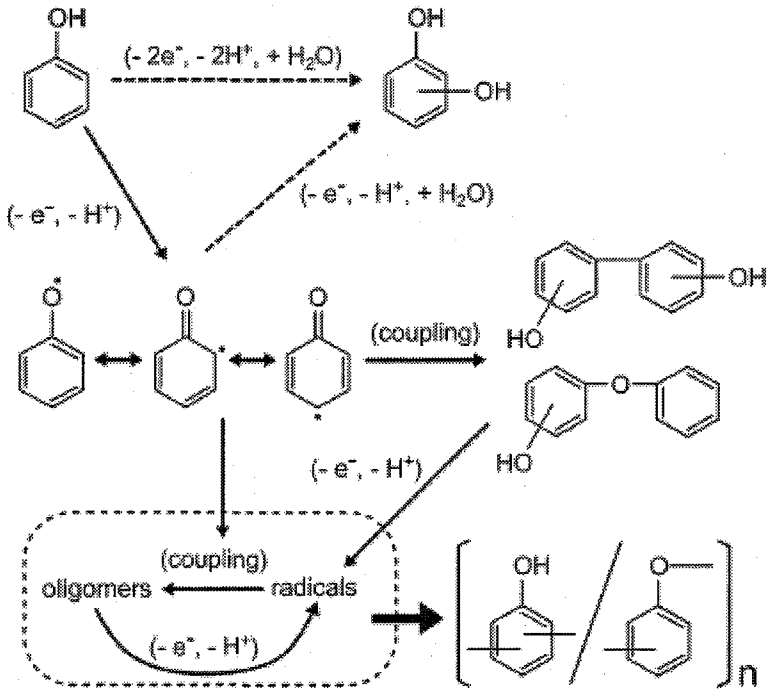

Figure 2. Postulated reaction pathways for oxidation of phenol in the present photocatalytic system.

Physical Properties of nPt@hC

The polymer-covered sample obtained after 2.5-h photoirradiation was heated at 973 K under evacuation to induce carbonization and was treated with 50 % aqueous hydrofluoric acid to remove TiO_2 components. Transformation of phenolic polymers on the TiO_2 surface into a carbon framework through the thermal treatment was confirmed by Raman spectroscopy (Figure 3). Two broad peaks at 1340 and 1580 cm^{-1}, attributable to in-plane vibration of crystalline and disordered amorphous carbon, respectively, are generally observed for less-crystalline carbon materials such as activated carbon.

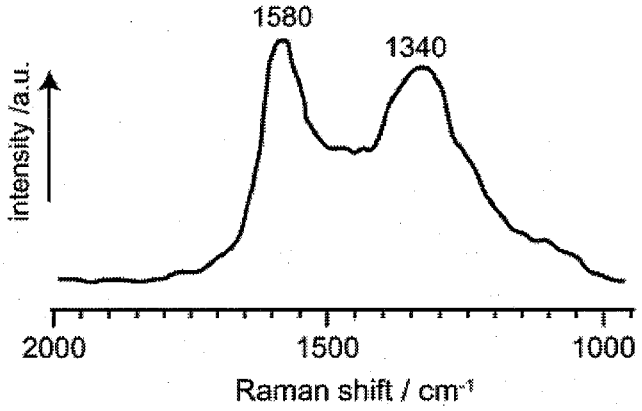

Figure 3. Raman spectrum of *n*Pt@*h*C.

The TEM image of the resultant black powder indicates that it was composed of hollow carbon spheres with average wall thickness of less than 4 nm, each of which encapsulates several Pt nanoparticles (Figure 4). Since the diameters of the hollow spaces (ca. 20 nm) were about the same as the diameter of original TiO_2 particles we consider that TiO_2 acted as a mold to form the hollow structure of carbon. Although we could not clearly obtain a selected-area electron diffraction (SAED) from the sample shown in Figure 4, SAED of hollow carbon spheres prepared from a solution containing larger amounts of hexachloroplatinic acid indicated diffraction rings that were indexed to face-centered-cubic Pt with a lattice constant of ca. 0.39 nm (see Figure 5c). This indicates the formation of the *n*Pt@*h*C composite through the above-described procedure.

Measurement of more than 200 Pt nanoparticles in randomly selected regions in TEM images of *n*Pt@*h*C and ICP analysis of Pt components showed that Pt nanoparticles in *n*Pt@*h*C have an average diameter of 2.9 nm and there was 1.4 wt% of Pt in carbon components in the present preparation conditions. From separate experiments, the size and content of Pt were found to be dependent on the content of H_2PtCl_6 during photoirradiation (Figure 5 and Table 1). However, since lower loading reduced the total yield of *n*Pt@*h*C due

to the decrease in photocatalytic activity and since higher loading induced a significant increase in the particle size of Pt, we focused on the *n*Pt@*h*C composite prepared under above-described conditions.

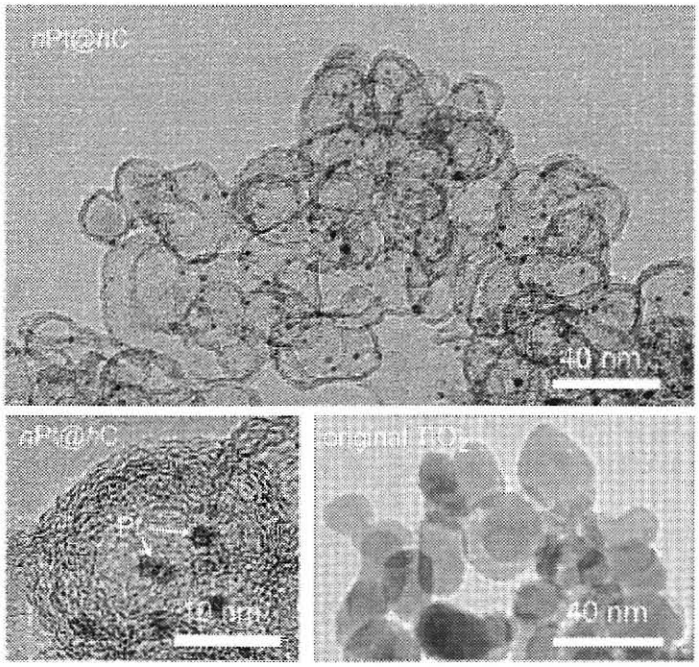

Figure 4. TEM images of *n*Pt@*h*C and original TiO_2.

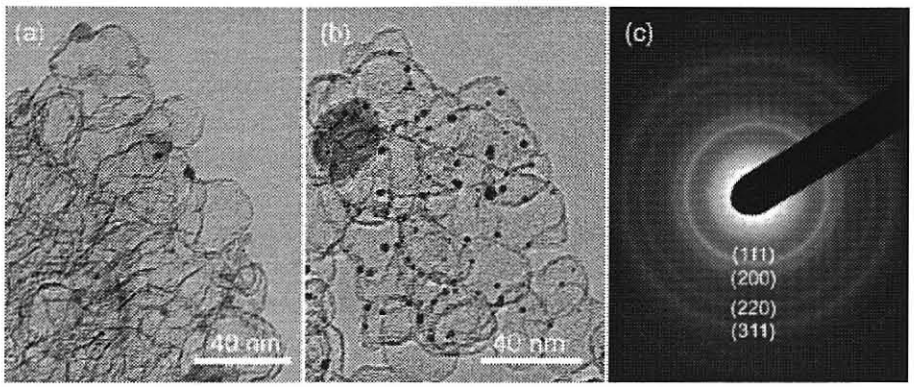

Figure 5. TEM images of *n*Pt@*h*C prepared from the aqueous TiO_2 suspensions with different contents of H_2PtCl_6: (a) 2.6 μmol and (b) 25.7 μmol of H_2PtCl_6, corresponding to 0.1 wt% and 1.0 wt% of Pt nanoparticles for TiO_2. A selected-area electron diffraction pattern (SAED) obtained from the sample shown in (b) is also shown in this figure (c)

Table 1. Properties of *n*Pt@*h*C powders synthesized from various amounts of H_2PtCl_6 [a]

Pt/TiO_2[b] (wt%)	H_2[c] / μmol	yield of *n*Pt@*h*C / mg	Pt size[d] /nm	Pt content[e] (wt%)
0.1	97	38	3.0 ±1.3	0.5
0.3	164	53	2.9 ±0.5	1.4
1.0	111	29	4.2 ±0.8	6.0

[a] TiO_2 (500 mg) was suspended in 400 cm^3 aqueous phenol solution (5.25 mmol dm^{-3}) containing small portions of H_2PtCl_6 and photoirradiated (> 290 nm) for 2.5 h under an Ar atmosphere. [b] Contents of H_2PtCl_6 in the reaction solution as Pt atoms for TiO_2. [c] Total amount of H_2 liberated in 2.5-h photoirradiation. [d] Average size of Pt nanoparticles in *n*Pt@*h*C samples determined from TEM images. [e] Contents of Pt nanoparticles in *n*Pt@*h*C estimated by ICP analyses of Pt.

The N_2 adsorption-desorption isotherm of *n*Pt@*h*C exhibits a characteristic type IV isotherm, indicating the presence of mesoporosity (Figure 6). The corresponding mesopore size distribution calculated by the BJH method from the adsorption branch revealed uniform pores centered at ca. 20 nm, which is attributable to the cavity of hollow carbon. Another noticeable feature of the isotherm is the steep increase in N_2 uptake at relative pressure (P/P_o) below 0.1. This indicates the presence of micropores in the carbon wall of *n*Pt@*h*C. The application of Horvath-Kawazoe (HK) formalism to the isotherm revealed that the carbon wall mainly comprised of ultramicropores (<0.8 nm) centered at 0.6 nm, as shown in Figure 2b. Accompanied by these ultramicropores, moreover, there are small portions of humps in the HK plot in the region of 0.8-1.5 nm, implying presences of relatively large micropores. Indeed, construction of an α_s-plot using the standard adsorption isotherm of a nonporous carbon black (Wako Pure Chemical, 86 $m^2 g^{-1}$) indicates a broad cooperative swing (CS), i.e., upward deviation at $\alpha_s > 0.5$, in addition to the deviation at $\alpha_s < 0.5$, termed filling swing (FS), representing existence of micropore systems in the region > 1 nm and those with pore size

smaller than 1 nm, respectively (Figure 6). Note that the specific surface area calculated from the slope of the α_s-plot reaches 1366 $m^2 g^{-1}$, which is remarkably high and comparable to that of representative activated carbon.[14]

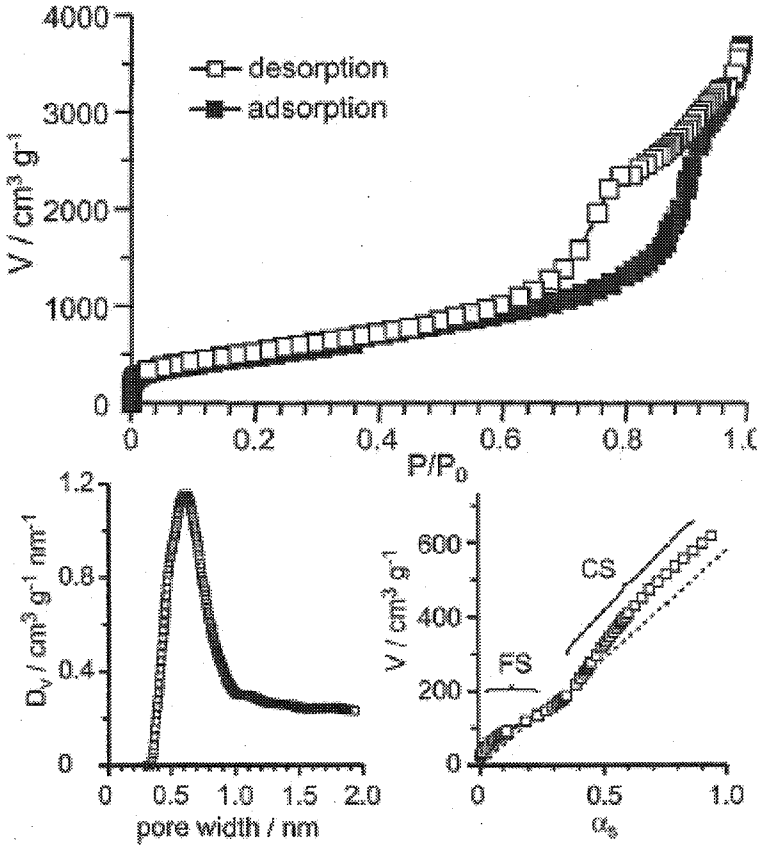

Figure 6. N_2 adsorption-desorption isotherm of *n*Pt@*h*C and its corresponding Horvath-Kawazoe (H-K) plot and a α_s-plot

Hydrogenation of Olefins using nPt@hC

The results of the above structural analysis suggest that the wall structure of *n*Pt@*h*C provides channels for the species being present outside the sphere to penetrate the carbon shell into the hollow spaces, which allows the Pt nanoparticles to act as catalysts. In order to evaluate the catalytic function of *n*Pt@*h*C, we chose hydrogenation of some olefins as model

reactions. As summarized in Table 2, *n*Pt@*h*C exhibits catalytic activities for hydrogenation of primary, secondary, and cyclic olefins (entries 1-3). When the activity was compared to that over a commercial Pt catalyst supported on an activated carbon (Pt/AC), *n*Pt@*h*C was found to have a much higher activity level (entries 4-6). We also confirmed reusability of *n*Pt@*h*C for the hydrogenation of cyclohexene (entry 7). All the results showed that *n*Pt@*h*C has the potential ability to serve as a high-performance catalytic material.

Table 2. Liquid phase hydrogenation of olefins catalyzed by nPt@hC and commercial Pt/AC powders [a].

Entry	Catalyst	Substrate	Product	t [h] [b]	Conv. [%] [c]
1	*n*Pt@*h*C	1-hexene	hexane	2	> 99
2	*n*Pt@*h*C	2-hexene	hexane	2	> 99
3	*n*Pt@*h*C	cyclohexene	cyclohexane	1	98
4	Pt/AC [d]	1-hexene	hexane	2	19
5	Pt/AC [d]	2-hexene	hexane	2	20
6	Pt/AC [d]	cyclohexene	cyclohexane	1	10
7	*n*Pt@*h*C reuse [e]	cyclohexene	cyclohexane	1	97

[a] All reactions were carried out with 0.1 μmol of catalysts (Pt) and 5 mmol of substrates under H2 (210 KPa in absolute pressure) at 348 K. [b] Reaction time. [c] Conversion of substrates. [d] A commercial catalyst supplied from N. E. Chemcat. [e] Catalyst was reused after the reaction (Entry 3).

2.4 Conclusions

In conclusion, we have demonstrated the fabrication of Pt nanoparticles encapsulated in hollow carbon nanospheres using TiO_2 nanoparticles as both the photocatalyst and the inorganic mold. These spheres were found to have high surface area and ultra-thin shell with well-developed microporosity, leading to the availability as catalysts. The preparation technique provides a new imprinting method which can be used to synthesize any desired nanostructures using pre-designed TiO_2 photocatalysts, such as nanorod- and ordered-mesoporous forms of TiO_2,[15] as core materials. Furthermore, the present concept should be applicable to other semiconductor photocatalysts and to fabrications of hollow carbon nanospheres including various metal nanoparticles other than Pt.

2.5 References

[1] a) S. Jun, S. H. Joo, R. Ryoo, M. Kruk, M. Jaroniec, Z. Liu, T. Ohsuna, O. Terasaki, *J. Am. Chem. Soc.* **2000**, *122*, 10712. b) J. Lee, S. Yoon, S. M. Oh, S. Shin, T. Hyeon, *Adv. Mater.* **2000**, *12*, 359. c) S. H. Joo, S. J. Choi, I. Oh, J. Kwak, Z. Liu, O. Terasaki, R. Ryoo, *Nature* **2001**, 412, 169.

[2] a) T. W. Kim, I. S. Park, R. Ryoo, *Angew. Chem. Int. Ed.* **2003**, *42*, 4375. b) Y. Xia, R. Mokaya, *Adv. Mater.* **2004**, *16*, 1553. c) C. N. Mbilenia, F. F. Prinsloob, M. J. Witcombc, N. J. Covillea, *Carbon* **2006**, *44*, 1476.

[3] a) S. B. Yoon, K. Sohn, J. Y. Kim, C. H. Shin, J. S. Yu, T. Hyeon, *Adv. Mater.* **2002**, *14*, 19. b) M. Kim, K. Sohn, H. B. Na, T. Hyeon, *Nano Lett.* **2002**, *2*, 1383. c) M. Kim, S. B. Yoon, K. Sohn, J. Y. Kim, C. H. Shin, T. Hyeon, J. S. Yu, *Microporous Mesoporous Mater.* **2003**, *63*, 1. d) G. S. Chai, S. B. Yoon, J. H. Kim, J. S. Yu, *Chem. Commun.* **2004**, 2766.

[4] a) J. Jang, B. Lim, *Adv. Mater.* **2002**, *14*, 1390. b) Y. Oda, K. Fukuyama, K. Nishikawa, S. Namba, H. Yoshitake, T. Tatsumi, *Chem. Mater.* **2004**, *16*, 3860.

[5] a) A. J. Bard, *J. Photochem.* **1979**, *10*, 59. b) S.-i. Nishimoto, B. Ohtani, H. Kajiwara, T. Kagiya, *J. Chem. Soc., Faraday Trans. 1* **1983**, *79*, 2685.

[6] a) P.D. Cozzoli, R. Comparelli, E. Fenizza, M.L. Curri, A. Agostiano, D. Laub, *J. Am. Chem. Soc.* **2004**, *126*, 3868. b) S. C. Chan, M. A. Barteau, *Langmuir*, **2005**, *21*, 5588.

[7] a) J. Disdier, J. M. Herrmann, P. J. Pichat, *J. Chem. Soc., Faraday Trans. 1* **1983**, *79*, 651. b) S.-i. Nishimoto, B. Ohtani, H. Kajiwara, T. Kagiya, *J. Chem. Soc., Faraday Trans. 1* **1985**, *81*, 61. c) B. Ohtani, Y. Ogawa, S.-i. Nishimoto, *J. Phys. Chem. B* **1997**, *101*, 3746.

[8] a) R. Lapuente, F. Cases, P. Garces, E. Morallon, J. L. Vazquez, *J. Electroanal. Chem.* **1998**, *451*, 163. b) J. Arana, E. Tello-Rendon, J. M. Dona-Rodriguez, J. A. Herrera-Melian, O. Gonzalez-Diaz, J. Perez-Pena, *Appl. Catal. B* **2001**, *30*, 1.

[9] In control experiments in which SiO_2 and Al_2O_3 were employed instead of TiO_2, no formation of polymeric compounds was observed under the present reaction conditions. Thus, the observed polymerization occurred through the photocatalytic reaction of TiO_2.

[10] M. Gattrell, D. W. Kirk, *J. Electrochem. Soc.* **1993**, *140*, 903.

[11] It is less probable for the formation of resorcinol through such phenoxy-radical intermediates. Hence, other pathways should also be included. Details for further identifications are still underway.

[12] S. Shanmugam, A. Gabashvili, D. S. Jacob, J. C. Yu, A. Gedanken, *Chem. Mater.* **2006**, *18*, 2275.

[13] a) K. S. W. Sing, D. H. Everett, R. A, W. Haul, L. Moscou, R. A. Pierotti, J. Rouquerol, T. Siemieniewska, *Pure Appl. Chem.* **1985**, *57*, 603. b) M. El-Merraoui, H. Tamai, H.

Yasuda, T. Kanata, J. Mondori, K. Nadai, K. Kaneko, *Carbon* **1998**, *36*, 1769.

[14] The presence of CS on activated carbons generally leads to an overestimation of specific surface area (SA) of the samples by routine BET analysis. Therefore, we determined SA of the present materials using the slope of the α_s plot.

[15] a) P. D. Cozzoli, A. Kornowski, H. Weller, *J. Am. Chem. Soc.* **2003**, *125*, 14539. b) Z. Zhong, T.-P. Ang, J. Luo, H.-C. Gan, A. Gedanken, *Chem. Mater.* **2005**, *17*, 6814. c) T. Peng, D. Zhao, K. Dai, W. Shi, K. Hirao, *J. Phys. Chem. B* **2005**, *109*, 4947.

CHAPTER 3

Development of *n*Pt@*h*C with Controllable Carbon Shell Density, Porosity and Morphology

3.1 Controllable Carbon Shell Density and Porosity of *n*Pt@*h*C

3.1.1 Introduction

Porous carbon materials have recently been the focus of intense study, especially in the field of catalysis as a support material owing to their promising properties such as high surface area, high stability in acidic and basic media, and controllable porosity.[1-3] The most efficient approach utilized for preparing these porous carbons is the templating method in which silica-based porous materials or colloidal crystals are mainly used as sacrificial molds. The availability of a wide variety of materials, such as zeolites, MCM-48, SBA-15, and colloidal silica, provides vast opportunities for the synthesis of porous carbon with various imprinted structures.[4-6]

The basic strategy of this method is filling the solid template with a carbon precursor, e.g., glucose, sucrose, pitch, or furfuryl alcohol, followed by carbonization of the resulting composite and dissolution of the template by chemical etching. Hence, by the selection of appropriate carbon precursors, silica-based templates, and carbonization setting, e.g., temperature and gas medium, various carbon materials with different degree of porosity, graphitization and density can be obtained through the medhod.[7-9] Indeed, there are many examples in the literature for better control of such structural properties of carbon. However, the ability for fine tuning to yield carbon materials with promising properties still remains a desirable research goal that has not been fully explored.

Besides efficient control of the structural properties of carbons themselves, fabrication of metal-carbon composites is another important subject for their application especially in the field of catalysis. Loading of these metals on carbon materials is generally involve multi-step process, i.e., post-loading of the respective metal ions onto carbons followed by reduction of them in a hydrogen atmosphere. Thus, a rather simplified fabrication method to prepare

carbon-metal composites with well-defined structures has recently been formulated.

In Chapter 2, we have demonstrated an alternative method for preparing porous hollow carbon encapsulating Pt nanoparticles (*n*Pt@*h*C) by using photocatalytic reaction on titanium(IV) oxide (TiO_2) particles.[10] The principle of the fabrication is based on the redox ability of photoirradiated TiO_2 nanoparticles to induce simultaneous photoreduction of Pt(IV) ions and photooxidative polymerization of phenol, which eventually result in Pt-loaded TiO_2 covered by a phenolic polyemer. This methodology enables loading of Pt nanoparticles and coverage of the carbon precursor on the TiO_2 template in a one-step process, and subsequent carbonization of the polymer layer and removal of TiO_2 yield the *n*Pt@*h*C composite. One of the significant aspects of *n*Pt@*h*C thus-obtained was that it works as an efficient catalyst for hydrogenation of various olefins.

It was also shown in Chapter 2 that polymerization of phenol seemed to proceed even after the surface of TiO_2 was fully covered after photoirradiation for a certain period, while this was not clearly clarified at the preceding stage. In subsequent study of the system, however, we found that this phenomenon induced remarkable alterations in properties of the thus-derived carbon shells. In this Chapter 3, therefore, we investigated in detail the effect of photoirradiation time on structural characteristics of the phenolic polymer covered on the TiO_2 surface and thus-derived *n*Pt@*h*Cs composite. The correlation of structures of *n*Pt@*h*Cs with their catalytic functions for hydrogenation of olefins was also examined.

3.1.2 Experimental

Preparation of Materials. An anatase TiO_2 powder supplied by Ishihara Sangyo (ST-21, average particle size: 20 nm, BET surface are: 50 $m^2\ g^{-1}$) was used. In a typical procedure, 500 mg ST-21 powder was dispersed in 400 cm^3 aqueous solution containing 200 mg phenol

and 7.7 μmol hexachloroplatinic acid (H_2PtCl_6). The amount of H_2PtCl_6 added corresponds to 0.3 wt% of TiO_2 as Pt metal. The suspension was then evacuated several times in a quartz inner-irradiation-type vessel connected to a closed gas circulation and evacuation system to ensure complete air removal. Photoirradiation of the suspension was performed with a high-pressure Hg lamp (450 W) under a reduced-pressure argon (Ar) atmosphere (30 kPa) at 293 K. The brownish samples obtained after the photoirradiation for various periods were retrieved by filtration, washed with 2 dm^3 distilled water to remove excessive phenol, and dried at 353 K in air to yield Pt-loaded TiO_2 covered with a phenolic polymer (Poly/Pt/TiO_2). The Poly/Pt/TiO_2 samples were then subjected to carbonization at 973 K for 6 h in vacuum followed by immersion of the samples in 10 cm^3 of 50 % hydrofluoric acid for 24 h at room temperature to remove the TiO_2 cores (*Caution: HF acid is highly corrosive and must be handled with extreme care!*). Finally, the black powders were washed several times with acetone and dried at 353 K to produce *n*Pt@*h*C powders. Poly/Pt/TiO_2 and *n*Pt@*h*C samples obtained with different photoirradiation times were designated as Poly/Pt/TiO_2 (photoirradiation time) and *n*Pt@*h*C (photoirradiation time), respectively; e.g., samples prepared with 1-h photoirradiation are designated as Poly/Pt/TiO_2(1) and *n*Pt@*h*C(1).

Characterization of Materials. The amount of hydrogen gas (H_2) generated from the suspension during photoirradiation was measured at certain time intervals by using a Shimadzu GC-8A gas chromatograph equipped with a MS-5A column (GL Sciences) and a TCD detector. The amount of polymer attached on the TiO_2 particles was measured by thermogravimetry (TG) analysis using a Bruker 2000A TG-DTA in air from room temperature to 873 K, with a heating ramp of 5 K min^{-1}. The polymer species was characterized by Fourier transform infrared (FT-IR) spectroscopy on a Nicolet 470 FT-IR spectrometer equipped with a MCT detector using a KBr disc technique. Typically, 2 mg Poly/Pt/TiO_2 was ground with 198

mg KBr to a fine powder. The mixture powders were then pressurized to form a KBr disc containing 1 wt% dispersed sample. Microscopic features of the samples were observed using a Hitachi H-9000 transmission electron microscope (TEM). Surface and pore analyses of *n*Pt@*h*C were performed by using a Quantachrome AUTOSORB-1 automated gas-sorption system employing Ar as an adsorbate after pretreatment of the sample at 473 K for 2 h. The content of Pt in *n*Pt@*h*C was determined by inductively coupled plasma (ICP) analysis on a Perkin-Elmer OPTIMA 3000-XL ICP emission spectrometer. For the ICP analysis, *n*Pt@*h*C samples were immersed in aqua regia for 2 h to dissolve the Pt particles. The undissolved carbon particles were filtered by using a Millipore syringe-driven membrane filter. The clear solution was then diluted to an appropriate concentration before the measurement. The amount of CO irreversibly held (CO_{irr}) on the surface of Pt nanoparticles in *n*Pt@*h*C was measured by the pulse CO adsorption experiment. Prior to the measurement, the sample was treated in H_2 flow (10 cm^3 min^{-1}) at 623 K for 30 min and flushed with helium flow (30 cm^3 min^{-1}) for 30 min at the same temperature. After the temperature was cooled to room temperature, CO pulses were injected. The amount of adsorbed CO was determined using a Shimadzu GC-14B gas chromatograph equipped with an active carbon column and a TCD detector.

Catalytic Activity Measurement. Catalytic hydrogenation was conducted in a glass tube equipped with a H_2-filled balloon. Certain amounts of *n*Pt@*h*C (corresponding to 0.08 μmol Pt), 1 ml of ethanol, and 0.5 mmol of substrate (1-hexane, 1-decene or 1-hexadecene) were put into the glass tube and connected to the H_2-filled balloon. After three vaccum/H_2 cycles to replace air inside the reaction tube with H_2, the mixture of the substrate and *n*Pt@*h*C in EtOH was stirred at room temperature for 30 min. After centrifugal separation of *n*Pt@*h*C at 2330 g for 10 min, the solution was injected into a Shimadzu GC 2010 gas chromatograph equipped

with a flame ionization detector and a TC-FFAP capillary column to determine the amounts of substrates and products. The *n*Pt@*h*C sample retrieved from centrifugation was washed three times in ethanol and reused in 1-decene hydrogenation using the same procedures as described above. The *n*Pt@*h*C composite after reaction was characterized by TEM to study the stability of the structure.

3.1.3 Results and Discussion

Photocatalytic Polymerization of Phenol in Various Irradiation Times

Due to the low catalytic ability of a bare TiO_2 surface for reduction of H_2O, photogenerated e^- in TiO_2 was initially utilized for reduction of H_2PtCl_6 to form Pt deposits when an aqueous suspension containing TiO_2, H_2PtCl_6, and phenol was irradiated by light with energy greater than the band-gap of TiO_2. After the formation of Pt metal on TiO_2, the photogenerated e^- was then consumed to reduce H_2O on the deposited Pt metal to a gaseous product of H_2 (Figure 1).[11] Because of these processes, an appreciable induction period was observed on the time course curves of H_2 liberation in the initial 30-min photoirradiation as shown in the inset of Figure 1a. On the other hand, photogenerated h^+ was likely to be instantly consumed in the oxidation of phenol: the color of TiO_2 particles became pale brown immediately after 15-min photoirradiation, indicating the deposition of polymeric compounds on the surface as a result of oxidative polymerization of phenol (see below). Based on the fact that neither liberation of H_2 nor changes in the color of particles was observed when reference systems using photocatalytically inert oxides such as Al_2O_3 instead of TiO_2 were performed (Figure 1b), observed reactions were confirmed to proceed as a result of redox reaction on TiO_2.

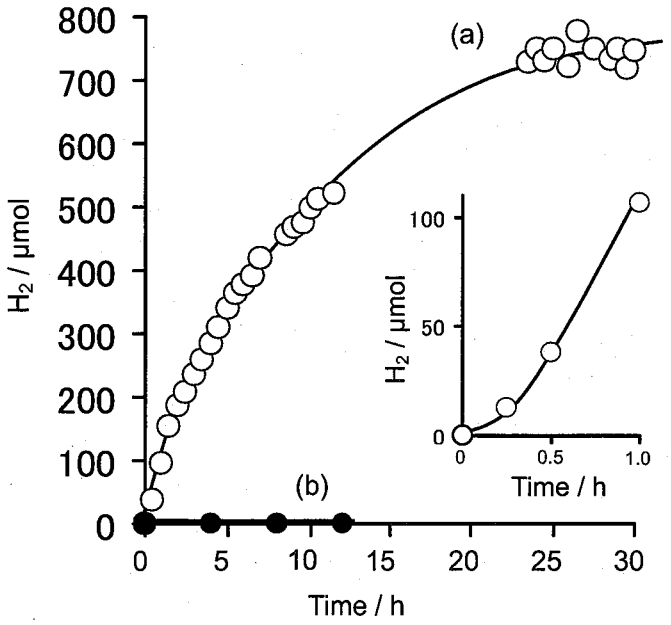

Figure 1. Time-course curves of H_2 liberation from an aqueous solution containing phenol, H_2PtCl_6 and TiO_2 (open circles) or Al_2O_3 (filled circles) under UV irradiation. The inset shows the initial rate of H_2 liberation from the TiO_2 system.

Prolonged photoirradiation induced change in the color of TiO_2 particles to deep brownish accompanied by a gradual decrease in rate of H_2 liberation as shown in Figure 1a. This suggests an increase in the amount of polymeric compounds attached on the TiO_2 particles: subsequent surface coverage of polymeric compounds reduced available active site(s), resulting in a decrease in the rate of H_2 liberation. In order to obtain quantitative information of these compounds on the surface of TiO_2, TG measurements were carried out for the TiO_2 samples after photoirradiation for various periods (Poly/Pt/TiO_2) and the results are shown in Figure 2. As a reference, the result for bare TiO_2 is also shown in this figure. While the TG curve of bare TiO_2 only showed a slight weight loss below 150 °C attributable to dehydration and desorption of water, all of the Poly/Pt/TiO_2 samples exhibited an additional large weight

loss between ca. 200 °C and ca. 500 °C in the TG curves. Since the weight loss was accompanied by a major exothermic events starting at ca. 200 °C in the DTA curve (data not shown), it was ascribed to combustion of surface-covered organic components on TiO_2. Hence, when the remaining powder above 500 °C is assumed to be composed of TiO_2 and a very small amount of Pt-deposits, the weight loss represents the amount polymeric compounds on TiO_2. Among the samples examined, it is clear that the total amount of polymeric compounds increased in proportion to photoirradiation time: polymeric compounds included in Poly/Pt/TiO_2(1), Poly/Pt/TiO_2(2.5), Poly/Pt/TiO_2(12) and Poly/Pt/TiO_2(30) samples are estimated to be ca. 5%, 14%, 18% and 26%, respectively. Another notable point is that all of the TG curves of Poly/Pt/TiO_2 samples exhibited analogous decomposition profiles comprised of two-step degradation starting at ca. 200 °C and 400 °C. Because of the similarity of these profiles to the decomposition profile of a phenolic polymer,[12] the surface-covered polymeric compound is likely to be an analogue(s) of this polymer, as expected from the above-described photocatalytic redox mechanism.

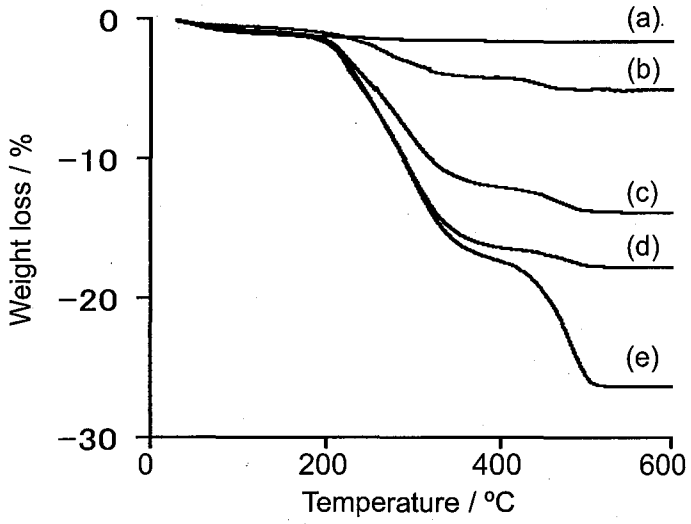

Figure 2. TG curves of (a) original TiO_2, (b) Poly/Pt/TiO_2(1), (c) Poly/Pt/TiO_2(2.5), (d) Poly/Pt/TiO_2(12) and (e) Poly/Pt/TiO_2(30)

FT-IR spectra of Poly/Pt/TiO_2 samples obtained using 200 mg KBr disc containing 1 wt% Poly/Pt/TiO_2 exhibit several identical absorption bands in addition to the absorption band at 1640 cm^{-1} assigned to the OH bending mode of adsorbed water on TiO_2 (Figure 3), indicating that the TiO_2 surface were covered by almost the same organic species regardless of photoirradiation time.[13] Overall enhancement in intensities of these absorption bands with increase in the duration of photoirradiation suggested an increase in the amount of polymer accumulated on the surface of TiO_2. Since these absorption bands are characteristics of a phenolic polymer,[14] the polymer covering the surface of TiO_2 was confirmed to have resulted from polymerization of phenol, as was analogized from the above TG analyses.

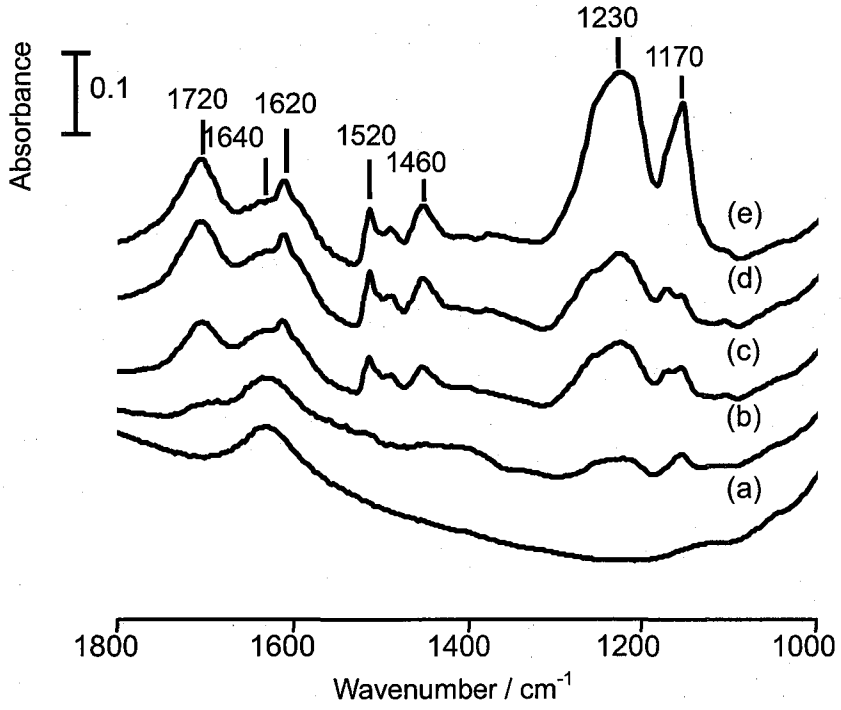

Figure 3. FTIR spectra of (a) original TiO_2, (b) Poly/Pt/TiO_2(1), (c) Poly/Pt/TiO_2(2.5), (d) Poly/Pt/TiO_2(12) and (e) Poly/Pt/TiO_2(30)

Figure 4 shows TEM images of Poly/Pt/TiO_2 samples after photoirradiation for 1, 2.5, 12 and 30 h. After photoirradiation for 1 h, the entire surface of TiO_2 was surrounded by a thin polymer layer (ca. 3 nm in thickness), indicating that complete coverage of a phenolic polymer on TiO_2 was achieved by photoirradiation for even such a short duration (Figure 4a). Moreover, the fact that Pt nanoparticles were observed as small black dots between the polymer layer and TiO_2 in the TEM images displays successful photoreduction of H_2PtCl_6 by TiO_2 during photoirradiation.

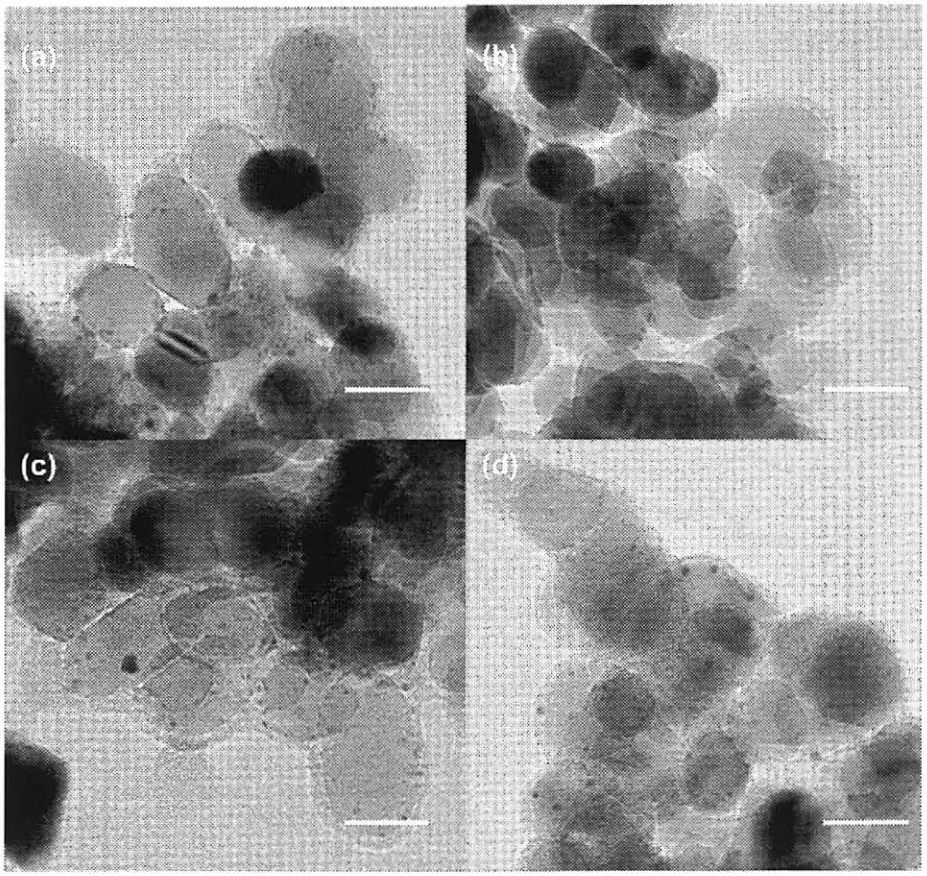

Figure 4. TEM images of (a) Poly/Pt/TiO_2(1), (b) Poly/Pt/TiO_2(2.5), (c) Poly/Pt/TiO_2(12) and (d) Poly/Pt/TiO_2(30). Scale bars correspond to 20 nm.

The thickness of the polymer layers in Poly/Pt/TiO_2 particles obtained after various durations of photoirradiation was determined from TEM images shown in Figure 4 by measuring more than 200 Poly/Pt/TiO_2 particles.[15] As a result, despite the monotonic increase in the amount of the polymer with the duration of photoirradiation (see above), the thickness of the layers was almost constant between these Poly/Pt/TiO_2 samples (ca. 3 nm). These results strongly suggest the occurrence of densification of the surface-covered polymers during prolonged photoirradiation.

Since the high oxidation potential of photogenerated h^+ in TiO_2 leads to complexity of the phenol polymerization process, the exact chemical pathway during densification of phenolic polymer is not understood at present. However, when a reaction pathway of the electrochemical oxidative phenol polymerization reported by Gattrell and Kirk was applied to the present system,[16] positive h^+ generated on TiO_2 was initially used to oxidize phenol into phenoxy radicals, and these radical species coupled with other phenols to form dimer, oligomer and polymer radicals. As discussed in Chapter 2, the existence of such C–O and C–C coupling processes was evident from the presence of phenoxy-phenol and biphenyl in the reaction suspension after 10-min photoirradiation. Due to the insolubility of these elongated phenolic species in aqueous solution, they attached to and probably self-terminated on the surface of TiO_2, resulting in the formation of a coarsely covered polymer layer on TiO_2. Once the entire surface of TiO_2 was covered by such a layer after a short duraction of photoirradiation, the subsequent polymerization process did not lead to the formation of a multi-layer polymer coating that would increase the thickness of the polymer layer, as shown in Figure 4. A possible model to explain the above results is that free phenol, which continuously penetrated the loosely packed polymer to reach the accessible surface sites of TiO_2, was photoexcited to form radical species followed by reaction with the surrounding

polymer backbone to form a densified polymer layer. Due to the gradual densification during photoirradiation, penetration of fresh phenol into the polymer layer to reach the TiO_2 surface was gradually suppressed, leading to decrease in the rate of overall reaction, as has been observed in the time course of H_2 liberation (see Figure 1a).

Densification of Carbon Shell of nPt@hC

Chapter 2 has shown that the Poly/Pt/TiO_2 sample obtained after 2.5-h photoirradiation (Poly/Pt/TiO_2(2.5)) was converted into the *n*Pt@*h*C composite by carbonization of the polymer layer at 700 °C under vacuum followed by removal of the TiO_2 core particles by a chemical etching method using 50 % aqueous HF. Since the surface-covered polymers obtained by photoirradiation for various durations have different packing densities as described above, carbon shells derived from them are expected to have different properties. Based on this idea, the *n*Pt@*h*C composites were fabricated from these Poly/Pt/TiO_2 samples by the above-mentioned procedure. Figure 5 shows typical TEM images of samples thus-obtained. All of the samples exhibited the same morphology regardless of duration of photoirradiation: hollow structured carbons encapsulating Pt nanoparticles. It is noted that both thickness of the carbon shells and particle size of Pt nanoparticles calculated by measuring more than 200 nPt@hC samples in randomly selected regions in these TEM images (Table 1) were comparable among these samples. The constant thickness of these shells indicates the densification of carbon components took place during photoirradiation. In addition, the fact that the diameters of void spaces in these samples are almost the same as that of TiO_2 used proves inversely replication of TiO_2 templates for the formation of the present hollow carbon structure.

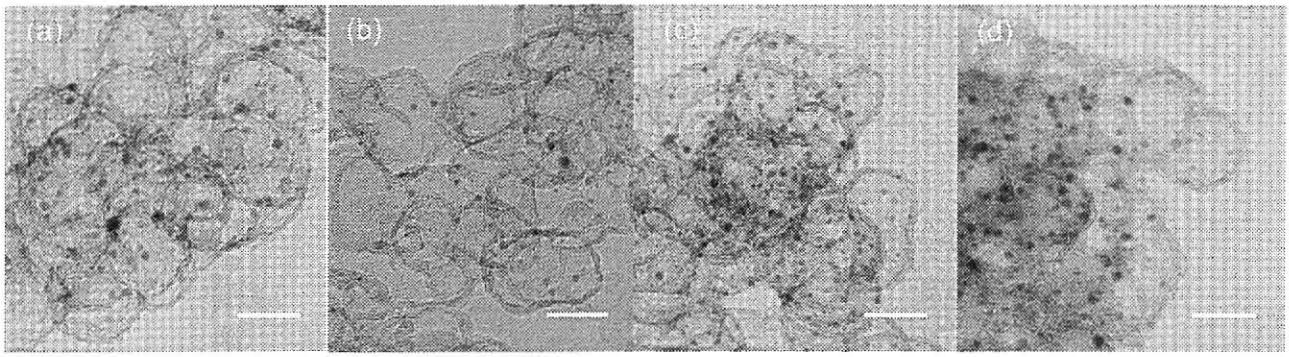

Figure 5. TEM images of (a) *n*Pt@*h*C(1), (b) *n*Pt@*h*C(2.5), (c) *n*Pt@*h*C(12) and (d) *n*Pt@*h*C(30). Scale bars correspond to 20 nm.

Figure 6 shows Ar sorption isotherms of *n*Pt@*h*C derived from various photoirradiation times. All the isotherms are categorized into type IV and show large hysterisis loops appeared from relative pressure (P/P_o) 0.4 to 0.9. This feature is typical for mesoporous materials having large pore sizes with narrow size distributions. Their corresponding pore size distributions determined from the BJH method from the adsorption data and the desorption data exhibit two different peaks centered at 21-22 nm and 8.5-9.0 nm, respectively (Figure xx). As discussed in Chapter 2, the former is corresponded to the diameter of void spaces of *n*Pt@*h*C, where the TiO_2 particles were originally existed. The latter is likely to be appeared by the presence of the window, i.e., an interconnected channel within the *n*Pt@*h*C particles, as has been typically observed in mesocellular materials with foam-like morphologies which consist of aggregates of hollow spheres.[17] The formation of such window in the present *n*Pt@*h*C is originated from the aggregated form of the TiO_2 mold. Besides these mesoporosities in *n*Pt@*h*C samples, steep increases in Ar uptake at $P/P_o < 0.1$ in these isotherms show existences of micropores inside the carbon shells. Indeed, micropore size distributions calculated by using HK formalism indicate appreciable peaks centered at ca.

0.6-0.7 nm (Figure 7 and Figure 8).

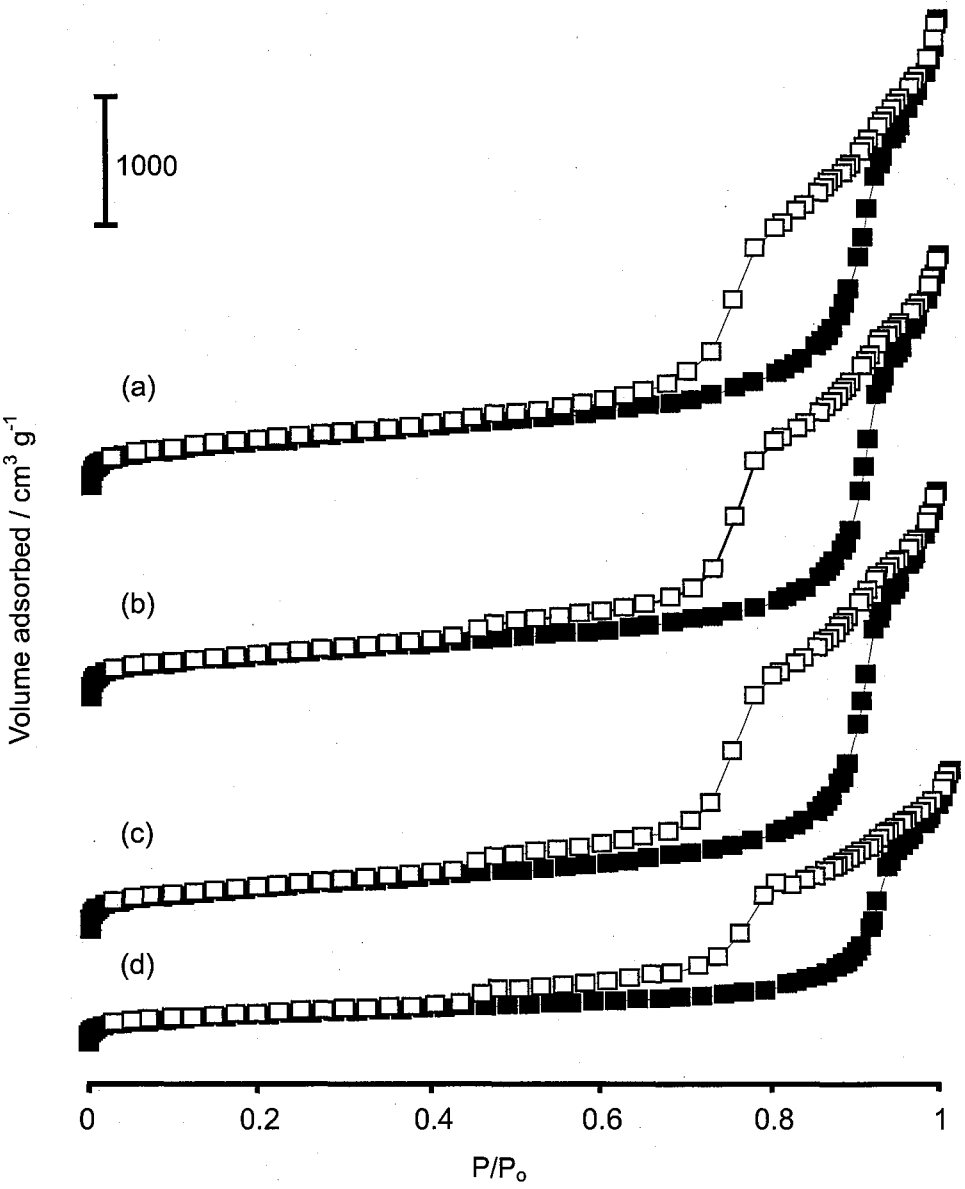

Figure 6. Ar sorption isotherms of (a) *n*Pt@*h*C(1), (b) *n*Pt@*h*C(2.5), (c) *n*Pt@*h*C(12) and (d) *n*Pt@*h*C(30). Filled and open squares denote adsorption and desorption branches, respectively.

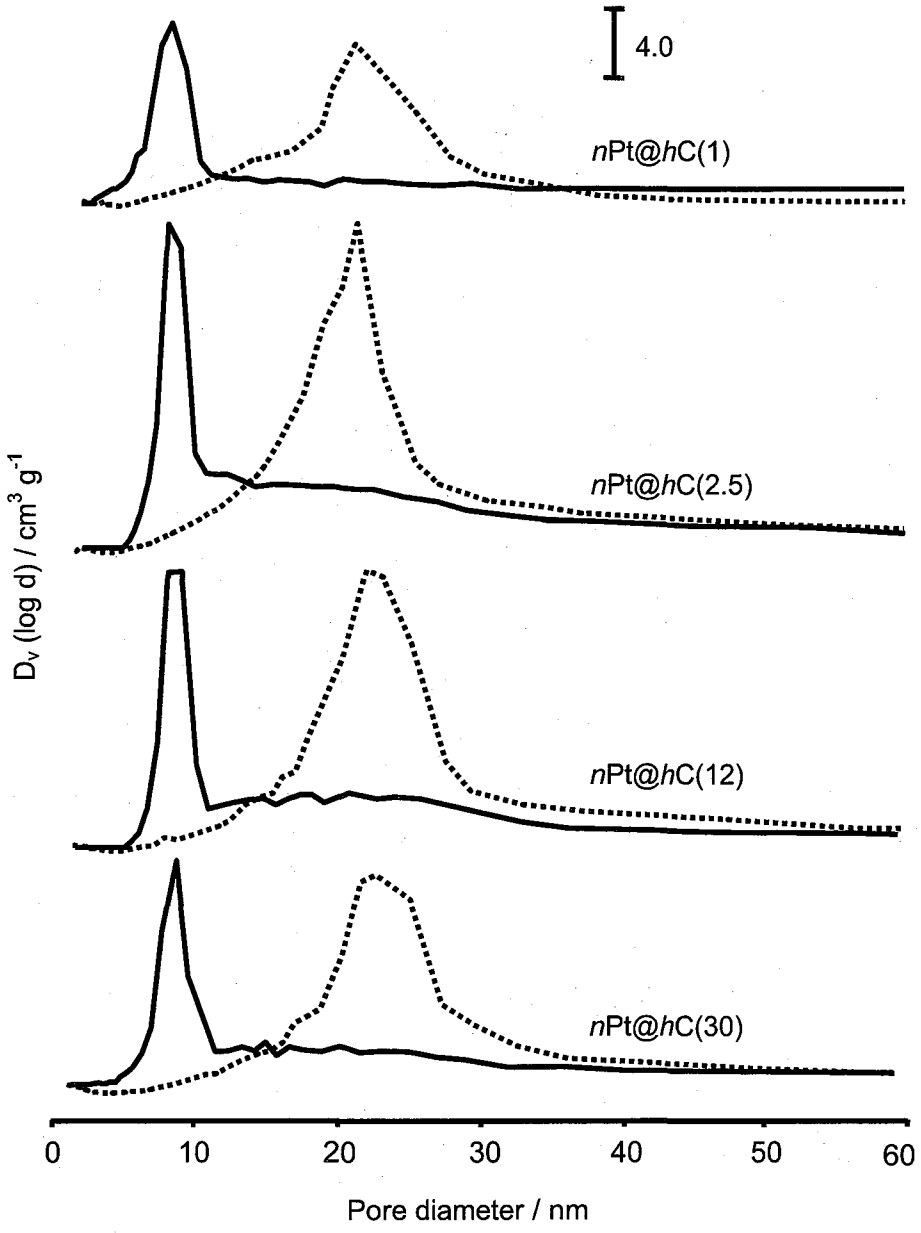

Figure 7. Mesopore size distribution of *n*Pt@*h*C samples derived from adsorption branch (dotted line) and desorption branch (solid line) of argon isotherm

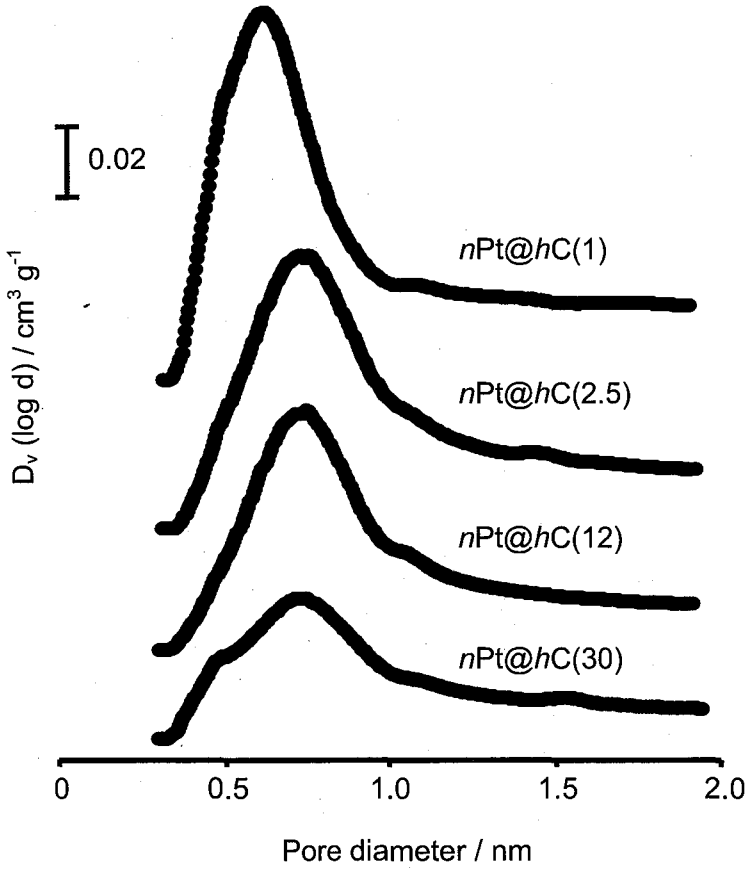

Figure 8. Micropore size distribution of *n*Pt@*h*C samples

The structural parameters deduced from these isotherms are listed in Table 1 together with other physical properties obtained from different techniques. The mesopore sizes exhibit insignificant difference between the *n*Pt@*h*C samples, as expected from their structural similarities observed in TEM images (Figure 5). Moreover, there is also no significant difference of the micropore sizes in these samples. Nevertheless, their BET surface areas and micropore show appreciable differences between these samples: both of them monotonically decreased with increase in duration of photoirradiation during the formation of Poly/Pt/TiO_2 samples. Hence, change in the density of the polymer layer in Poly/Pt/TiO_2 induced by

duration of photoirradiation strongly influences the density of the resulting carbon shell in *n*Pt@*h*C without any alterations of pore sizes. These results imply that the densification of the carbon shell leads to filling of certain parts of the micropore systems inside the carbon shell to lose its microporosity. In addition, as a consequence of densification of the carbon shell, the content of Pt in the *n*Pt@*h*C sample gradually decreased with increase in duration of photoirradiation, as we expected.

Table 1. Physical properties of *n*Pt@*h*C samples derived from various durations of photoirradiation

Catalyst	T_{shell}[a] / nm (σ[b])	Pt[c] / nm (σ[b])	D_{ads}[d] / nm	D_{des}[e] / nm	W_{micro}[f] / nm	S_{BET}[g] / m^2g^{-1}	V_{micro}[h] / cm^3g^{-1}	Pt content[i] / wt%
*n*Pt@*h*C(1)	2.8 (0.68)	2.8 (0.58)	21	8.5	0.6	1320	0.43	3.3
*n*Pt@*h*C(2.5)	2.8 (0.63)	2.8 (0.60)	21	8.5	0.7	1080	0.35	1.5
*n*Pt@*h*C(12)	2.8 (0.82)	2.7 (0.58)	22	9.0	0.7	980	0.33	1.3
*n*Pt@*h*C(30)	2.8 (0.80)	2.7 (0.65)	22	9.0	0.7	690	0.23	1.0

[a] Thickness of carbon shell [b] Standard deviation [c] Pt size [d] Diameter of mesopore from adsorption branch of isotherm [e] Diameter of mesopore from desorption branch of isotherm [f] Micropore width [g] BET surface area [h] Micropore volume calculated using HK formalism. [i] Pt content determined by ICP analysis.

Effect of Carbon Shell Densification on the Catalytic Activity.

Alteration in the porosity of support materials often has a significant influence in catalytic activity for several considerations, such as change in available surface area and modification of the diffusion mode for substrate(s) and product(s).[18] From this viewpoint, effects of densification of the carbon matrix in the present *n*Pt@*h*C sample on its catalytic function are one of the attractive subjects. Thus, we evaluated catalytic activities for hydrogenation of

some normal olefins using *n*Pt@*h*C(1) and *n*Pt@*h*C(30) samples having the lowest and the highest densities of carbon shell among the present samples, respectively. Figure 8 shows representative results of hydrogenation of 1-hexene, 1-decene, and 1-hexadecene over these samples. It is clear that remarkable activity is achieved with *n*Pt@*h*C(1): almost all of the substrates are converted into their corresponding normal alkanes by *n*Pt@*h*C(1), whereas the reactions do not go to completion with *n*Pt@*h*C(30) under the present reaction condition. It should be noted that we confirmed the reusability of *n*Pt@*h*C(1) for the hydrogenation of 1-decene for at least three runs of reactions without significant loss of catalytic activity (data not shown). A TEM image of *n*Pt@*h*C(1) taken after the reaction revealed that there is no change in the structure of the catalyst (Figure 9).

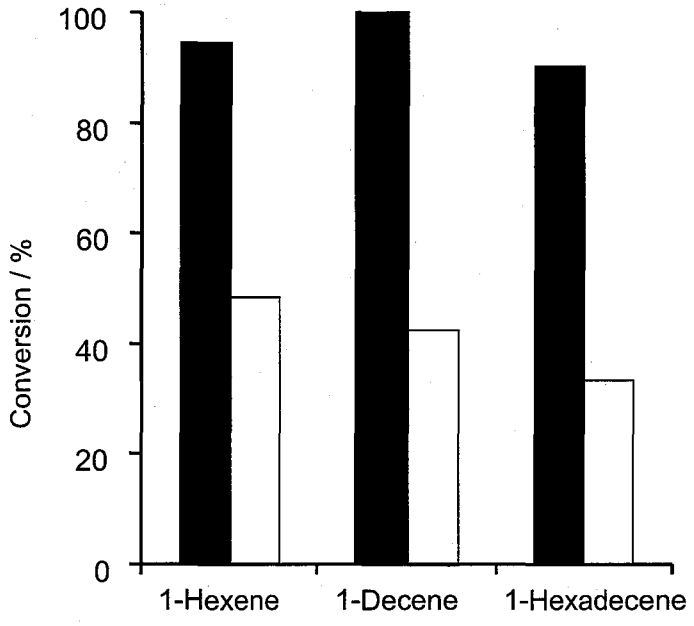

Figure 8. Liquid-phase hydrogenation of olefins catalyzed by *n*Pt@*h*C(1) (black blocks) and *n*Pt@*h*C(30) (white blocks) at ambient temperature and pressure.

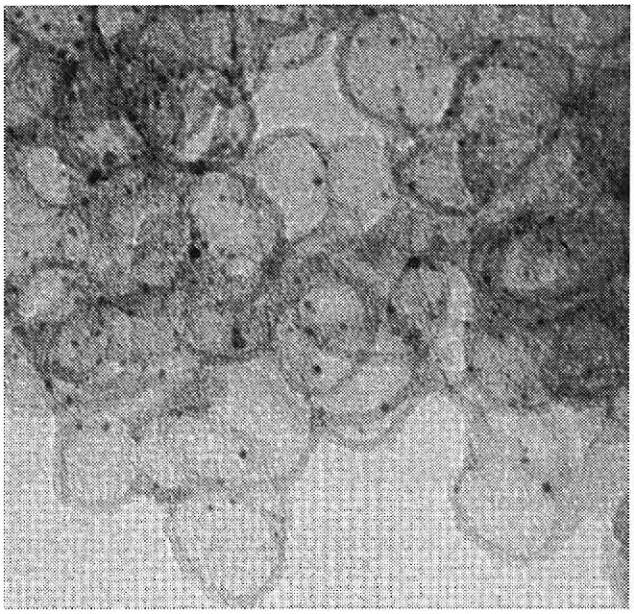

Figure 9. TEM image of *n*Pt@*h*C after hydrogenation reaction.

The above results clearly indicate significant effects of carbon densification on the catalytic activity of the *n*Pt@*h*C composites. From cross-sectional imaging of an *n*Pt@*h*C sample (will be discussed in Chapter 4),[19] we found that the Pt nanoparticles were actually embedded in the matrix of the carbon shell instead of being "rattled" inside the hollow structure. Therefore, one of the most possible explanations for the reduction of catalytic activity on the *n*Pt@*h*C(30) sample is the surface coverage of Pt nanoparticles by the growing carbon shell, leading to decrease in available active site(s). Actually, CO adsorption analyses of *n*Pt@*h*C(1) and *n*Pt@*h*C(30) at room temperature indicate that Pt dispersion (CO_{irr}/Pt), i.e., the ratio of surface Pt atoms available for CO adsorption to the total number of Pt atoms, of *n*Pt@*h*C(30) (CO_{irr}/Pt = 0.21) is smaller than that of *n*Pt@*h*C(1) (CO_{irr}/Pt = 0.36). Because the sizes of Pt nanoparticles in both samples are almost the same (Table 1), it is likely that the decrease in Pt dispersion is directly related to the decrease in active site(s) for the present catalytic reaction.

Besides the surface coverage of Pt nanoparticles with the carbon layer which act as a physical barrier between substrate(s) and Pt catalyst, decrease in micropore volume in the dense carbon shell prepared from longer irradiation time might limit the rate of substrate diffusion. Therefore, another probable explanation for the activity drops in the *n*Pt@*h*C(30) sample is that the dense carbon layer in *n*Pt@*h*C(30) obstructs permeation of the substrate through it to reach to the Pt catalyst. However, since other structural parameters in porosity such as micropore and mesopore sizes are almost comparable between *n*Pt@*h*C(1) and *n*Pt@*h*C(30) samples (Table 1) and since reactions of normal olefins employed in this chapter should not provide clear size dependence, such effects of substrate diffusion have not yet proved. Hence, further investigations to identify factors determining the overall rate using various bulky substrates in different catalytic systems are now in progress.

3.1.4 Conclusions

In this section, a photocatalytic method for fabrication of hollow carbon encapsulating Pt nanoparticles was investigated, focusing on control of structural characteristics of the carbon shell. We proved that the density of the phenolic polymer, a carbon precursor, could be controlled by changing duration of photoirradiation during the deposition of Pt metal and the polymer onto TiO_2 particles, leading to tunability of density and porosity of the resulting hollow carbon shell. Moreover, the densification of carbon was found to reduce number of active surfaces on Pt nanoparticles, resulting in changes in catalytic activity of Pt for hydrogenation of olefins with H_2. Due to its simplicity, the present strategy can be used as a tool for tuning properties of carbon-based materials when appropriate photocatalyst particles are employed.

3.1.5 References

[1] (a) Ma, Z.; Kyotani, T.; Liu, Z.; Terasaki, O.; Tomita, A. *Chem. Mater.* **2001**, *13*, 4413. (b) Wang, J. N.; Zhang, L.; Niu, J. J.; Yu, F.; Sheng, Z. M.; Zhao, Y. Z.; Chang, H.; Pak, C. *Chem. Mater.* **2007**, *19*, 453. (c) Yang, Z.; Xia, Y.; Mokaya, R. *J. Am. Chem. Soc.* **2007**, *129*, 1673. (d) Lu, A.; Li, W.; Salabas, E.; Spliethoff, B.; Schuth, F. *Chem. Mater.* **2006**, *18*, 2086. (e) Ikeda, S.; Ishino, S.; Harada, T.; Okamoto, N.; Sakata, T.; Mori, H.; Kuwabata, S.; Torimoto, T.; Matsumura, M. *Angew. Chem. Int. Ed.* **2006**, *45*, 7063.

[2] (a) Toda, M.; Takagaki, A.; Okamura, M.; Kondo, J. N.; Hayashi, S.; Domen, K.; Hara, M. *Nature* **2005**, *438*, 178. (b) Okamura, M.; Takagaki, A.; Toda, M.; Kondo, J. N.; Domen, K.; Tatsumi, T.; Hara, M.; Hayashi, S. *Chem. Mater.* **2006**, *18*, 3039. (c) Wang, X.; Liu, R. Waje. M. M.; Chen, Z.; Yan, Y.; Bozhilov, K. N.; Feng, P. *Chem. Mater.* **2007**, *19*, 2395.

[3] (a) Xia, Y.; Yang, Z.; Mokaya, R. *Chem. Mater.* **2006**, *18*, 140. (b) Yu, C.; Fan, J.; Tian, B.; Zhao, D.; Stucky, G. D. *Adv. Mater.* **2002**, *14*, 1742. (c) Lee, J. S.; Joo, S. H.; Ryoo, R. *J. Am. Chem. Soc.* **2002**, *124*, 1156. (d) Lu, A.; Schmidt, W.; Spliethoff, B.; Schueth, F. *Adv. Mater.* **2003**, *15*, 1602.

[4] Kyotani, T.; Ma, Z.; Tomita, A. *Carbon* **2003**, *41*, 1451.

[5] (a) Lee, J.; Kim, J.; Hyeon, T. *Adv. Mater.* **2006**, *18*, 2073. (b) Ryoo, R.; Joo, S. H.; Kruk, M.; Jaroniec, M. *Adv. Mater.* **2001**, *13*, 677.

[6] Gierszal, K. P.; Jaroniec, M. *J. Am. Chem. Soc.* **2006**, *128*, 10026.

[7] (a) Delhaes, P. *Carbon* **2002**, *40*, 641. (b) Jeong, H. J.; Park, H. D.; Lee, J. D.; Park, J. O. *Carbon* **1996**, *34*, 417.

[8] (a) Yoon, S. B.; Chai, G. S.; Kang, S. K.; Yu, J. S.; Gierszal, K. P.; Jaroniec, M. *J. Am. Chem. Soc.* **2005**, *127*, 4188. (b) Gierszal, K. P.; Kim, T. W.; Ryoo, R.; Jaroniec, M. *J. Phys. Chem. B* **2005**, *109*, 23263.

[9] (a) Arriagada, R.; Bello, G.; Garcia, R.; Rodriguez-Reinoso, F.; Sepulveda-Escribano, A. *Micro. Meso. Mater.* **2005**, *81*, 161. (b) Lei, S.; Miyamoto, J.; Ohba, T.; Kanoh, H.; Kaneko, K. *J. Phys. Chem. C* **2007**, *111*, 2459.

[10] Ng, Y. H.; Ikeda, S.; Harada, T.; Higashida, S.; Sakata, T.; Mori, H.; Matsumura, M. *Adv. Mater.* **2007**, *19*, 597.

[11] (a) Ohtani, B.; Ogawa, Y.; Nishimoto, S. –I. *J. Phys. Chem. B* **1997**, *101*, 3746. (b) Kraeutler, B.; Bard, A. J. *J. Am. Chem. Soc.* **1978**, *100*, 4317. (c) Kawai, T.; Sakata, T. *J. Chem. Soc. Chem. Commun.* **1980**, 694. (d) Yamaguti, K.; Sato, S. *J. Phys. Chem.* **1985**, *89*, 5510. (e) Ikeda, S.; Sugiyama, N.; Murakami, S. –Y.; Kominami, H.; Kera, Y.; Noguchi, H.; Uosaki, K.; Torimoto, T.; Ohtani, B. *Phys. Chem. Chem. Phys.* **2003**, *5*, 778. (f) Abe, R.; Sayama, K.; Sugihara, H. *J. Phys. Chem. B.* **2005**, *109*, 16052.

[12] Uyama, H.; Maruichi, N.; Tonami, H.; Kobayashi, S. *Biomacromolecules* **2002**, *3*, 187.

[13] Peaks at 1230 and 1170 cm^{-1} in the FT-IR spectra of Poly/Pt/TiO_2 samples were ascribed to the asymmetric vibrations of the C–O–C bending and C–OH vibration, respectively. The presence of a benzene ring was verified by absorption bands at 1460, 1520 and 1620 cm^{-1} of aromatic C–C stretching vibration. A C=O stretching band contributed from ester groups generated as a result of benzene ring-opening reaction, or from benzoquinone groups produced as typical derivatives from phenol oxidation was also observed at 1720 cm^{-1}.

[14] (a) Gattrell, M.; Kirk, D. W. *J. Electrochem. Soc.* **1992**, *139*, 2736. (b) Lapuente, R.; Cases, F.; Garces, P.; Morallon, E.; Vazqueq, J. L. *J. Electroanal. Chem.* **1998**, *451*, 163.

[15] Thickness of the polymer layer in each Poly/Pt/TiO_2 sample was defined as the thin grayish layer covered on the relatively black TiO_2 particles in the TEM image.

[16] Gattrell, M.; Kirk, D. W. *J. Electrochem. Soc.* **1993**, *140*, 903.

[17] (a) Schimidt-Winkel, P.; Lukens, W. W., Jr.; Ying, P.; Margolese, D. I.; Lettow, J. S.; Ying, J. Y.; Stucky, G. D. *Chem. Mater.* **2000**, *12*, 686. (b) Lettow, J. S.; Han, Y. J.; Schmidt-Winkel, P.; Yang, P.; Zhao,D.; Stucky, G. D.; Ying, J. Y. *Langmuir*, **2000**, *16*, 8291. (c) Oda,Y.; Fukuyama, K.; Nishikawa, K.; Namba, S.; Yoshitake, H.; Tatsumi,T. *Chem. Mater.* **2004**, *16*, 3860.

[18] (a) Viswanadham, N.; Dixit, L.; Gupta, J. K.; Garg, M. O. *J. Mol. Catal. A: Chem.* **2006**, *258*, 15. (b) Arino, M.; Pinna, F.; Strukul, G. *Appl. Catal. B: Environ.* **2004**, *53*, 161.

[19] Pt nanoparticles were found to be embedded in the carbon shell. The carbon matrix kinetically locked the motion of Pt nanoparticles, resulting in remarkable thermal stability. The results will be submitted elsewhere.

3.2 Morphological Control of Carbon in *n*Pt@*h*C

3.2.1 Introduction

Metal nanoparticles with sizes less than 10 nm exhibit unexpectedly excellent catalytic activities for various reactions owing to their large surface area and size-dependent properties different from bulk metals.[1] A problem accompanied by their homogeneities in reaction solutions is, however, difficulty in separation from products as-formed. One of the solutions to overcome the problem is immobilization of these metal nanoparticles on insoluble materials. Hence, studies on fabricating supported metal nanoparticles using various preparation methods and support materials have been reported extensively.[2]

Among a wide variety of supports employed so far, carbon is one of the most promising materials because of its stability in acid and basic media, high surface area derived from well-developed porosity, and inertness to most chemical reactions.[3] Various types of carbon materials have therefore been developed and proved to work as efficient catalysts when certain metal nanoparticles were loaded.[4] However, when these catalysts are utilized to reactions under a severe condition such as vigorous agitation, high pressure, and high temperature, appreciable leaching and/or agglomeration often occur, probably due to the relatively weak interaction between the loaded metal nanoparticles and carbon supports.[5]

In order to improve the stabilities, we have developed a rattle-type nanostructure composed of naked metal nanoparticles (core) and hollow porous carbon shell (not included in this thesis).[6] Since the nanostructure is effective for preventing aggregation of metal nanoparticles core and since the void space between the core and porous carbon shell is suitable as a catalytic reaction site, this material has been proved to work as highly active catalysts for various hydrogenations. Besides, Zhao and co-workers reported another type of nanocomposites, i.e., metal nanoparticles entrapped in carbon matrixes; the novel composite

is probed to have high resistance to agglomeration and leaching.[7]

In Chapter 2, we introduced the fabrication of Pt nanoparticles incorporated with a hollow porous carbon shell (*n*Pt@*h*C) by using a titanium(IV) oxide (TiO_2) photocatalytic reaction.[8] Due to certain specific properties of the *n*Pt@*h*C nanostructure, this material was found to work as an active and reusable catalyst in hydrogenation reactions.

In the previous section of this chapter, we have also evaluated in details the pore structures of various *n*Pt@*h*C samples obtained from different duration of photoirradiation. Consequently, we have proved that prolonged irradiation induced a densification of the carbon matrix. This results in a decrease in pore volume and thereby reduces catalytic functions. These results led us to investigate the effect of relatively short photoirradiation duration on the structure of the *n*Pt@*h*C nanostructure. In this section, we therefore studied in detail structures and catalytic functions of the Pt nanoparticles and carbon composites obtained *via* short photoirradiation duration.

3.2.2 Experimental

Preparation of Materials. An anatase TiO_2 powder supplied by Ishihara Sangyo (ST-41, average particle size: 120 nm, BET surface area: 13 $m^2 g^{-1}$) was used. In a typical procedure, 500 mg ST-41 powder was dispersed in 500 cm^3 aqueous solution containing 200 mg phenol and 7.7 μmol hexachloroplatinic acid (H_2PtCl_6). The suspension was then evacuated several times in a quartz inner-irradiation-type vessel connected to a closed gas circulation and evacuation system to ensure complete air removal. Photoirradiation of the suspension was performed under reduced-pressure Ar atmosphere (30 kPa) with a high-pressure Hg lamp through a water jacket to keep the reactor temperature constant at 293 K. The brownish

sample obtained after photoirradiation for various periods were retrieved by filtration, washed with 2 dm^3 distilled water to remove excessive phenol, dried at 353 K in air to yield phenolic polymer-coated platinized TiO_2 nanocomposites. These nanocomposites were then subjected to carbonization at 973 K for 6 h in vacuum. The resulting black powder was subsequently immersed in 10 ml 50 % hydrofluoric acid for 24 h at room temperature to dissolve TiO_2 core particles to give the carbon-supported Pt nanocomposites (*Caution: HF acid is highly corrosive and must be handled with extreme care!*). The as-prepared samples are called *n*Pt@*h*C(photoirradiation time), e.g., *n*Pt@*h*C(0.5) represents a sample obtained after 0.5-h photoirradiation.

Characterizations of Materials. The amount of polymer attached on the TiO_2 particles was measured by thermogravimetry (TG) analysis using a Bruker 2000 A TG-DTA in air from room temperature to 873 K, with a heating ramp of 5 K min-1. Amounts of Pt in polymer-coated platinized TiO_2 and *n*Pt@*h*C samples were determined by inductively coupled plasma (ICP) analysis on a Perkin-Elmer OPTIMA 3000-XL ICP emission spectrometer. For the ICP analysis, the samples were immersed in aqua regia for 2 h to dissolve the Pt particles. After filtration of undissolved components by using a Millipore syringe-driven membrane filter, the clear solution was diluted to an appropriate concentration for the analysis. Surface area and porosity of the samples were analyzed using a Quantachrome AUTOSORB-1. Microscopic features of the samples were observed using a Hitachi S-5000 FEG scanning electron microscope (SEM) and a Hitachi H-9000 transmission electron microscope (TEM)

Catalytic Activity Measurement. Oxidation of 1-phenylethanol with molecular oxygen (O2) was performed as a model reaction. Typically, a mixture of 1-phenylethanol (0.25 mmol), catalyst (Pt: 0.5 μmol) and distilled water (5 cm^3) was put into a reaction vessel equipped with a reflux condenser. Then the mixture was heated at 333 K for 24 h under an atmospheric

pressure of O_2 with vigorous stirring. After the reaction, the solution was transferred into a sample tube and extracted with diethyl ether. A portion of the diethyl ether solution was withdrawn and injected into a Shimadzu GC 2010 gas chromatograph equipped with a flame ionization detector and a TC-FFAP capillary column to determine the amounts of substrates and products. When the catalyst was reused, the residual reaction solution after the extraction with diethyl ether was centrifuged and the collected catalyst powder was heated at 353 K overnight in an oven before reuse.

3.2.3 Results and Discussion

Deposition Behaviors of Pt particle and Phenolic Polymer

Figure 1 shows SEM images of TiO_2 powders after photoirradiation in the aqueous solution containing H_2PtCl_6 and phenol for various photoirradiation duration. For the samples obtained after 0.25 h and 5 h photoirradiation, corresponding TEM images are also shown in the insets (panels a and d). After 0.25 h irradiation, Pt particles (with size of 2 – 3 nm) are clearly observed as the bright dots on the plain TiO_2 surface (Figure 1a). When the photoirradiation was performed for 0.5 h, some irregular components adjacent to the Pt metals started to appear on the TiO_2 surface, as shown in Figure 1b. Since the sample exhibited an appreciable exothermic peak at ca. 623 K in the TG-DTA measurement, the roughly shaped component on the TiO_2 surface should be an organic components. As is analogized from the electrochemical oxidation of phenol to generate phenolic polymer on the electrode surface reported by Grattrell and Kirk,[9] the observed organic component was assigned to the phenolic polymer grown by oxidative polymerization of phenol with positive h^+ in TiO_2. Indeed, we have proved appropriateness of the assignment by FT-IR and GS-MS analyses.[8a,8b]

As shown in Figure 1c, an increment of coverage of phenolic polymer was clearly observed by extending the photoirradiation duration (0.75 h). Finally, whole TiO_2 particles are covered with a layer of phenolic polymer by prolonged photoirradiation after 5 h (Figure 1d). Because of the surface coverage by the polymer layer, Pt particles are hardly observed in these SEM images because they have been covered by the polymer layer. However, their existence is confirmed by the TEM image shown in the inset of Figure 1d, indicating the entrapment of Pt particles beneath the polymer layer on the TiO_2.

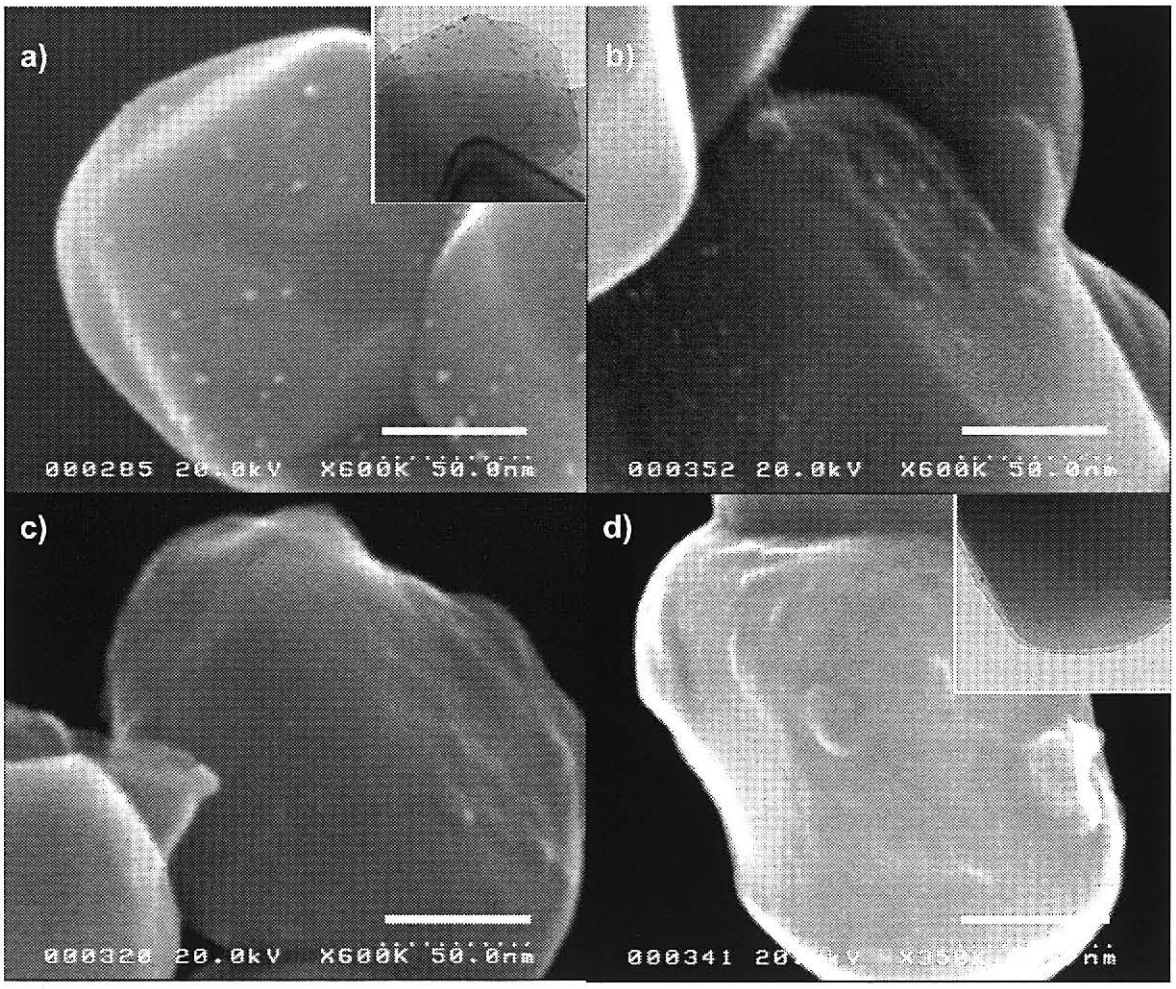

Figure 1. SEM images of TiO_2 after irradiated with H_2PtCl_6 and phenol for (a) 0.25 h, (b) 0.5 h, (c) 0.75 h and (d) 5 h. Insets of (a) and (d) represent the corresponding TEM images. Scale bars correspond to 50 nm.

It is worth noting that the surface coverage of Pt particles seems to be in a certain level irrespective of the photoirradiation duration. In order to understand the photodeposition pathways of Pt particles, amounts of them in various photoirradiation durations were quantified by IPC analyses. Figure 2 shows the results. Amounts of gaseous product of molecular hydrogen (H_2) and surface covered phenolic polymer determined by GC and TG analyses, respectively, were also shown in this figure. It is clear that the amount of the Pt component on TiO_2 achieves saturation within first 0.25 h of photoirradiation (Figure 2a). This indicates that photogenerated e^- in TiO_2 rapidly reduces $PtCl_6^{2-}$ ions to form Pt nanoparticles on the surface of TiO_2. Since the reduction of H_2O into H_2 predominantly occurs on such deposited Pt particles, the monotonic liberation of gaseous H_2 without appreciable induction period shown in Figure 2b supports this prediction.

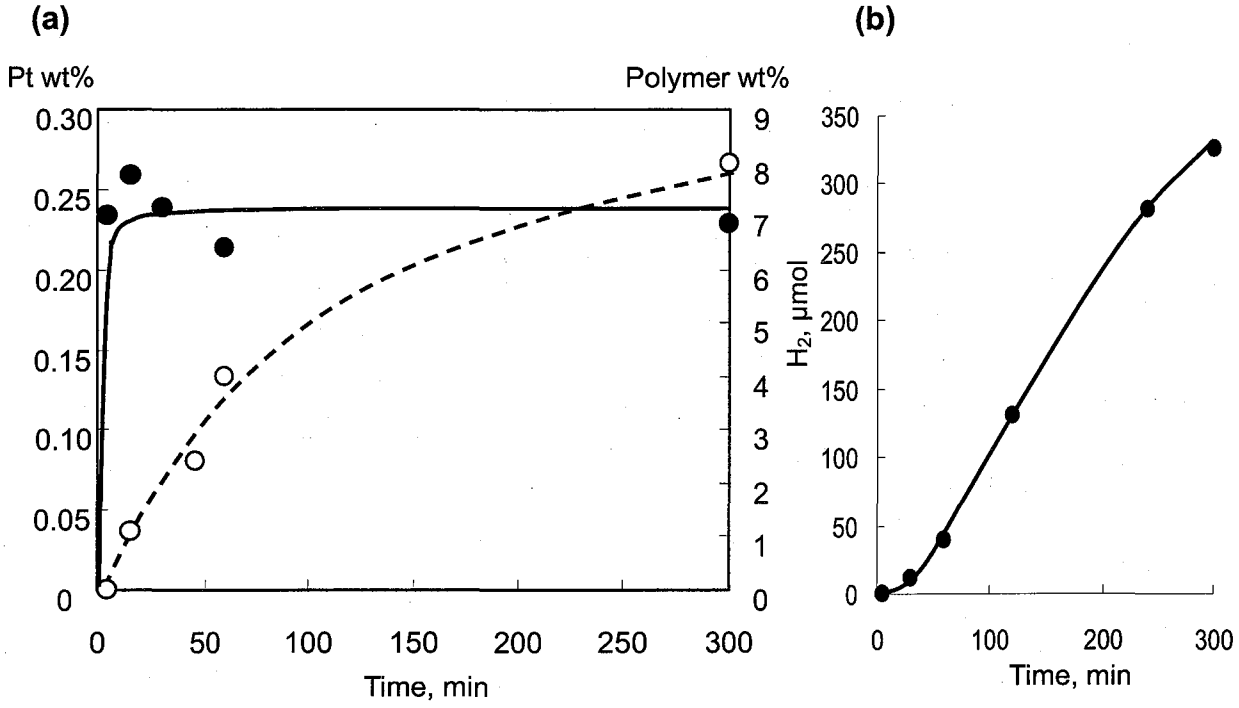

Figure 2. (a) Deposition rate of Pt nanoparticles and phenolic polymer on TiO_2 and (b) H_2 liberation from the reaction suspension during photoirradiation

In comparison with the above Pt photodeposition, oxidative polymerization of phenol with positive holes (h^+) proceeded in a much slower manner: a continuous increase in the amounts of attached phenolic polymer proceeded along with irradiation time. As reported in the previous section,[8a] gradual decrease in the deposition rate correspondence to the deceleration of H_2 liberation indicates the progress of surface coverage with the phenolic polymer in agreement with the above SEM observation.

Structure of Carbon Components Obtained by Different Irradiation Durations

After subjecting these polymer-coated Pt-TiO_2 nanocomposites to carbonization at 973 K in vacuum followed by removal of TiO_2 core particles by a chemical etching method using aqueous HF, *n*Pt@*h*C composites were obtained. Figure 3 shows TEM images of *n*Pt@*h*C prepared from various irradiation times. Apparently, sample prepared from 0.5 h irradiation labeled as *n*Pt@*h*C(0.5) shows non-defined structure where the carbon barely exhibits any clear configuration. *n*Pt@*h*C(0.75) derived from 0.75 h irradiation started to exhibit edges and boundaries with sheet-like 2-dimensional structure. Formation of edges and boundaries in this nanosheet-like *n*Pt@*h*C(0.75) is likely to be attributed to the incomplete coverage of phenolic polymer on TiO_2 nanoparticles during the short irradiation time. In contrast, when the complete coverage of phenolic polymer on TiO_2 nanoparticles is achieved with 5 h or longer irradiation, well-defined hollow carbon nanospheres encapsulated Pt nanoparticles *n*Pt@*h*C(5) is obtained. This *n*Pt@*h*C(5) nanosphere demonstrates undoubtedly the inverse structure of TiO_2 nanoparticles used as template.

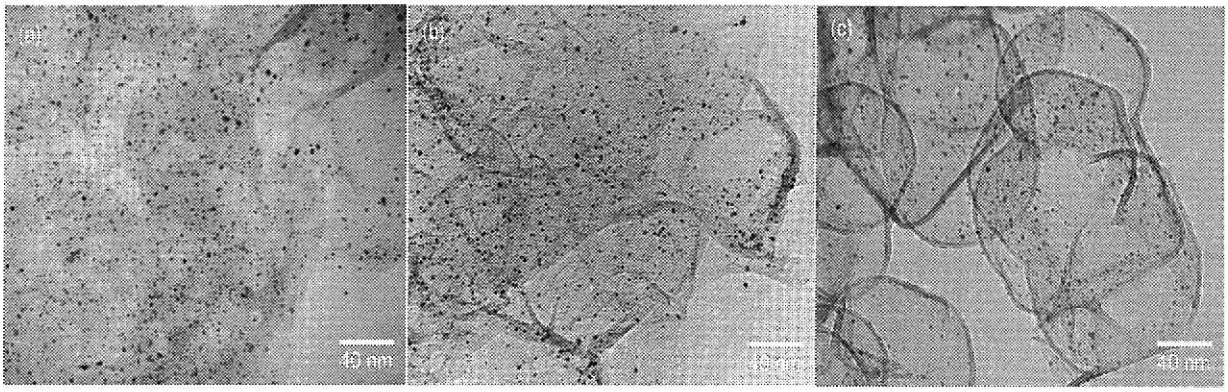

Figure 3. TEM images of carbon-supported Pt derived from a) 0.25 h, b) 0.75 h and c) 5 h irradiation.

Figure 4 reveals the micropore size distribution of *n*Pt@*h*C(0.5), *n*Pt@*h*C(0.75) and *n*Pt@*h*C(5) obtained by using N_2 sorption analyses. Despite the very different morphology of carbon derived from short and long irradiation time shown in TEM images, they all possess identical micropore structure indicate the analogous nature of all carbon components. This result shows that the pore characteristic of carbon is alike while its morphology is pre-determined by the coverage of polymer on TiO_2 as precursor composite. Another noticeable feature in Figure 4 is the gradual decrease in micropore volume of *n*Pt@*h*C samples along with the increased irradiation time. This slight reduction of micropore volume from 0.24 $cm^3\ g^{-1}$ of *n*Pt@*h*C(0.5) nanosheet to 0.19 $cm^3\ g^{-1}$ of *n*Pt@*h*C(5) nanospheres is compliant with the results shown in the previous section regarding the irradiation time-dependent densification of carbon components, i.e., longer irradiation time leads to the filling of micropore system of the originally loosely-packed carbon to give a relatively more densified carbon components. Owing to this well-developed microporosity, all *n*Pt@*h*C samples exhibit high surface area at ca. 600 – 700 $m^2\ g^{-1}$, leading to the high expectation of their catalytic performance.

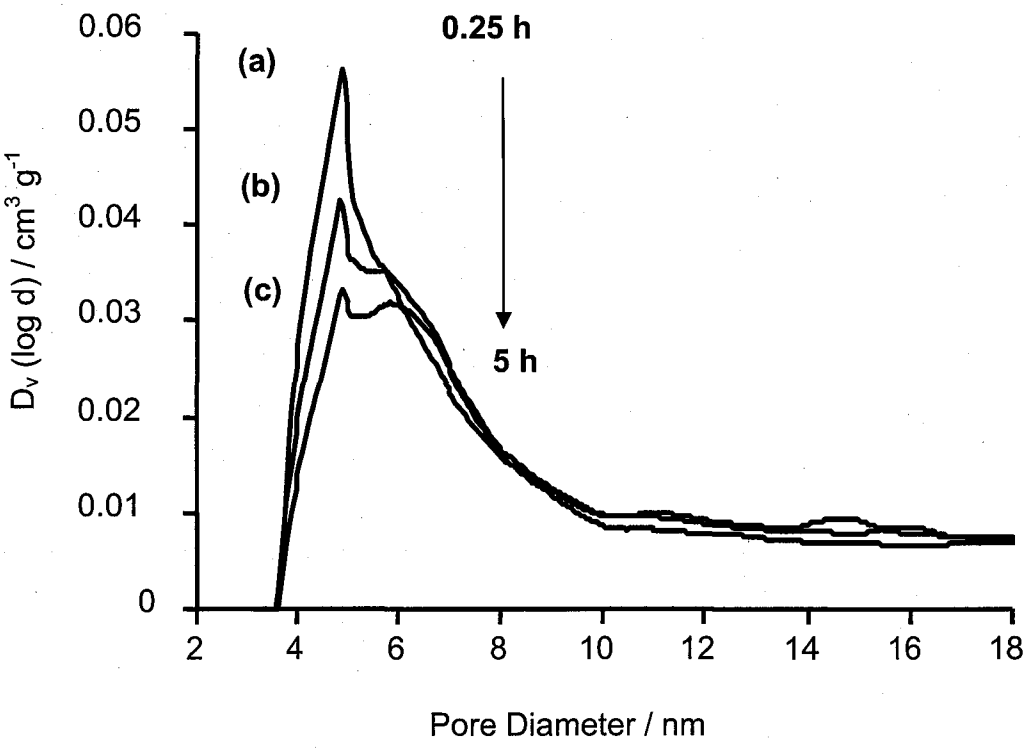

Figure 4. Micropore size distribution of *n*Pt@*h*C samples derived from (a) 0.25 h, (b) 0.75 h and (c) 5 h photoirradiation time.

Catalytic Activities of nPt@hC Nanosheets and Nanospheres

Activity of various Pt catalysts was evaluated in oxidation of 1-phenylethanol under 1 atm O_2 in water, as shown in Table 1. *n*Pt@*h*C(5) nanospheres exhibited the most efficient activity to oxidize 1-phenylethanol to acetophenone (entry 1). *n*Pt@*h*C(0.75) nanosheet, on the other hand, was found to be relatively less effective but still preceding the activity of a commercial Pt/AC catalyst (entries 2 and 3). Other Pt catalysts such as commercial Pt supported on alumina (Pt/Al_2O_3), Pt-black and Pt nanoparticles stabilized with polyvinylpyrrolidone (Pt-PVP) yielded poor results (entries 4-6).[10] Most commercial Pt catalysts demonstrate low activity of alcohol oxidation in aqueous system owing to the hydrophilic nature of their support result in a less efficient mass contact between active sites

and organic substrate. On the other hand, PVP is covering the Pt metals leads to the suppression of active sites accessibility in Pt-PVP sample. Hence, a hydrophobic porous carbon is suitable to serve as a good support for metal catalysts in organic reactions using water as solvent. However, despite of the similar nature of carbon components in *n*Pt@*h*C(0.75) nanosheet and *n*Pt@*h*C(5) nanosphere, they demonstrated appreciable difference in catalytic activity.

Table 1. Oxidation of 1-phenylethanol using various Pt metal catalysts[a].

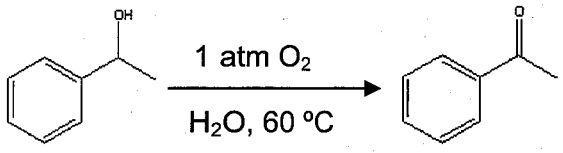

Entry	Catalyst	M/S[b], %	Conv.[c], %	TON[d]
1	PtC@nanosphere	0.2	70	350
2	PtC@nanosheet	0.2	48	240
3	Pt/AC (Wako)	0.2	38	190
4	Pt-black	0.5	45	90
5	Pt/Al_2O_3	0.2	5	25
6	Pt-PVP	1	3	3

[a]All reactions were carried out in water under 1 atm of oxygen at 60 °C for 24 h. [b] Metal/substrate molar ratio. [c] Conversion. [d] Turnover number.

One of the possibilities contributes to this phenomenon is the influence of location of Pt nanoparticles in these nanocomposites. As will be discussed in Chapter 4,[8c] the Pt nanoparticles in *n*Pt@*h*C nanosphere were well dispersed and were embedded in the carbon matrix which contains highly developed micropore and mesopore systems. Besides inducing preferential adsorption of the organic substrate to prepare a higher concentration of substrate in the Pt surrounding microenvironment, this hydrophobic porous carbon also provide three-dimensional channels and spaces for efficient mass transfer to accelerate the catalytic reaction. In contrast, when a short irradiation time was employed, the coverage of polymer coating on Pt-TiO_2 is incomplete, results in the thus-obtained sheet-like *n*Pt@*h*C(0.75) which does not reflect the shape of TiO_2 nanoparticles. It is reasonable to anticipate that, in a shorter irradiation condition in which the surface of platinized TiO_2 is just partly covered by phenolic polymer, only a portion of Pt nanoparticles are embedded but the rest of them are attached on the thus-derived carbon. Therefore, in comparison with nanospheres composite where embedment of Pt in carbon took place, *n*Pt@*h*C(0.75) nanosheet receives less profound effect from the highly concentrated microenvironment. Generally, Pt nanoparticles of commercial catalysts are anchored on the surface of carbon. Although this catalyst benefits from being excellently dispersed and also has a hydrophobic carbon to adsorb organic alcohol, its inhomogeneity of Pt particle size distribution and weak interaction with carbon are believed to be the reasons of its lower activity.

In addition to providing a higher concentration of substrate in Pt surrounding microenvironment, embedment of Pt in carbon matrix also enhances the reusability of catalyst in alcohol oxidation. It is generally accepted that Pt metals are easily susceptible to deactivation by oxygen, i.e., overoxidation of Pt.[11] The insertion of oxygen atom into the interstices and lattices of Pt metals significantly diminishes their catalytic ability. However,

encapsulating Pt nanoparticles within the carbon matrix successfully represses the deactivation as indicated in Figure 5. One of the most noticeable features in Figure 5 is that the reused *n*Pt@*h*C(5) nanosphere maintained its high activity level while a marked decrease in activity level was observed on Pt/AC sample. Meanwhile, *n*Pt@*h*C(0.75) nanosheet in which the environment of Pt metals is somehow fall in between *n*Pt@*h*C(5) nanosphere and Pt/AC shows moderate decrease of activity in the reusability test. Though deactivation of *n*Pt@*h*C(5) nanosphere is occurred in the third run of reaction, rate of activity loss was rather mild when compared to that of the *n*Pt@*h*C(0.75) nanosheet and Pt/AC sample, indicating that embedding Pt nanoparticles in a hollow porous carbon is a practical structure to suppress deactivation of Pt catalyst. One of the possible reasons for the suppression of Pt deactivation is that the carbon matrix acts as an oxygen diffusion barrier to lower the concentration of dissolved oxygen on the surface of Pt metal so that the oxygen supply is only consumed to oxidize the substrate instead of Pt metal. Unlike Pt/AC or conventional supported Pt catalysts that the Pt metals are directly contact with dissolved oxygen in reaction system, oxygen must be diffused through the carbon matrix before reaching Pt in *n*Pt@*h*C(5) nanosphere. Van Dam *et al.* had demonstrated that activated carbon served as an oxygen diffusion barrier in oxidation of glucose.[12] However, due to the impregnation method that they employed to deposit Pt metals on activated carbon, they encountered the clustering of Pt crystallites as the main problem that hampered their quantitative study. By encapsulating Pt nanoparticles within carbon matrix, *n*Pt@*h*C(5) nanosphere effectively prevents the agglomeration of Pt nanoparticles during reaction. Therefore, current synthesis method would be an appropriate model to study the oxygen diffusion effect induced by carbon materials on the overoxidation of Pt metal. Works in this direction are now underway.

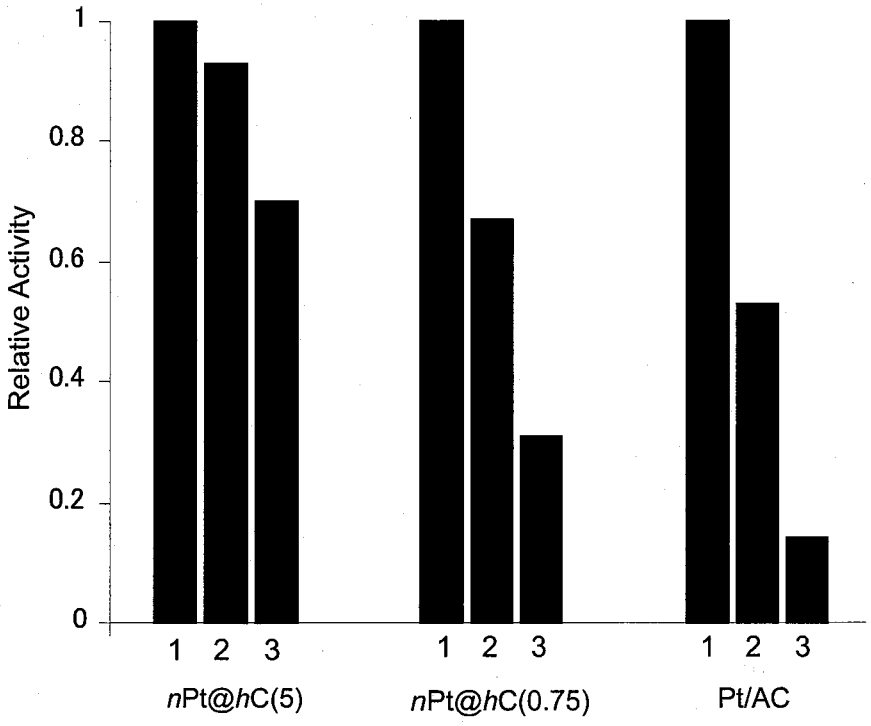

Figure 5. Reusability test for *n*Pt@*h*C(5), *n*Pt@*h*C(0.75) and Pt/AC in oxidation of 1-phenylethanol.

3.2.4 Conclusion

In this section, we observed the deposition of Pt nanoparticles and phenolic polymer on TiO_2 as the precursor of carbon-supported Pt nanocomposites. Rapid deposition rate of Pt metal compared to phenolic polymer ensured the encapsulation of Pt nanoparticles in between polymer layer and TiO_2 core. We also demonstrated that by using different irradiation duration, Pt embedded in hollow porous carbon nanospheres [*n*Pt@*h*C(5) nanospheres] and Pt embedded in and anchored on carbon nanosheet [*n*Pt@*h*C(5) nanosheet] were fabricated. Owing to the unique location of Pt in *n*Pt@*h*C(5) nanosphere, it exhibited higher level of catalytic activity and reusability. The carbon which simultaneously served as the Pt carrier

and as the oxygen diffusion barrier might be the reason for the resistance of *n*Pt@*h*C(5) nanosphere to Pt deactivation. We believe that the current system would be helpful in studying the deactivation mechanism of Pt metal in oxidation reaction.

3.2.5 References

[1] (a) M. Haruta and M. Date, *Appl. Catal. A* 222 (**2001**) 427. (b) S. H. Joo, S. J. Choi, I. Oh, J. Kwak, Z. Liu, O. Terasaki and R. Ryoo, *Nature* 412 (**2001**) 169. (c) T. Mallat and A. Baiker, Chem. Rev. 104 (2004) 3037. (d) P. J. Collier, J. A. Iggo and R. Whyman, *J. Mol. Catal. A* 146 (**1999**) 149.

[2] (a) M. Yang, Y. Yang, Y. Liu, G. Shen and R. Yu, *Biosens. Bioelectron.* 21 (**2006**) 1125. (b) S. Mandal, D. Roy, R.V. Chaudhari and M. Sastry, *Chem. Mater.* 16 (**2004**) 3714. (c) N. Zheng and G. D. Stucky, *Chem. Commun.* (**2007**) 3862. (d) Y. Lin, X. Cui, C. Yen and C. M. Wai, *J. Phys. Chem. B* 109 (**2005**) 14410. (e) S. Ivanova, C. Petit and V. Pitchon, *Appl. Catal. A* 267 (**2004**) 191. (f) P. Braunstein, H. –P. Kormann, W. Meyer-Zaika, R. Pugin and G. Schmid, *Chem. Eur. J.* 6 (**2000**) 4637. (g) J. He, T. Kunitake and A. Nakao, *Chem. Mater.* 15 (**2003**) 4401. (h) M. Sasaki, M. Osada, N. Higashimoto, T. Yamamoto, A. Fukuoka and M. Ichikawa, *J. Mol. Catal. A* 141 (**1999**) 223. (i) Y. Zhou, H. Itoh, T. Uemura, K. Naka and Y. Chujo, *Langmuir* 18 (**2002**) 277.

[3] E. Auer, A. Freund, J. Pietsch and T. Tacke, *Appl. Catal. A* 173 (**1998**) 259.

[4] (a) M. Endo, Y. A. Kim, M. Ezaka, K. Osada, T. Yanagisawa, T. Yanagisawa, T. Hayashi, M. Terrones and M. S. Dresselhaus, *Nano Lett.* 3 (**2003**) 723. (b) H. E. Van Dam and H. Van Bekkum, *J. Catal.* 131 (**1991**) 335. (c) M. C. Roman-Martinez, D. Cazorla-Amoros, A. Lineares-Solano, C. Salinas-Martinez De Lecea, H. Yamashita and M. Anpo, *Carbon* 33 (**1995**) 3. (d) J. Jang and H. Yoon, *Adv. Mater.* 15 (**2003**) 2088.

[5] (a) J. D. Aiken and R. G. Finke, *J. Mol. Catal. A* 145 (**1999**) 1. (b) Y. I. Matatov-Meytal and M. Sheintuch, *Ind. Eng. Chem. Res.* 37 (**1998**) 309. (c) F. Alardin, B. Delmon, P. Ruiz and M. Devillers, *Catal. Today* 61 (**2000**) 255. (d) S. Hermans and M. Devillers, *Catal. Lett.* 99 (**2005**) 55. (e) M. Besson and P. Gallezot, *Catal. Today*, 57 (**2000**) 127.

[6] (a) S. Ikeda, S. Ishino, T. Harada, N. Okamoto, T. Sakata, H. Mori, S. Kuwabata, T. Torimoto and M. Matsumura, *Angew. Chem., Int. Ed.* 45 (**2006**) 7063. (b) T. Harada, S. Ikeda, Y. H. Ng, T. Sakata, H. Mori, T. Torimoto, M. Matsumura, *Adv. Funct. Mater.* 18 (**2008**) 2190. (c) T. Harada, S. Ikeda, N. Okamoto, Y. H. Ng, S. Higashida, T. Torimoto, M. Matsumura, *Chem. Lett.* 37 (**2008**) 948.

[7] F. Su, F. Y. Lee, L. Lv, J. Liu, X. N. Tian and X. S. Zhao, *Adv. Funct. Mater.* 17 (**2007**) 1926.

[8] (a) Y. H. Ng, S. Ikeda, T. Harada, S. Higashida, T. Sakata, H. Mori and M. Matsumura, *Adv. Mater.* 19 (**2007**) 597. (b) Y. H. Ng, S. Ikeda, T. Harada, S. Park, T. Sakata, H. Mori and M. Matsumura, *Chem. Mater.* 20 (**2008**) 1154. (c) Y. H. Ng, S. Ikeda, T. Harada, T. Sakata, H. Mori, A. Takaoka and M. Matsumura, *Langmuir* 24 (**2008**) 6307. (d) Y. H. Ng, S. Ikeda, T. Harada, Y. Morita and M. Matsumura, *Chem. Commun.* (**2008**) 3181.

[9] M. Gattrell and D. W. Kirk, *J. Electrochem. Soc.* 140 (**1993**) 903.

[10] Polyvinylpyrrolidone-stabilized Pt (Pt-PVP) was synthesized as follows: PVP (66 mg) was added to a solution of hexachloroplatinic acid ($H_2PtCl_6 \cdot 6H_2O$; 0.03 mmol, 15.5 mg) in water (5 ml) and ethanol (45 ml) and the mixture was heated under reflux for 3 h.

[11] T. Mallat and A. Baiker, *Catal. Today* 19 (**1994**) 247.

[12] (a) H. E. Van Dam, P. Duijverman, A. P. G. Kieboom and H. Van Bekkum, *Appl. Catal.* 33 (**1987**) 373. (b) H. E. Van Dam, A. P. G. Keiboom and H. Van Bekkum, *Appl. Catal.* 33 (**1987**) 361.

CHAPTER 4

Embedment of Platinum Nanoparticles in Carbon Shell for Improving Sintering Resistance

4.1 Introduction

Metal nanoparticles (MNPs) show specific physical and chemical characteristics different from those of their bulky counterparts. These distinct properties are derived from quantum confinement phenomena induced by changes in densities of electronic energy levels of metals.[1] In general, these MNPs are energetically unstable owing to their high surface-to-volume ratios leading to a propensity for coalescence or sintering to minimize their surface chemical potentials. Therefore, synthesis of MNPs with excellent dispersion has been drawing much attention. One of the promising approaches to overcome this problem is loading of highly dispersed MNPs on solid supports such as polymers, oxides, and carbon materials to form MNP-support nanocomposites.[2-9] Among a wide variety of these nanocomposites, carbon-supported MNPs are of particular interest for their various promising applications such as heterogeneous catalysis, fuel cells and nanoreactors.[6-8] Ion-exchange or impregnation of metal ions onto carbon materials followed by reduction with hydrogen (H_2) is a widely used procedure. Although high dispersion of MNPs on carbon materials can be achieved by using this method, these MNPs thus-obtained are generally irregular in size and still have a tendency to be sintered at a moderate temperature to form stable larger clusters because of relatively weak interaction between loaded MNPs and carbon surfaces.[9] These propensities of MNPs often result in a great loss of catalytic activity. A method for fabrication of carbon-supported MNPs with uniform particle sizes and high resistance toward sintering at a high temperature is therefore needed.

In Chapter 2 and 3, we have developed a novel method to incorporate Pt nanoparticles in a carbon material by using TiO_2 nanoparticles.[10] Using this method, the photocatalytic function of TiO_2 nanoparticles was utilized to form Pt nanoparticles-loaded TiO_2 covered by phenolic polymers as precursor composites, *i.e.*, highly active electrons (e^-) and positive holes

(h^+) generated in TiO_2 particles by ultraviolet (UV) light irradiation simultaneously induced reduction of $PtCl_6^{2-}$ and oxidation of phenol, respectively, to form such composites. Subsequent calcination of thus-obtained composites in vacuum to convert surface phenolic polymers into carbon components followed by removal of TiO_2 core particles by a chemical etching yielded porous hollow carbons encapsulating Pt nanoparticles (*n*Pt@*h*C). In the case of conventional templating approach, a multi-step process, including fabrication of carbon nanostructure, loading of metal ions followed by reduction of them to form dispersed MNPs, is required to fabricate such composites. In contrast, this unique methodology based on the bifunctional utilization of TiO_2 particles as photocatalysts and templates offers a facile alternative to complete the loading of both carbon precursors and MNPs in a one-pot synthesis. In addition, *n*Pt@*h*C composites exhibited excellent catalytic activity for hydrogenation of various olefins as shown in Chapter 2.

In previous chapters, we have investigated some phenomenological aspects regarding the formation of *n*Pt@*h*C to prove the effectiveness of the proposed photocatalytic method for fabrication of MNP-carbon nanocomposites.[10] Despite successful preparation of *n*Pt@*h*C with novel structure, numerous structural features of thus-obtained composites still not fully clarified at that stage, for instance, behavior of Pt nanoparticles. In this chapter, therefore, we paid attention to their structures, focusing on the location of Pt nanoparticles in *n*Pt@*h*C using an electron tomography technique and the properties resulted from this unique position. Resistibility of these Pt nanoparticles to sintering, leading to minimization of loss of catalytic activity for hydrogenation reactions upon heat treatment of the *n*Pt@*h*C composite is observed and discussed.

4.2 Experimental

Preparation Procedures: The *n*Pt@*h*C sample was synthesized using the procedures described in previous chapters.[10] To 400 cm^3 of aqueous solution containing 200 mg of phenol and 7.7 μmol of hexachloroplatinic acid (H_2PtCl_6) was added 500 mg anatase TiO_2 powder supplied by Ishihara Sangyo (ST-21, average particle size: 20 nm, BET surface area: 50 $m^2 g^{-1}$). The suspension was then evacuated several times in a quartz inner-irradiation-type vessel connected to a closed gas circulation and evacuation system to ensure complete air removal. Photoirradiation of the suspension was performed under reduced-pressure Ar atmosphere (30 kPa) with a high-pressure Hg lamp through a water jacket to keep the reactor temperature constant at 293 K. After photoirradiation for 2.5 h, the brownish phenolic polymer-coated powder were retrieved by filtration, washed with 2 dm^3 distilled water to remove excessive unreacted phenol, dried at 353 K in air, and finally subjected to carbonization at 973 K for 6 h in vacuum. The resulting black powder was subsequently immersed in 10 ml 50% hydrofluoric acid for 24 h at room temperature to dissolve TiO_2 core particles to give *n*Pt@*h*C (*HF solution is very hazardous and corrosive and should be handled according to the MSDS guidelines.*).

For a reference sample, Pt/AC, an activated carbon (AC) supplied by Wako Pure Chemicals (BET surface area: 1400 m^2g^{-1}) loaded with Pt particles, was prepared as follows. To 100 mg of AC was added an ethanolic solution containing 7.7 μmol of H_2PtCl_6, the amount of which corresponded to 1.5 wt% loading of Pt. The mixture was gently stirred at ca. 333 K, evaporated to dryness, and then further dried at 383 K for 24 h in an oven. Then reduction of the Pt ions loaded on AC was performed in an H_2 atmosphere at 573 K for 2 h to yield the Pt/AC sample.

Characterization: Microscopic features of the samples were observed using a Hitachi H-800 transmission electron microscope (TEM). An XP spectrum of TiO_2 after photoirradiation was recorded on a Shimadzu ESCA-1000 X-ray photoelectron spectrometer. An electron tomogram of *n*Pt@*h*C was obtained using a 3D-TEM system based on a Hitachi H-9500 TEM equipped with a CCD camera and its operating software (EMmenu-3) developed by TVIPS. Briefly, the *n*Pt@*h*C sample in the TEM chamber was tilted from –60° to +60° in 1° steps and an image was taken for each step to accumulate a total of 121 images. These images as-obtained were reconstructed using the IMOD software[11] to give the desired tomogram. The content of Pt in *n*Pt@*h*C was determined by inductively coupled plasma (ICP) analysis on a Perkin-Elmer OPTIMA 3000-XL ICP emission spectrometer. Typically, *n*Pt@*h*C samples were immersed in aqua regia for 2 h to dissolve the Pt particles. The undissolved carbon particles were filtered by using a Millipore syringe-driven membrane filter. The clear solution was then diluted to an appropriate concentration before analysis. Raman spectra were obtained using a JASCO NRS-3100 Laser Raman Spectrophotometer.

Catalytic Hydrogenation of Olefins: Catalytic hydrogenation of 1-hexene was conducted in a stainless-steel autoclave equipped with a glass reactor of 50 cm^3 capacity. Certain amounts of *n*Pt@*h*C or Pt/AC powder (corresponding to 0.1 μmol of Pt), 10 cm^3 acetone, and 5 mmol of 1-hexene were put into the reactor and purged with N_2 several times to remove air. The reactor was then pressurized to 200 kPa with H_2, and the catalytic reaction was carried out at 348 K for 30 min under the condition of stirring (1200 rpm). After the reaction, catalyst powders were separated by centrifugation (3500 rpm, 10 min), and the solution was injected into a Shimadzu GC 2010 gas chromatograph equipped with a flame ionization detector and a TC-FFAP capillary column to determine the amounts of substrates and products.

4.3 Results and Discussion

Embedment of Platinum Nanoparticles in the Carbon Shell

Figure 1 shows a representative TEM image of TiO_2 particles after UV-light irradiation in an aqueous solution containing H_2PtCl_6 and phenol. A layer of polymer with ca. 3 nm in thickness entirely covers the TiO_2 particles. The layer encapsulates dispersed Pt nanoparticles that appear as black dots in this image.[12] In comparison with the inset of Figure 1 which represents the oval shape of original TiO_2 particles, this result demonstrates the feasibility of TiO_2 photocatalytic reaction to simultaneously deposit a polymer layer and Pt metal based on the redox capability of TiO_2 particles under irradiation.

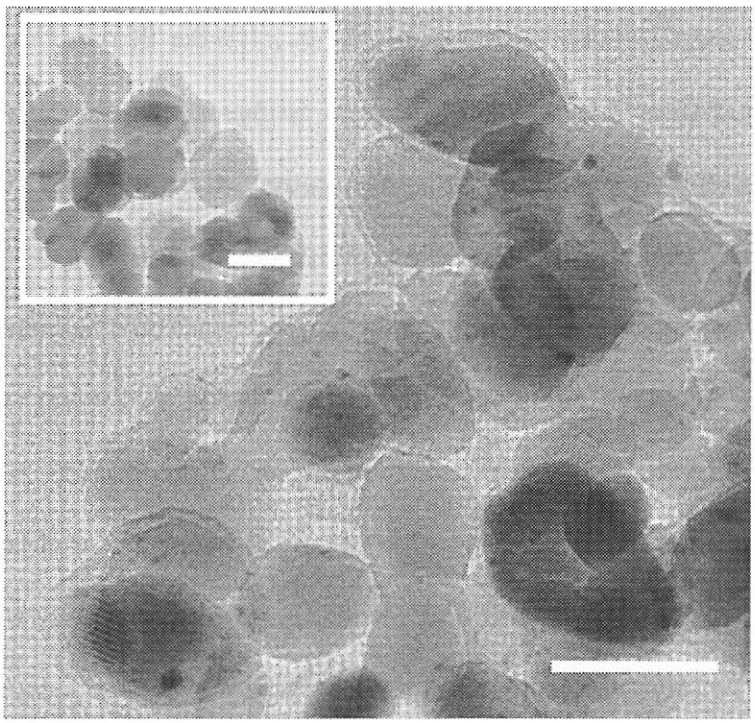

Figure 1. TEM image of TiO_2 particles after UV-light irradiation in an aqueous solution containing H_2PtCl_6 and phenol. The inset shows the TEM image of original TiO_2. Scale bars in TEM image correspond to 10 nm.

Figure 2 shows a TEM of the typical *n*Pt@*h*C sample obtained from above photoirradiated TiO_2 particles. Corresponding size distributions of Pt nanoparticles on the sample are shown in this figure. The *n*Pt@*h*C sample was comprised of a thin carbon shell of *ca.* 3-5 nm in thickness with a hollow structure including dispersed Pt nanoparticles with a narrow size distribution centered at 2.8 nm. The content of Pt in *n*Pt@*h*C measured by ICP analysis indicated the presence of 1.5 wt% of Pt in the present preparation condition. In addition, diameters of void spaces of *n*Pt@*h*C (*ca.* 20 nm) shown in this figure seem to correspond to those of original TiO_2 particles as shown in the inset of Figure 1a, indicating that TiO_2 particles acted as molds to form the hollow structure. It is noted that the carbon shell of *n*Pt@*h*C was found to have two types of micropore systems, *i.e.*, those with pore size larger and smaller than 1 nm, as determined by N_2 sorption measurements.[13]

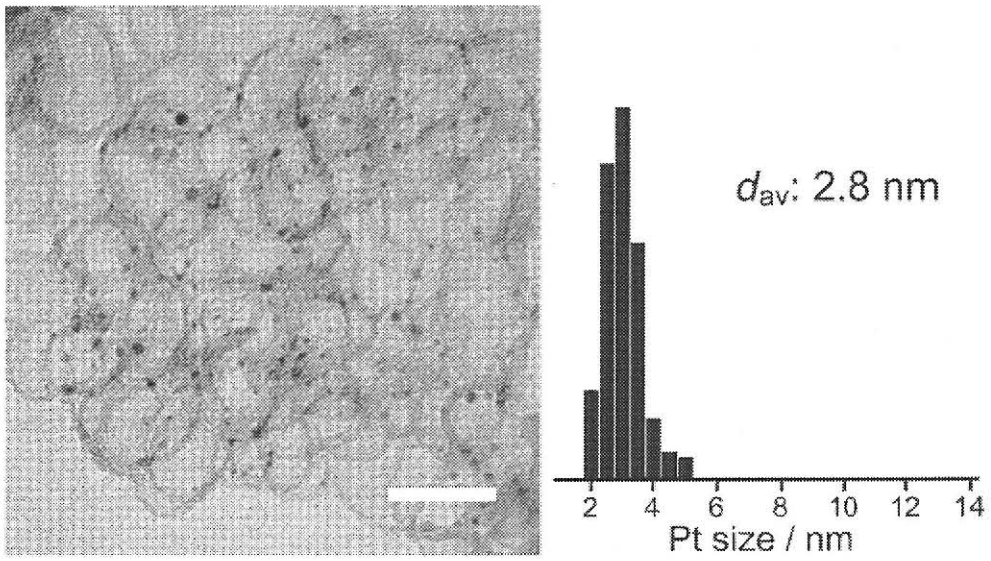

Figure 2. TEM image and Pt particle size distributions of *n*Pt@*h*C. Scale bar corresponds to 15 nm. d_{av} denotes average diameter of Pt particles.

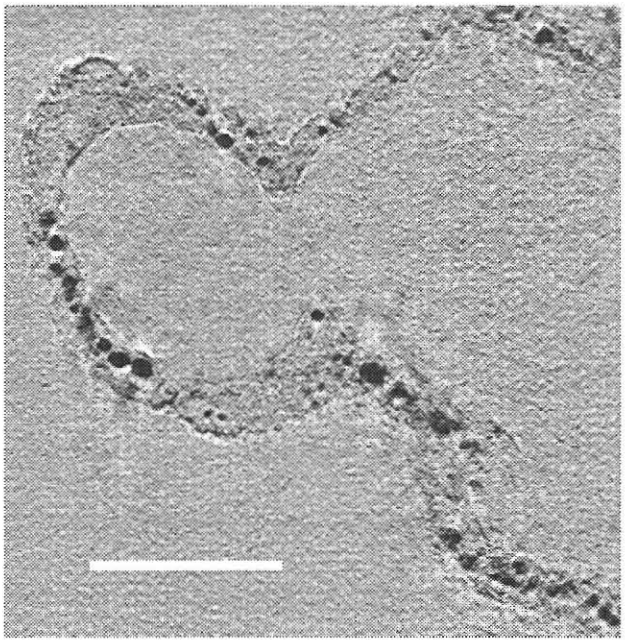

Figure 3. Typical tomogram of *n*Pt@*h*C. Scale bar corresponds to 15 nm.

Figure 3 shows a tomogram (*i.e.*, a cross-sectional image) of the *n*Pt@*h*C sample, obtained by taking tilted TEM images of the sample from –60° to +60° using a 3D-TEM system followed by reconstruction of these images using a software program (see Experimental).[14] The tomogram clearly indicates that most of the Pt nanoparticles are embedded in the thin carbon shell and a small portion of Pt nanoparticles is seen encapsulated in the hollow space of *n*Pt@*h*C.

When an aqueous suspension containing TiO_2, H_2PtCl_6, and phenol is irradiated by UV light with energy greater than the band-gap of TiO_2, photogenerated e^- and h^+ in TiO_2 reduce Pt(IV) ions ($PtCl_6^{2-}$ ions) and oxidize phenol, respectively. The former reaction immediately produces Pt nanoparticles on the surface of TiO_2 (see Figure 1) and the latter induces polymerization following a reaction pathway analogous to the electrochemical oxidative

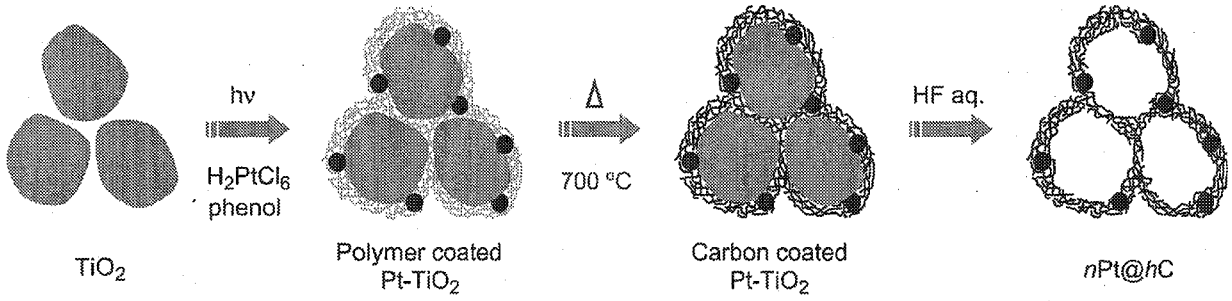

Scheme 1. An illustration scheme of the preparation procedure of *n*Pt@*h*C

phenol polymerization reported by Grattrell and Kirk,[15] resulting in successive surface coverage of a thin layer of the phenolic polymer on the platinized TiO_2. Due to the oval/spherical shape of Pt nanoparticles, it is likely that only a small part of the surfaces of these nanoparticles adheres to the surface of TiO_2, leaving most of surfaces of Pt nanoparticles available for possible further modification. Hence, during the progress of surface coverage of the phenolic polymer, the polymer encloses the majority part of all Pt nanoparticles resulting in embedment of the Pt nanoparticles inside the polymer matrix as shown in Scheme 1. As a result, the *n*Pt@*h*C possesses a structure as shown in Figure 2, *i.e.*, subsequent carbonization of the phenolic polymer followed by removal of TiO_2 core particles results in well-developed microporosity of the hollow carbon shell with Pt nanoparticles being entirely incorporated in the porous carbon shell.

Improved Sintering Resistance of Platinum Nanoparticles

Because the entrapment of Pt nanoparticles inside a porous carbon shell physically separates the particles and kinetically locks their motion, we can expect suppression of their sintering induced by thermal treatment at elevated temperatures. Thus, the *n*Pt@*h*C samples were subjected to thermal treatments in N_2 at various temperatures for 2 h. Figure 4 shows TEM images and Pt-size distributions of resulting samples. In comparison with the

as-synthesized *n*Pt@*h*C shown in Figure 2, the thermal treatment at temperatures below 700 °C had negligible effects on the morphology of *n*Pt@*h*C, *i.e.*, Pt nanoparticles on these samples remained highly dispersed in hollow porous carbons with narrow size distributions (Figures 4a and 4b). When thermal treatment at 800 °C was performed, however, Pt nanoparticles obviously started to sinter, resulting in a broader particle size distribution to give an average particle size of 4.9 nm in diameter (Figure 4c). Sintering became significant on the sample treated at 900 °C: Pt nanoparticles on the sample exhibited an average particle size of 5.1 nm in diameter, as shown in Figure 4d.

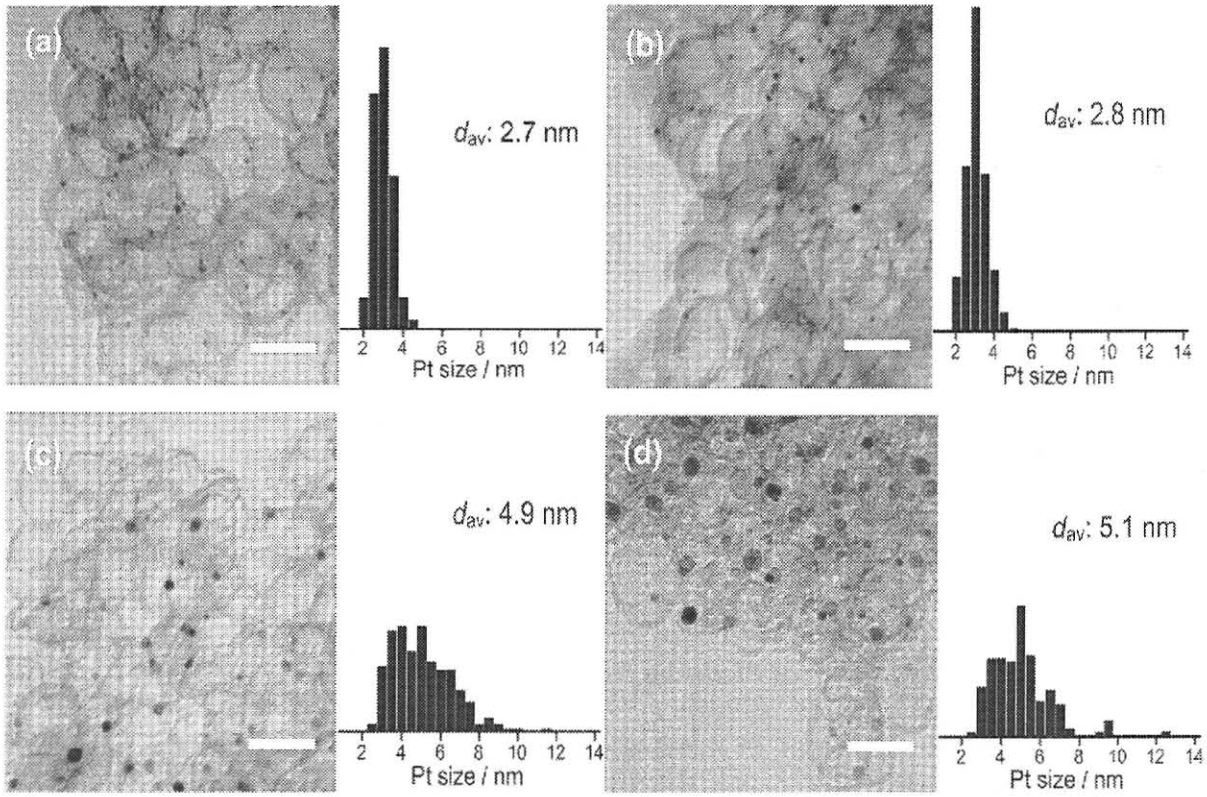

Figure 4. TEM images and Pt particle size distributions of *n*Pt@*h*C samples treated at (a) 500 °C, (b) 700 °C, (c) 800 °C and (d) 900 °C. Scale bars in TEM images correspond to 20 nm. d_{av} denotes average diameter of Pt particles.

For comparison, an activated carbon (AC) loaded with Pt nanoparticles (Pt/AC, 1.5wt% loading of Pt to AC) was prepared by a conventional impregnation method and the samples were subjected to similar heat treatments. Figure 5 shows TEM images and Pt size distributions of resulting samples. While the use of the conventional impregnation/H_2-reduction method results in production of highly dispersed Pt nanoparticles with almost the same average particle size as that of *n*Pt@*h*C (3.2 nm), the size distribution of Pt nanoparticles on Pt/AC is broad in comparison with that on *n*Pt@*h*C (Figure 2). As mentioned above, this inhomogeneity of loaded Pt nanoparticles often occur when such a conventional technique is used, indicating that there is a potential advantage of the present photocatalytic methodology for production of Pt nanoparticles with a narrow size distribution.

Another different feature of the present *n*Pt@*h*C sample from that of Pt/AC is relatively high resistance to sintering at an elevated temperature: Pt nanoparticles in Pt/AC started to sinter even at 500 °C of thermal treatment and continually growing in accordance with the heating temperature much appreciable than that observed on *n*Pt@*h*C as shown in Figures 5b-e. Since Pt nanoparticles in Pt/AC are only attached to the carbon by metal-support interactions, each particle is likely to migrate to neighboring Pt nanoparticles even at a moderate temperature, leading to coalescence or agglomeration. On the other hand, the unique structure of *n*Pt@*h*C, *i.e.*, Pt nanoparticles isolated from each other by a carbon matrix that acts as a physical barrier to minimize their possible migration, effectively inhibits sintering of Pt nanoparticles at relatively high temperatures.

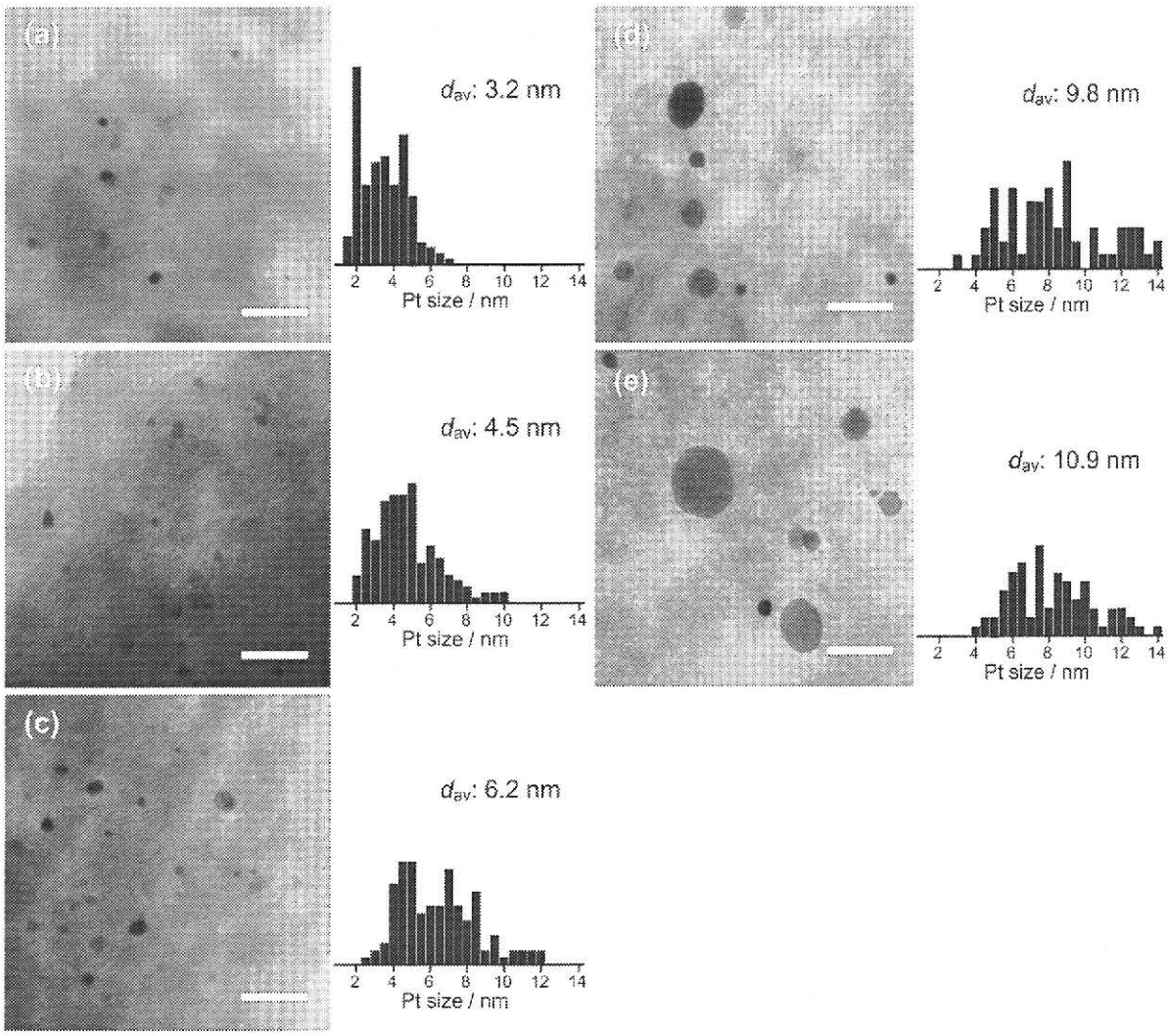

Figure 5. TEM images and Pt particle size distributions of (a) an as-synthesized Pt/AC sample and samples treated at (b) 500 °C, (c) 700 °C, (d) 800 °C and (e) 900 °C. Scale bars in TEM images correspond to 20 nm. d_{av} denotes average diameter of Pt particles.

Figure 6 shows Raman spectra of an as-synthesized *n*Pt@*h*C sample and a sample after heat treatment at 900 °C. Both samples exhibit two broad bands at 1350 cm^{-1} and 1580 cm^{-1}, the former of which is assigned to disordered amorphous carbon (D-band) and the latter of which is ascribed to graphitic sp^2 carbon structures (G-band)[16] as typically observed on less-crystalline carbon materials such as AC. It is clear from this figure that thermal treatment at 900 °C in N_2 changed neither the wavenumber nor intensity ratio of these two peaks from those of the as-synthesized *n*Pt@*h*C. Furthermore, specific surface area of both samples obtained from the N_2 absorption-desorption isotherm showed almost comparable values (1740 $m^2\ g^{-1}$ for the as-synthesized *n*Pt@*h*C and 1670 $m^2\ g^{-1}$ for the *n*Pt@*h*C sample treated at 900 °C). Due to the long carbonization time at 700 °C under evacuation during the fabrication of *n*Pt@*h*C allowing complete transformation of the phenolic polymer into respective stable phases of amorphous carbon and graphite,[17] the nature of carbon remained unaltered during the heat treatment. Hence, an effect of structural alteration of the carbon framework of *n*Pt@*h*C on the stability of Pt nanoparticles against sintering can be excluded in the present work.

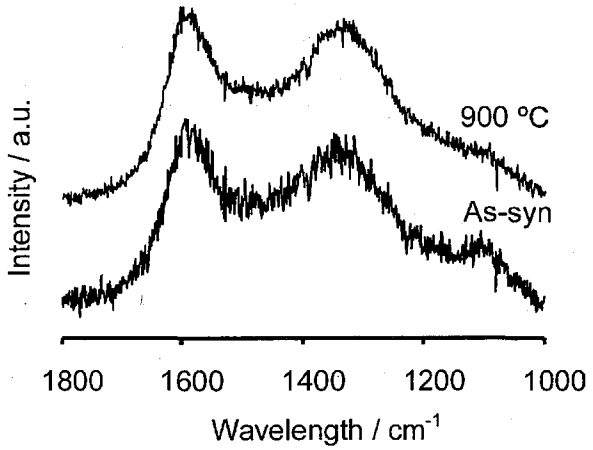

Figure 6. Raman spectra of (a) an as-synthesized *n*Pt@*h*C sample and (b) a sample treated at 900 °C under N_2.

Table 1. Catalytic activities of various Pt catalysts for 1-hexene hydrogenation[a]

Entry	Catalyst	T / °C[b]	Pt size / nm	Conv. / %[c]	TOF / h^{-1}	$Act._R$[d]
1	*n*Pt@*h*C	–[e]	2.8	92	91000	1.00
2	*n*Pt@*h*C	500	2.7	88	86000	0.95
3	*n*Pt@*h*C	700	2.8	93	92000	1.01
4	*n*Pt@*h*C	900	5.1	51	57000	0.63
5	Pt/AC	–[e]	3.2	30	32000	1.00
6	Pt/AC	500	4.5	22	28000	0.88
7	Pt/AC	700	6.2	20	25000	0.78
8	Pt/AC	900	10.9	11	12000	0.38

[a]All reactions were carried out with 1.3 mg of samples (Pt: 0.1 μmol) and 5 mmol of substrates under H_2 (210 kPa in absolute pressure) at 348 K for 30 min. [b]Temperature of thermal treatment under N_2. [c]Conversion of 1-hexene. [d]Relative catalytic activity defined as ratio of TOF of corresponding sample to that of as-synthesized. [e]As-synthesized sample without heat treatment.

In order to evaluate the effectiveness of *n*Pt@*h*C as a catalyst, hydrogenation of 1-hexene using gaseous H_2 was performed on *n*Pt@*h*C samples before and after various thermal treatments, and results are summarized in Table 1. For comparison, catalytic activities of several Pt/AC samples in the same reaction are also shown in this table. The as-synthesized *n*Pt@*h*C showed a remarkably higher turnover frequency (TOF) (entry 1) compared to that of Pt/AC (entry 5). As discussed in previous chapters,[10] the well-developed microporosity inside the carbon shell of *n*Pt@*h*C allows sufficient three-dimensional spaces for feasible mass transfer of substrates, directing them to reach the Pt active sites embedded within the

carbon. Although Pt/AC possesses microporosity as well, the advantages of being microporous is not fully utilized since the Pt nanoparticles are only impregnated, therefore attached to the surface of carbon, not within the carbon. Moreover, the hydrophobic nature of the carbon shell would adsorb the hydrophobic substrate of 1-hexene efficiently in the relatively polar solvent (acetone). These two effects result in the excellent contact rate between substrates and reaction sites on Pt nanoparticles embedded in the carbon shell, leading to the high catalytic activity. Besides, homogeneity of Pt particle size in *n*Pt@*h*C allowing efficient utilization of all of the loaded Pt particles might also contribute to its excellent activity compare to that of Pt/AC.

One of the most attractive features shown in Table 1 is that the *n*Pt@*h*C samples after heat treatment at 500 °C and 700 °C maintained the high activity level of the original sample (entries 2 and 3), while a marked decrease in activity level was observed on Pt/AC samples after the same heat treatments (entries 6 and 7). Based on results of TEM observations as discussed above, the maintenance of catalytic activities observed in heated *n*Pt@*h*C samples is attributed to retention of high dispersion of Pt nanoparticles in the *n*Pt@*h*C sample without agglomeration after heat treatment at temperatures up to 800 °C. Due to the induction of sintering of Pt nanoparticles in *n*Pt@*h*C samples by heat treatments at higher temperature, an appreciable drop in catalytic activities was observed (entry 4). However, when compared to the Pt/AC sample, rate of activity loss of *n*Pt@*h*C samples was rather low: *n*Pt@*h*C treated at 900 °C exhibited about more than 60% of its original activity, while Pt/AC treated at the same temperature retained below 40% of its original activity (entry 8). This large decrease in activity observed on Pt/AC is attributable to the occurrence of significant Pt agglomeration on Pt/AC as mentioned above. When Pt nanoparticles sintered to a larger cluster in high temperature, active surface area of Pt is greatly reduce resulting in activity drop. These results,

therefore, indicate the superiority of the present structure, *i.e.*, entrapment of Pt nanoparticles in the carbon matrix with well-developed porous structure, for effective prevention of loss of catalytic activity against high temperature processing.

4.4 Conclusions

We have demonstrated a photocatalytic method for synthesizing a Pt-carbon nanocomposite in which the Pt nanoparticles are embedded in microporous carbon with a hollow structure. We showed that sintering behavior of Pt nanoparticles at high temperature, which is commonly observed in a carbon supported metal composite, was effectively suppressed due to the unique structure of the present *n*Pt@*h*C sample. Since the high resistibility led to the minimization of loss of catalytic activity, the present nanostructure is a promising candidate for applying in processes requiring more rigorous conditions. Hence, we believe that the basic concept shown in this study will open up a wider usage of MNPs-carbon nanocomposites for various chemical reactions when appropriate MNPs other than Pt are employed.

4.5 References

[1] Alivisatos, A. P. *Science* **1996**, *271*, 933.

[2] (a) Yang, C. M.; Sheu, H. S.; Chao, K. J. *Adv. Funct. Mater.* **2002**, *12*, 143. (b) Zhang, L. X.; Shi, J. L.; Yu, J.; Hua, Z. L.; Zhao X. G.; Ruan, M. L. *Adv. Mater.* **2002**, *14*, 1510. (c) Konya, Z.: Puntes, V. F.; Kiricsi, I.; Zhu, J.; Ager, J. W.; Ko, M. K.; Frei, H.;

Alivisatos, P.; Somorjai, G. A. *Chem. Mater.* **2003**, *15*, 1242. (d) Tsung, C. K.; Hong, W. B.; Shi, Q. H.; Kou, X. S.; Yeung, M. H.; Wang, J. F.; Stucky, G. D. *Adv. Funct. Mater.* **2006**, *16*, 2225.

[3] (a) Justus, B. L.; Tonucci, R. J.; Berry, A. D. *Appl. Phys. Lett.* **1992**, *61*, 3151. (b) Takahashi, T.; Yanagimoto, Y.; Matsuoka, T.; Kai, T. *Microporous Mater.* **1996**, *6*, 189. (c) Enke, D.; Janowski, F.; Schwieger, W. *Microporous Mesoporous Mater.* **2003**, *60*, 19.

[4] (a) Selvan, S. T.; Spatz, J. P.; Klok, H. A.; Moller, M. *Adv. Mater.* **1998**, *10*, 132. (b) Koenig, S.; Chechik, V. *Chem. Commun.* **2005**, 4110. (c) Cen, L.; Neoh, K. G.; Kang, E. T. *Adv. Mater.* **2005**, *17*, 1656. (d) Feng, X. M.; Huang, H. P.; Ye, Q. Q.; Zhu, J. J.; Hou, W. H. *J. Phys. Chem. C* **2007**, *111*, 8463.

[5) (a) Joo, S. H.; Choi, S. J.; Oh, I.; Kwak, J.; Liu, Z.; Terasaki, O.; Ryoo, R. *Nature* **2001**, *412*, 169. (b) Kim, M.; Sohn, K.; Na, H. B.; Hyeon, T. *Nano Lett.* **2002**, *2*, 1383. (c) Choi, W. C.; Woo, S. I.; Jeon, M. K.; Sohn, J. M.; Kim, M. R.; Jeon, H. J. *Adv. Mater.* **2005**, *17*, 446. (d) Kim, Y. T.; Ohshima, K.; Higashimine, K.; Uruga, T.; Takata, M.; Suematsu, H.; Mitani, T. *Angew. Chem. Int. Ed.* **2006**, *45*, 407. (e) Sakai, G.; Yoshimura, T.; Isohata, S.; Uota, M.; Kawasaki, H.; Kuwahara, T.; Fujikawa, D.; Kijima, T. *Adv. Mater.* **2007**, *19*, 237.

[6] (a) Li, W.; Liang, C.; Zhou, W.; Qiu, J.; Zhou, Z.; Sun, G.; Xin, Q. *J. Phys. Chem. B* **2003**, *107*, 6292. (b) Wang, C.; Waje, M.; Wang, X.; Tang, J. M.; Haddon, R. C.; Yan, Y. *Nano Lett.* **2004**, *4*, 345. (c) Chai, G. S.; Shin, I. S.; Yu, J. S. *Adv. Mater.* **2004**, *16*, 2057.

(d) Su, F.; Zeng, J.; Bao, X.; Yu, Y.; Lee, J. Y.; Zhao, X. S. *Chem. Mater.* **2005**, *17*, 3960.

[7] (a) Kim, Y. T.; Mitani, T. *J. Catal.* **2006**, *238*, 394. (b) Cui, G.; Zhi, L.; Thomas, A.; Kolb, U.; Lieberwirth, I.; Mullen, K. *Angew. Chem. Int. Ed.* **2007**, *46*, 3463.

[8] (a) Narayanan, R.; El-Sayed, M. A. *J. Catal.* **2005**, *234*, 348. (b) Ikeda, S.; Ishino, S.; Harada, T.; Okamoto, N.; Sakata, T.; Mori, H.; Kuwabata, S.; Torimoto, T.; Matsumura, M. *Angew. Chem. Int. Ed.* **2006**, *45*, 7063. (c) Hermans, S.; Diverchy, C.; Demoulin, O.; Dubois, V.; Gaigneaux, E. M.; Devillers, M. *J. Catal.* **2006**, *243*, 239. (d) Harada, T.; Ikeda, S.; Miyazaki, M.; Sakata, T.; Mori, H.; Matsumura, M. *J. Mol. Catal. A: Chem.* **2007**, *268*, 59. (e) Su, F.; Lee, F. Y.; Lv, L.; Liu, J.; Tian, X. N.; Zhao, X. S. *Adv. Funct. Mater.* **2007**, *17*, 1926.

[9] (a) Harris, P. J. F. *J. Catal.* **1986**, *97*, 527. (b) Antolini, E.; Cardellini, F.; Giacometti, E.; Squadrito, G. *J. Mater. Sci.* **2002**, *37*, 133. (c) Narayanan, R.; El-Sayed, M.A. *J. Am. Chem. Soc.*, **2003**, *125*, 8340. (d) Miao, S.; Liu, Z.; Han, B.; Huang, J.; Sun, Z.; Zhang, J.; Jiang, T. *Angew. Chem. Int. Ed.* **2006**, *45*, 266.

[10] (a) Ng, Y. H.; Ikeda, S.; Harada, T.; Higashida, S. Sakata, T.; Mori, H.; Matsumura, M. *Adv. Mater.* **2007**, *19*, 597. (b) Ng, Y. H.; Ikeda, S.; Harada, T.; Park, S.; Sakata, T.; Mori, H.; Matsumura, M. *Chem. Mater.* **2008**, *20*, 1154.

[11] Kremer, J. R.; Mastronarde, D. N.; Mcintosh, J. R. *J. Struct. Biol.* **1996**, *116*, 71.

[12] Concentration of the Pt species prepared by the current procedure was too low to obtain the detailed information about their valence state by XPS or XRD. However, a

polymer-coated Pt-TiO_2 prepared with a higher Pt concentration (10 wt% of TiO_2) indicates the existence of Pt metal and a small amount of Pt^{2+} compound which might be attributed to the oxidation in atmosphere, as obtained from the XPS analysis.

[13] Pore analyses of the carbon shell are discussed in detail in our previous report (see reference 10).

[14] For the construction of this tomogram image, the *n*Pt@*h*C sample containing 6.0 wt% Pt, which was obtained by adding 25.7 μmol of H_2PtCl_6 during photoirradiation, was employed.

[15] (a) Gattrell, M.; Kirk, D. W. *J. Electrochem. Soc.* **1992**, *139*, 2736. (b) Gattrell, M.; Kirk, D. W. *J. Electrochem. Soc.* **1993**, *140*, 903.

[16] (a) Eklund, P. C.; Holden, J. M.; Jishi, R. A. *Carbon* **1995**, *33*, 959. (b) Shimodaira, N.; Masui, A. *J. Appl. Phys.* **2002**, *92*, 902. (c) Osswald, S.; Flahaut, E.; Gogotsi, Y. *Chem. Mater.* **2006**, *18*, 1525.

[17] (a) Li, Z.; Jaroniec, M.; Lee, Y. J.; Radovic, L. R. *Chem. Commun.* **2002**, 1346. (b) Fuertes, A. B.; Alvarez, S. *Carbon*, **2004**, *42*, 3049. (c) Yoon, S. B.; Chai, G. S.; Kang, S. K.; Yu, J. S.; Gierszal, K. P.; Jaroniec, M. *J. Am. Chem. Soc.* **2005**, *127*, 4188. (d) Mattia, D.; Rossi, M. P.; Kim, B. M.; Korneva, G.; Bau, H. H.; Gogotsi, Y. *J. Phys. Chem. B* **2006**, *110*, 9850.

CHAPTER 5

Catalytic Activity of *n*Pt@*h*C in Oxidation of Alcohols: Mechanistic Study and Suppression of Pt Deactivation

5.1 Catalytic Activity of *n*Pt@*h*C for Oxidation of Alcohols

5.1.1 Introduction

Oxidation of alcohols into aldehydes, ketones and carboxylic acids is one of the most crucial reactions in fine chemical and pharmaceutical industries.[1] Stoichiometric quantities of oxidants such as chromates and mineral acids are traditionally employed for these reactions. However, the stoichiometric oxidation process suffers from low atom efficiency and a large amount of waste production, leading to a severe environmental impact.[2] Heterogeneously catalyzed liquid-phase oxidations using molecular oxygen (O_2) as the sole oxidant are an attractive alternative. Among the various catalysts exploited so far,[3] platinum (Pt) supported on activated carbon (Pt/AC) has been studied extensively as a suitable candidate for alcohol oxidation because it works in water under atmospheric pressure of O_2,[4] However, the major drawback of the use of Pt/AC is rapid deactivation due to by-product poisoning and over-oxidation of the Pt catalyst. A common method to minimize these deactivation processes is the introduction of a second metal component such as gold (Au), bismuth (Bi) and lead (Pb).[5] Except for the case of Au addition, however, leaching of these heavy metals is a serious ecological problem for its operation.[6]

In previous chapters, we have fabricated Pt nanoparticles embedded in the porous wall of a hollow carbon shell (*n*Pt@*h*C) by using a titanium(IV) oxide (TiO_2) photocatalytic reaction.[7] The immobilization of Pt nanoparticles inside the framework of porous carbon could prevent particle aggregation, movement and leaching. Due to the specific properties of the *n*Pt@*h*C nanostructure, this material was found to work as an active and reusable catalyst for hydrogenation of various olefins. We therefore decided to investigate the catalytic activity of *n*Pt@*h*C for alcohol oxidation. Herein we report the application of *n*Pt@*h*C to aerobic

oxidation of various alcohols in water to prove its efficient promotion of the reaction with high recyclability.

5.1.2 Experimental

Preparation Procedures: The *n*Pt@*h*C sample was synthesized using the procedures described in previous chapters.[10] To 400 cm^3 of aqueous solution containing 200 mg of phenol and 7.7 μmol of hexachloroplatinic acid (H_2PtCl_6) was added 500 mg anatase TiO_2 powder supplied by Ishihara Sangyo (ST-21, average particle size: 20 nm, BET surface area: 50 $m^2 g^{-1}$). The suspension was then evacuated several times in a quartz inner-irradiation-type vessel connected to a closed gas circulation and evacuation system to ensure complete air removal. Photoirradiation of the suspension was performed under reduced-pressure Ar atmosphere (30 kPa) with a high-pressure Hg lamp through a water jacket to keep the reactor temperature constant at 293 K. After photoirradiation for 2.5 h, the brownish phenolic polymer-coated powder were retrieved by filtration, washed with 2 dm^3 distilled water to remove excessive unreacted phenol, dried at 353 K in air, and finally subjected to carbonization at 973 K for 6 h in vacuum. The resulting black powder was subsequently immersed in 10 ml 50% hydrofluoric acid for 24 h at room temperature to dissolve TiO_2 core particles to give *n*Pt@*h*C (*HF solution is very hazardous and corrosive and should be handled according to the MSDS guidelines.*).

Characterization: Microscopic features of the samples were observed using a Hitachi H-800 transmission electron microscope (TEM). The content of Pt in *n*Pt@*h*C was determined by inductively coupled plasma (ICP) analysis on a Perkin-Elmer OPTIMA 3000-XL ICP emission spectrometer. Typically, *n*Pt@*h*C samples were immersed in aqua regia for 2 h to dissolve the Pt particles. The undissolved carbon particles were filtered by

using a Millipore syringe-driven membrane filter. The clear solution was then diluted to an appropriate concentration before analysis. Raman spectra were obtained using a JASCO NRS-3100 Laser Raman Spectrophotometer.

Catalytic Oxidation of Alcohols: A general procedure for oxidation of 1-phenylethanol is as follows: Into a reaction vessel equipped with a reflux condenser and balloon were placed the nPt@hC (4.7 mg, Pt: 0.5 μmol), 1-phenylethanol (025 mmol), and water (2.5 cm^3). Then the mixture was heated at 333 K for 24 h under an atmospheric pressure of O_2 with stirring. After the reaction, the solution was transferred into a sample tube and extracted with diethyl ether. A portion of the diethyl ether solution was withdrawn and subjected to GC analysis.

5.1.3 Results and Discussion

Efficient and Reusable nPt@hC in Oxidation of Alcohols in Aqueous Solution

High-resolution transmission electron microscopy (HRTEM) analysis of *n*Pt@*h*C revealed that the Pt nanoparticles were embedded in the carbon shell and were physically separated from each other by the carbon matrix, and the Pt nanoparticles had a mean diameter of 3.0 nm with a very narrow size distribution (Figure 1).

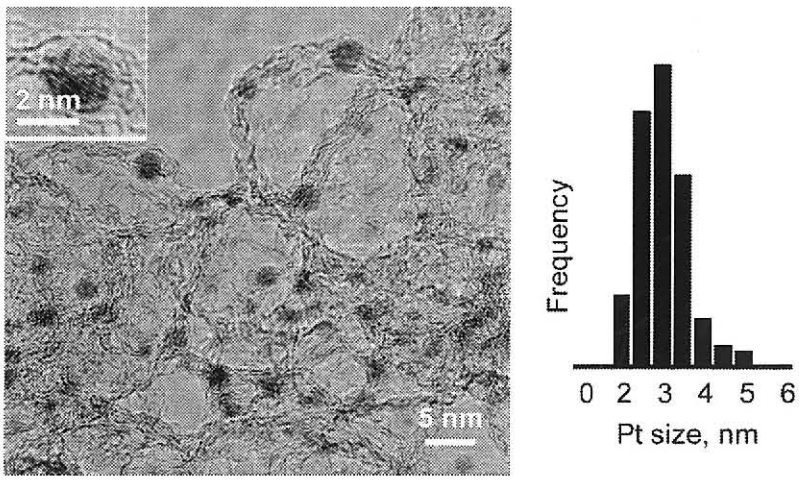

Figure 1. HRTEM and Pt size distribution of *n*Pt@*h*C.

Table 1. Oxidation of benzyl alcohol using various Pt metal catalysts[a].

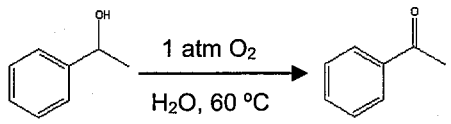

Entry	Catalyst	M/S[b], %	Conv.[c], %	TON[d]
1	*n*Pt@*h*C	0.2	81	446
2	Pt/AC (Wako)	0.2	36	185
3	Pt/AC (N. E.)	0.2	30	158
4	Pt/AC (impreg.)	0.2	20	107
5	Pt-black	1.0	88	91
6	Pt/Al_2O_3	0.2	5	30
7	Pt-PVP	0.2	2	11
8	Pt/AC (Wako)[e]	0.2	10	49
9	Pt/AC (N. E.)[e]	0.2	8	40
10	*n*Pt@*h*C[f]	0.2	76	426

[a] All the reactions were carried out in water under atmospheric oxygen at 60 °C for 24 h. [b] Metal/Substrate molar ratio [c] Conversion [d] Turnover number [e] After 1 successive run [f] After 2 successive runs

Oxidations of 1-phenylethanol were initially carried out using various Pt catalysts under 1 atm of O_2 in water, as shown in Table 1. Among the catalysts examined, the *n*Pt@*h*C catalyst proved to be the most efficient for oxidation of 1-phenylethanol to give the corresponding ketone (entry 1). Commercial Pt/AC samples and a Pt/AC sample prepared by the conventional impregnation-reduction method were found to be less effective, while their

activities varied depending on the method for sample preparation or the supplier (entries 2-4). Other Pt catalysts such as Pt supported on alumina (Pt/Al_2O_3), Pt-black, and Pt nanoparticles stabilized with polyvinylpyrrolidone (Pt-PVP)[8] gave poor results (entries 5-7). In general, the catalytic activity of Pt/AC catalysts greatly declines after successive catalytic runs (entries 8-9). On the other hand, after simple extraction by diethyl ether followed by drying at 353 K overnight, the *n*Pt@*h*C catalyst could be readily reused without significant loss of its high level of catalytic activity for at least 2 successive runs (entries 10-11). Moreover, TEM observation of *n*Pt@*h*C after these reactions revealed that there is no appreciable change in structure of the catalyst. In addition, because the present system can be operated at a relatively low metal/substrate molar ratio (ca. 0.001), TON for Pt of *n*Pt@*h*C is also much larger than that obtained on recently developed resin-supported Pt catalysts.[9] These results indicate the potential ability of *n*Pt@*h*C as a heterogeneous oxidation catalyst.

The scope for oxidation using *n*Pt@*h*C is summarized in Table 2. Results obtained for a typical Pt/AC catalyst supplied by Wako are also shown for comparison. The *n*Pt@*h*C catalyst showed high levels of catalytic activity for oxidation of primary alcohols, i.e., benzyl alcohol and cinnamyl alcohol, to yield corresponding carbonyl compounds (entries 1-4). Although oxidation of a bulky secondary alcohol (benzhydrol) was less efficient compared to the other substrates, the activity level of *n*Pt@*h*C was still higher than that of Pt/AC (entries 5 and 6). Interestingly, aerobic oxidation of 2-adamantanol, a sterically hindered nonactivated alicyclic alcohol, also proceeded smoothly on the *n*Pt@*h*C catalyst (entries 7 and 8). To the best of our knowledge, oxidation of 2-adamantanol has only been performed using supported Ru and homogeneous complexes of Pd and Fe in organic solvents,[10] and oxidation using *n*Pt@*h*C is therefore the first example of Pt-catalyzed efficient oxidation of 2-adamantanol in water.

Table 2. Oxidation of various aromatic alcohols using *n*Pt@*h*C and Pt/C from wako[a].

Entry	Catalyst	Substrate	Product	M/S[b], %	Conversion, %	Selectivity[c], %	TON[d]
1	*n*Pt@*h*C	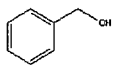	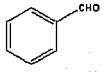	0.1	90	51	895
2	Pt/AC			0.1	89	49	887
3	*n*Pt@*h*C	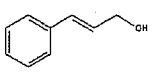	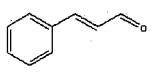	0.1	99	75	989
4	Pt/AC			0.1	69	95	695
5	*n*Pt@*h*C	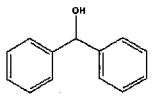	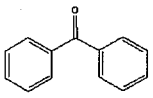	0.2	42	[e]	208
6	Pt/AC			0.2	16		79
7	*n*Pt@*h*C	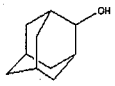	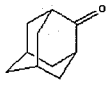	0.2	72	[e]	362
8	Pt/AC			0.2	21		104

[a] All the reactions were carried out in water under atmospheric oxygen at 60 °C for 24 hours. [b] Metal/Substrate molar ratio [c] The remain is carboxylic acid of the corresponding alcohols [d] Turnover number [e] Ketone is the sole product

As discussed in Chapter 4,[7] the Pt nanoparticles are embedded in the carbon matrix of *n*Pt@*h*C which contains well-developed micropore and mesopore systems. These pores provide three-dimensional channels and spaces for efficient mass transfer. Furthermore, the hydrophobic carbon covering the Pt induces preferential adsorption of the substrate results in a higher concentration of substrate in the Pt surrounding microenvironment compared to that of Pt/AC. Besides allowing the efficient contact between Pt and substrates, this special location of Pt also effectively prevents its agglomeration during reactions. Hence, the efficient and reusable catalytic function of nPt@hC is observed. Further studies on mechanistic details and possible extension to other organic syntheses are currently underway.

5.1.4 Conclusions

In conclusion, we have proved that *n*Pt@*h*C has high potential as a heterogeneous oxidation catalyst. Owing to the requirement of only a small amount of Pt to induce reactions in water under 1 atm of O_2, it is expected that this composite can be used for synthesis of a wide range of useful chemicals from alcohols.

5.1.5 References

[1] (a) T. Mallat and A. Baiker, *Chem. Rev.*, **2004**, *104*, 3037. (b) T. Mallat and A. Baiker, *Catal. Today*, **1994**, *19*, 247. (c) N. Kakiuchi, Y. Maeda, T. Nishimura and S. Uemura, *J. Org. Chem.*, **2001**, *66*, 6620. (d) T. Nishimura, N. Kakiuchi, M. Inoue and S. Uemura, *Chem. Commun.*, **2000**, 1245. (e) G. T. Brink, I. W. C. E. Arends and R. A. Sheldon, *Science*, **2000**, *287*, 1636. (f) A. Abad, C. Almela, A. Corma and H. Garcia, *Chem. Commun.*, **2006**, 3178. (g) H. Tsunoyama, H. Sakurai, Y. Negishi and T. Tsukuda, *J. Am. Chem. Soc.*, **2005**, *127*, 9374. (h) M. Nechab, C. Einhorn and J. Einhorn, *Chem. Commun.*, **2004**, 1500. (i) T. Matsushita, K. Ebitani and K. Kaneda, *Chem. Commun.*, **1999**, 265. (j) K. Yamaguchi and N. Mizuno, *Angew. Chem. Int. Ed.*, **2002**, *41*, 4538.

[2] (a) W. J. Mijs and C. R. H. de Jonge, *Organic Synthesis by Oxidation with Metal Compounds*, Plenum Press, New York, **1986**. (b) B. M. Trost and I. Fleming, *Comprehensive Organic Synthesis*, Pergamon Press, Oxford, **1991**. (c) G. Cainelli and G. Cardillo, *Chromium Oxidations in Organic Chemistry*, Springer-Verlag, Berlin, **1984**.

[3] (a) Z. Opre, D. Ferri, F. Krumeich, T. Mallat and A. Baiker, *J. Catal.*, **2006**, *241*, 287. (b) N. Zheng and G. D. Stucky, *Chem. Commun.*, **2007**, 3862. (c) A. Abad, P. Concepcion, A. Corma and H. Garcia, *Angew. Chem. Int. Ed.*, **2005**, *44*, 4066. (d) A. Biffis, S. Cunial, P. Spontoni and L. Prati, *J. Catal.*, **2007**, *251*, 1. (e) Y. Uozumi and R. Nakao, *Angew. Chem.*

Int. Ed., **2003**, *42*, 194. (f) K. Yamaguchi and N. Mizuno, *Chem. Eur. J.*, **2003**, *9*, 4353. (g) K. Mori, K. Yamaguchi, T. Hara, T. Mizugaki, K. Ebitani and K. Kaneda, *J. Am. Chem. Soc.*, **2002**, *124*, 11572.

[4] (a) C. Donze, P. Korovchenko, P. Gallezot and M. Besson, *Appl. Catal. B*, **2007**, *70*, 621. (b) P. Korovchenko, C. Donze, P. Gallezot and M. Besson, *Catal. Today*, **2007**, *121*, 13. (c) C. Bronnimann, Z. Bodnar, R. Aeschimann, T. Mallat and A. Baiker, *J. Catal.*, **1996**, *161*, 720. (d) T. Mallat, C. Bronnimann and A. Baiker, *Appl. Catal. A-Gen.*, **1997**, *149*, 103.

[5] (a) H. H. C. M. Pinxt, B. F. M. Kuster and G. B. Marin, *Appl. Catal. A-Gen.*, **2000**, *191*, 45. (b) T. Mallat, Z. Bodnar, P. Hug and A. Baiker, *J. Catal.*, **1995**, *153*, 131. (c) P. Gallezot, *Catal. Today*, **1997**, *37*, 405. (d) N. Dimitratos, A. Villa, D. Wang, F. Porta, D. Su and L. Prati, *J. Catal.*, **2006**, *244*, 113. (e) R. Oi and S. Takenaka, *Chem. Lett.*, **1988**, 115. (f) A. Deffernez, S. Hermans and M. Devillers, *Appl. Catal. A-Gen.*, **2005**, *282*, 303. (g) C. Keresszegi, T. Mallat, J. Grunwaldt and A. Baiker, *J. Catal.*, **2004**, *225*, 138.

[6] (a) F. Alardin, B. Delmon, P. Ruiz and M. Devillers, *Catal. Today*, **2000**, *61*, 255. (b) S. Hermans and M. Devillers, *Catal. Lett.*, **2005**, *99*, 55. (c) M. Besson and P. Gallezot, *Catal. Today*, **2000**, *57*, 127.

[7] (a) Y. H. Ng, S. Ikeda, T. Harada, S. Higashida, T. Sakata, H. Mori and M. Matsumura, *Adv. Mater.*, **2007**, *19*, 597. (b) Y. H. Ng, S. Ikeda, T. Harada, S. Park, T. Sakata, H. Mori and M. Matsumura, *Chem. Mater.*, **2008**, *20*, 1154..

[8] Polyvinylpyrrolidone-stabilized Pt (Pt-PVP) was synthesized as follows: PVP (66 mg) was added to a solution of hexachloroplatinic acid ($H_2PtCl_6 \cdot 6H_2O$; 0.03 mmol, 15.5 mg) in water (5 ml) and ethanol (45 ml) and the mixture was heated under reflux for 3 h.

[9](a) Y. M. A. Yamada, T. Arakawa, H. Hocke and Y. Uozumi, *Angew. Chem. Int. Ed.*, **2007**, *46*, 704. (b) T. Wang, C. Xiao, L. Yan, L. Xu, J. Luo, H. Shou, Y. Kou and H. Liu, *Chem. Commun.*, **2007**, 4375. (c) A. Biffis and L. Minati, *J. Catal.*, **2005**, *236*, 405.

[10](a) S. E. Martin and D. F. Suarez, *Tetrahedron Lett.*, **2002**, *43*, 4475. (b) B. Zhan and A. Thompson, *Tetrahedron*, **2004**, *60*, 2817. (c) K. Yamaguchi and N. Mizuno, *New J. Chem.*, **2002**, *26*, 972. (d) M. J. Schultz, S. S. Hamilton, D. R. Jensen and M. S. Sigman, *J. Org. Chem.*, **2005**, *70*, 3343.

5.2 Mechanism of Oxidation of Benzyl Alcohol on *n*Pt@*h*C

5.2.1 Introduction

Liquid-phase oxidation of alcohols into carbonyl compounds (corresponding aldehydes and ketones) is a crucial transformation in the field of fine chemical and pharmaceutical industries. Traditional non-catalytic methods employ stoichiometric quantities of high-valent metal oxidants such as chromates, permanganate and mineral acids and are frequently used in halogenated organic solvents.[1] In addition to the low atom efficiency in these systems, disposal and isolation of enormous amounts of metal salts and harmful solvents are a serious drawback for the economical and environmental benefits. Owing to the increasing environmental concerns, the replacement of these toxic oxidants with clean and inexpensive molecular O_2 is of great importance. Homogeneously catalyzed oxidation by means of complexes of Pd, Cu, Ru, V and Co using molecular O_2 has been found active.[2] However, most of these systems require the presence of other additives such as bases and co-oxidant[3] and are difficult to recover after the usage, leading to hampering their further applications in green chemistry of catalysis.

Heterogeneous catalysts are readily serving the industrial interests in terms of easy handling, facile recovery and potential reusability. Hence, many methods for developing supported or immobilized metal catalysts active in alcohol oxidation have been reported. For example, Ru, Au, Pd, Pt and Mn supported on alumina, ceria, zeolite, polymer and carbon, respectively, have been extensively studied for this reaction.[4] Among these catalysts, Pt supported on activated carbon (Pt/C) receives the most attention because it performs excellently under mild conditions (20-90 °C, atmospheric pressure of O_2). Though there is no final agreement on the reaction mechanism, it has been generally accepted that the reaction

occurs through the oxidative dehydrogenation where the adsorbed alcohols dehydrogenate on the surface of Pt metal to yield the respective carbonyls whilst the abstracted hydrogen reacts with oxygen to produce water as the benign by-product.[5]

A major bottleneck for large scale application of Pt catalyzed alcohol oxidation is the rapid catalyst deactivation. Two major deactivation pathways have been proposed: Pt chemical poisoning by adsorption of intermediates or by-products, and Pt over-oxidation in the presence of excessive O_2 (formation of surface platinum oxide) during reaction.[4e, 5b and 5c] Besides, sintering and leaching of Pt from the supports are also contributing to the decline in activity.[6] Both pathways point to a decrease in the number of active catalytic sites. However, pathway of which dominates the deactivation still remains controversial. Mallat and Baiker have studied extensively the process of Pt chemical poisoning and have identified it as the primary cause of deactivation.[4e] In contrast, Vleeming *et al.* distinguished these two deactivation modes by investigating the response of the catalytic system to the change of O_2 supply. If deactivation could be eliminated by changing temporarily the O_2 flow to inert or reductive gas, deactivation by Pt chemical poisoning is unlikely. Therefore, their observation on the complete catalyst reactivation after *in situ* replacement of O_2 by nitrogen doubted the significant role of Pt chemical poisoning in the deactivation.[7] The nature and extent of Pt deactivation are supposed to be largely influenced by the reaction conditions, for instance, types of substrate, solvent and concentration of O_2.

We have previously reported the fabrication of carbon-encapsulated Pt nanoparticles (*n*Pt@*h*C) based on a titanium (IV) oxide (TiO_2) photocatalytic reaction.[8] The unique location of Pt nanoparticles being embedded inside the framework of porous carbon effectively inhibits the particle sintering and leaching.[8c] When compared to the commercial activated carbon-supported Pt catalyst (Pt/AC), *n*Pt@*h*C nanocomposites are found highly

active and reusable in aerobic oxidation of alcohols under atmospheric pressure of O_2 at 60 °C.[8d] Since the oxidation reaction was carried out in the O_2 atmosphere and Pt metal is normally very susceptible in O_2 rich condition, the durable activity of *n*Pt@*h*C in previous findings, hence, indirectly indicates the high resistance to deactivation of *n*Pt@*h*C. In this study, we expand the scope to provide the experimental proofs to alcohol oxidation mechanism on Pt metal surface and also present the insights of suppression of Pt deactivation using *n*Pt@*h*C.

5.2.2 Experimental

Catalyst Preparation. The *n*Pt@*h*C sample was synthesized using a previously reported procedure.[8] To 500 cm^3 of aqueous solution containing 200 mg of phenol and 7.7 μmol of hexachloroplatinic acid (H_2PtCl_6) was added 500 mg anatase TiO_2 powder (Ishihara ST-21, average particle size: 20 nm, BET surface area: 50 m^2g^{-1}). The suspension was then evacuated several times in a Pyrex inner-irradiation-type vessel connected to a closed gas circulation and evacuation system to ensure complete air removal. Photoirradiation was carried out for 5 h with a high-pressure Hg lamp (450 W) through a Pyrex water jacket (cutoff <320 nm) to keep the reactor temperature constant at 293 K under reduced-pressure argon (30 kPa). After irradiation, the thus-obtained brownish powder was retrieved by filtration, washed with distilled water (ca. 2000 cm^3) to remove excessive unreacted phenol and was subjected to carbonization at 973 K for 6 h in vacuum followed by immersion in a 50% hydrofluoric acid (HF) solution for 24 h at room temperature to dissolve the TiO_2 component (***CAUTION**: HF solution is hazardous and corrosive and should be handled with extreme care*). The black

powder sample obtained through centrifugation was washed with acetone and dried at 80 °C to give *n*Pt@*h*C. For comparison of activity, a commercially available Pt/AC supplied by Wako Chemical was used as purchased.

Characterizations of Materials. TEM images of *n*Pt@hC were obtained using a Hitachi H-9000 transmission electron microscope. Surface area of *n*Pt@*h*C was performed using a Quantachrome AUTOSORB-1 automated gas sorption system employing N_2 as an adsorbate after pretreatment of the sample at 473 K for 2 h. The content of Pt in *n*Pt@*h*C was determined by inductively coupled plasma (ICP) analysis on a Perkin-Elmer OPTIMA 3000-XL ICP emission spectrometer. For the ICP analysis, *n*Pt@*h*C samples were immersed in aqua regia for 2 h to dissolve the Pt particles. The undissolve carbon particles were filtered by using a Millipore syringe-driven membrane filter. The clear solution was then diluted to an appropriate concentration before the measurement. The amount of CO irreversibly held (CO_{chem}) on the surface of Pt nanoparticles in nPt@hC was measured by the pulse CO chemisorption experiment. Prior to the measurement, the sample was flushed with He flow (30 cm^3min^{-1}) at 623 K for 30 min. After the temperature was cooled to room temperature, CO pulses were injected. The amount of adsorbed CO was determined using a Shimadzu GC-14B gas chromatography equipped with an active carbon column and a FID detector.

Procedures for the aerobic oxidations of alcohols. Generally, into a test tube with 5 cm^3 volume capacity were placed the *n*Pt@*h*C or Pt/AC (0.5 μmol Pt) and toluene (1.5 cm^3). The suspension was ultrasonicated for 5 min followed by the addition of 0.25 mmol benzyl alcohol (or other alcohols). Unless otherwise stated, the reaction mixture was kept in air under vigorous stirring for certain duration. After the reaction, *n*Pt@*h*C powder was separated using centrifugation. A portion of the toluene containing reactant and product were injected into

Shimadzu GC 2010 and GC 353B gas chromatograph equipped with TC-FFAP and DB-1 capillary column, respectively, for activity determination.

5.2.3 Results and Discussion

Mechanistic Study of Oxidation of Benzyl Alcohol

Oxidation of alcohols using *n*Pt@*h*C was carried out in air at room temperature, as shown in Table 1. In general, oxidation of primary alcohols takes place faster than that of secondary alcohols. The reaction rates for oxidation of benzyl alcohol and 1-phenylethanol are 377 and 97 M min^{-1}, respectively. In the competitive oxidations, i.e., when an equimolar mixture of benzyl alcohol and 1-phenylethanol is present in the reaction, the selective conversion of benzyl alcohol to benzaldehyde is preferred. The formation of an alkoxy-metal species (metal alcoholate) is known to be important for the selective oxidation of primary alcohols to aldehydes.[9] In the present Pt/alcohol system, the oxidation is assumed to proceed *via* the formation of a similar Pt-alcoholate species, since primary alcohols were preferentially oxidized in the presence of their secondary counterparts. Besides, in order to examine the possibility of oxidation pathway involved radical intermediates, a radical scavengers, 2,2,6,6-tetramethylpiperidine-N-oxide (TEMPO) was added to the mixture prior to the reactions. Neither changes in reaction rate nor the presence of side product excluded the possibility of radical intermediates to play important role in oxidation mechanism.

Table 1. Oxidation of alcohols using *n*Pt@*h*C in air at room temperature.

Entry	Substrate	Product	Reaction Rate ($M\ min^{-1}$)
1	Benzyl alcohol	Benzaldehyde	377
2	1-Phenylethanol	Acetophenone	97
3	Competitive reaction		
	Benzyl alcohol	Benzaldehyde	95
	1-Phenylethanol	Acetophenone	32
4	Benzyl alcohol + TEMPO	Benzaldehdye	358

When *para*-substituent of benzyl alcohol is replaced with various electron donating/ electron withdrawing groups, their influences in the reactivity were plot as a function of log (k_X/k_H) and Brown-Okamoto parameters (σ^+) to constitute a Hammett plot (Figure 1a), where k_X and k_H represent the reaction rate of x-substituted benzyl alcohol and benzyl alcohol itself, respectively. Based on the slope of the Hammett plot, or also called sensitivity constant (ρ), information on the reaction and the associated mechanism can be obtained. Negative value of the slope (ρ= -0.313) indicates a positively charged benzyl alcohol is built during the reaction and the most probable location for this positively charged carbocation is at the benzylic carbon,[11] as verified in the kinetic isotope effect study (Figure 1b).

Figure 1b compares the reaction rates of benzyl alcohol and α-α-dideutero-benzyl alcohol (dideuterated at benzylic carbon) to examine the kinetic isotope effect (KIE). An isotopic substitution of hydrogen to deuterium will greatly modify the reaction rate if this isotopic replacement is in a chemical bond that is broken in the rate-determining step. When the rate-determining step occurs in places other than the isotope-substituted bond, the KIE will be masked and show insignificant discrepancy in the reaction rate. From the plots in Figure 1b, the ratio of k_H/k_D was calculated to be 6, which indicates a primary isotopic effect

had taken place. This result suggests that breaking of C–H bond of the benzylic carbon occurs as the rate-determining step in the oxidation of alcohol and the cleavage of C–H bond results in the transfer of H to metal surface to form metal-hydride species.[10] Besides, it also indirectly supports the formation of carbocation at benzylic carbon as the reaction intermediate since the removal of hydrogen reasonably generates a positive charge in benzylic alcohol, as revealed by the Hammett plot.

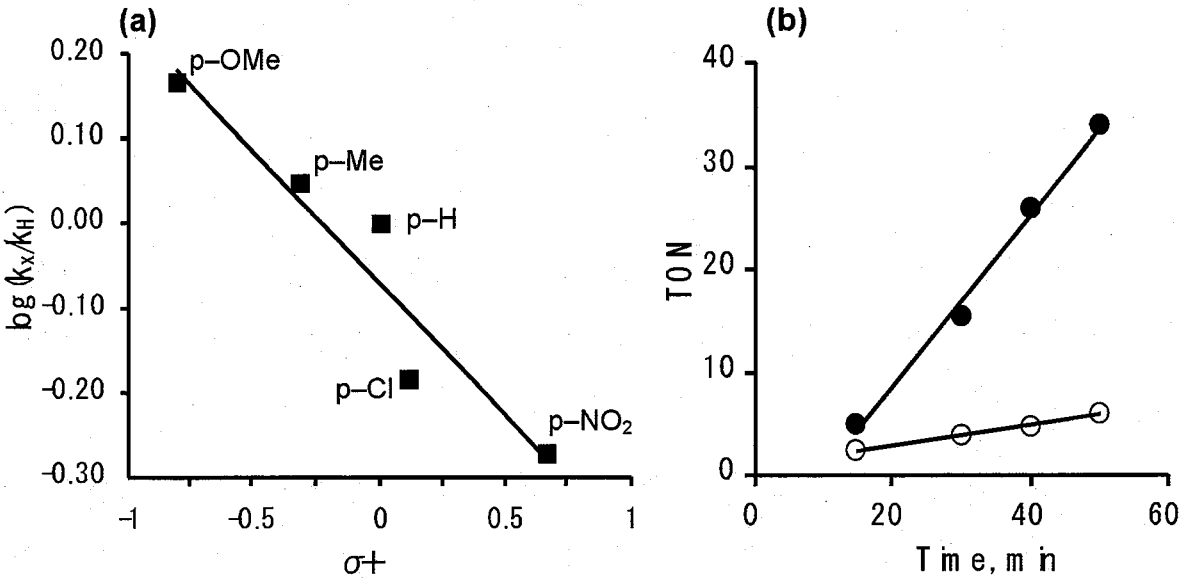

Figure 1. a) Hammett plot for competitive oxidation of benzyl alcohol and p-substituted benzyl alcohols, and b) kinetic isotopic effect in oxidation of benzyl alcohol (filled circles) and α-α-dideutero-benzyl alcohol (opened circles) using *n*Pt@*h*C.

Figure 2 shows a correlation between oxygen consumption and the benzaldehyde formation during the reaction. The plot reveals that the moles of benzaldehyde yielded are twice of the oxygen consumed, in good agreement with the reaction stoichiometry as indicated in Equation (4). The stoichiometric participation of O_2 in the reaction proves the oxidative dehydrogenation instead of a simple dehydrogenation has occurred. The adsorbed hydrogen species (Pt-hydride) generated during the formation of reversible alcoholate and the

C–H bond cleavage undergoes reoxidation by O_2 to recover the initial metallic site for continuous reaction.

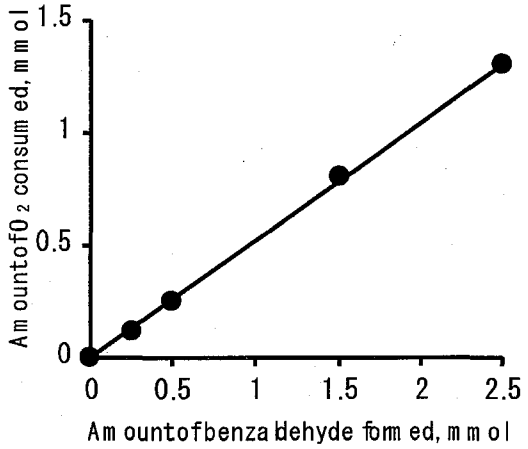

Figure 2. Relationship between amounts of benzaldehyde produced and O_2 consumed for the oxidation of benzyl alcohol by air using *n*Pt@*h*C.

The effects of reaction temperature on the *n*Pt@*h*C catalyzed oxidation of benzyl alcohol are shown in Figure 3. Good linearity was observed and afforded activation energy (E_a) of 10 kJ mol^{-1}. The activation energy is smaller than that of reported for the supported-Au and supported Ru catalyzed aerobic oxidation.

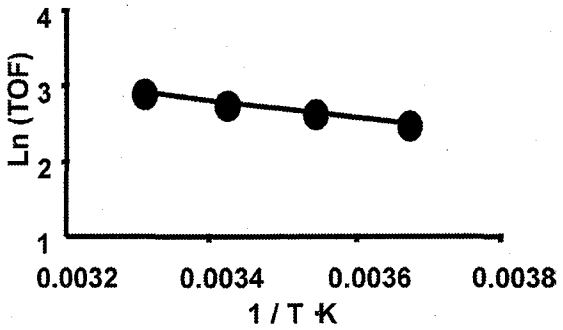

Figure 3. Arrhenius plot for the oxidation of benzyl alcohol using *n*Pt@*h*C.

On the basis of all above results, mechanism of Pt metal-catalyzed alcohol oxidation should follow the similar pathways as that of catalyzed by supported Ru and Au metal.[11] Oxidation of alcohols are supposed to occur on the surface of Pt through the following main reaction steps:

1) Formation of equilibrium state of Pt–alcoholate

$$2R_2R_1CH_2OH \leftrightarrow 2R_2R_1CH_2O_{ads}\ (\text{metal–alcoholate}) + 2H_{ads} \quad (1)$$

2) β-hydride transfer (rate-determining step)

$$2R_2R_1CH_2O_{ads} \rightarrow 2R_2R_1CHO\ (\text{product: aldehyde/ ketone}) + 2H_{ads} \quad (2)$$

3) Reoxidation of Pt-hydride

$$4H_{ads} + O_2 \rightarrow 2H_2O \quad (3)$$

$$2R_2R_1CH_2OH + O_2 \rightarrow 2R_2R_1CHO + 2H_2O \quad (4)$$

High and durable activity of nPt@hC in alcohol oxidation

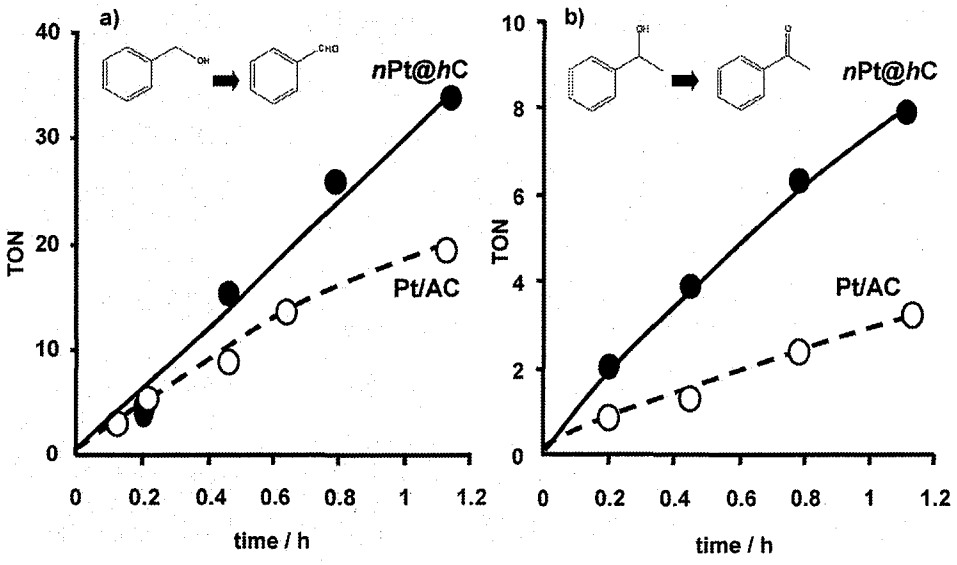

Figure 4. Initial reaction rate for oxidation of a) benzyl alcohol and b) 1-phenylethanol using *n*Pt@*h*C (filled circles) and commercial Pt/AC (opened circles) in air.

Figure 4 shows the initial reaction time courses for oxidation of benzyl alcohol and 1-phenylethanol in air using *n*Pt@*h*C and the commercial Pt/AC, respectively. As indicated in the previous mechanistic study, oxidation of primary alcohols proceeded faster than that of secondary one using these two Pt catalysts. Interestingly, in both reactions, *n*Pt@*h*C constantly demonstrates higher activity than Pt/AC, by a factor of 2-3. This enhancement in activity could be induced by the unique location of Pt nanoparticles in *n*Pt@*h*C.

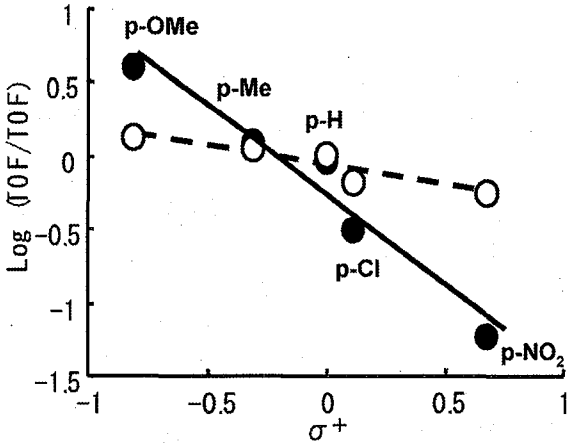

Figure 5. Hammett plot for competitive oxidation of benzyl alcohol and p-substituted benzyl alcohols using *n*Pt@*h*C (filled circles) and Pt/AC (opened circles).

When the reaction intermediates in the rate-determining step of this reaction are characterized by using Hammett plots (Figure 5), both *n*Pt@*h*C and Pt/AC demonstrate linear slope with negative value. The observation of negative linear slope in Hammett plots is agreed well with the oxidation of alcohols using other noble metals such as Ru and Au,[11] to indicate the development of a positively charged benzylic carbon during the reaction. Formation of this positively charged intermediate species is further supported by the kinetic isotopic effect study, as discussed in the previous section. The magnitudes of the slope, however, are

different in these two Pt catalysts to indicate the subtle variations in the reaction intermediates. The modification of the Pt microenvironment in *n*Pt@*h*C should result in delicate changes in the formation of reaction intermediates, leading to the facile discharge of β-hydrogen of the C–H bond at the benzylic carbon.

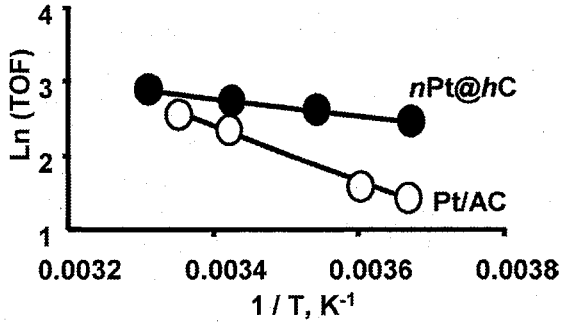

Figure 6. Arrhenius plots for the oxidation of benzyl alcohol using *n*Pt@*h*C and Pt/AC.

In order to confirm the facilitation of more efficient β-hydride elimination in the rate-determining step, Arrhenius plots to study the dependence of reaction rate on varied temperatures for both catalysts are shown in Figure 6. Based on the slope of the plots, apparent activation energies (E_a) for *n*Pt@*h*C and Pt/AC are calculated to be 10 kJ/mol and 31 kJ/mol, respectively. The smaller E_a of *n*Pt@*h*C verified the more facile pathway for oxidation reaction to take place on *n*Pt@*h*C compare to Pt/AC. The decrease of E_a in *n*Pt@*h*C is believed to be correlated to the stabilization of positively charged benzylic carbon (intermediate in rate-determining step). The electron-rich carbon matrix surrounded Pt nanoparticles in *n*Pt@*h*C stabilized the charge of reaction intermediate resulted in the easier breaking of benzylic C–H bond compared to that of Pt/AC, thus leading to the faster reaction.

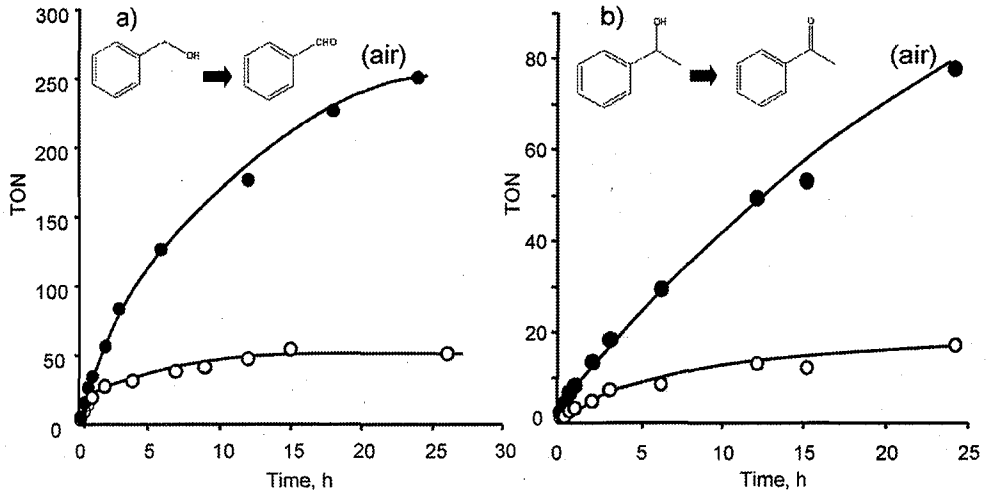

Figure 7. Reaction time courses for oxidation of a) benzyl alcohol and b) 1-phenylethanol using *n*Pt@*h*C (filled circles) and commercial Pt/AC (opened circles) in air over 25 hours.

Besides higher initial reaction rate, another remarkable feature of alcohol oxidation using *n*Pt@*h*C is its long durability. Figure 7 shows the reaction time courses for the oxidation of benzyl alcohol and 1-phenylethanol in air using *n*Pt@*h*C and Pt/AC over 25 hours. In both reactions, activity of Pt/AC is rapidly decreased after 1 h and the reaction is almost ceased after 5 h. Contrary, *n*Pt@*h*C shows reasonably good linearity in activity over the region of 25 h, this is very unlikely to happen in most Pt catalysts. This result indicates that *n*Pt@*h*C possesses greater suppression towards deactivation of Pt metal.

Although in general Pt metal efficiently catalyzes liquid phase oxidation of alcohols, the rapid deactivation of Pt remained as the main problem to be encountered. Pt metals are easily deactivated by blockage of the surface by strongly adsorbed molecules either impurities or reaction products. This deactivation is usually referred as Pt chemical poisoning. Traditional method to overcome the chemical poisoning is the incorporation of promoter in which the hazardous heavy metals like Pb and Bi are the most popular candidates.[12] However, leaching

of these heavy metals would be another serious environmental problem. Therefore, from a practical point of view, it is better to avoid deactivation without the introduction of other environmental harmful components into the catalytic system. *n*Pt@*h*C provides a practical model for this purpose.

Table 2. Pt Particle size and surface area of fresh and used *n*Pt@*h*C and Pt/AC.

Catalyst	Pt size (nm)[a]		CO_{chem}/Pt		Change in Pt metal
	fresh	used	fresh	used	
*n*Pt@*h*C	2.1	2.2	0.22	0.23	1.06
Pt/AC	2.6	2.6	0.57	0.36	0.69

[a] measured based on TEM images

Because the alcohol oxidation takes place on the active surface of Pt metal, the examination of the changes in active surface of Pt metal for both catalysts before and after reactions is necessary. Table 2 demonstrates the analyses of Pt particle size and pulse CO chemisorption for both catalysts after 25 h reaction with 1-phenylethanol. Pulse CO chemisorption analysis was carried out to measure the active surface of Pt. The amount of adsorbed CO on Pt nanoparticles indicates the Pt dispersion (CO_{chem}/Pt), i.e., the ratio of surface Pt atoms available for CO adsorption to the total number of Pt atoms. It is noted that $CO_{chem.}$/Pt for fresh Pt/AC is ca. 2.5 times large than that of *n*Pt@*h*C. As revealed in previous chapter, Pt nanoparticles of *n*Pt@*h*C were embedded inside a microporous carbon matrix resulted in the partial Pt surface coverage by the carbon network.[8b and 8c] Therefore, with the equivalent amount of Pt, *n*Pt@*h*C yields lower amount of CO_{chem}.

For samples recovered after 25 h reaction, Pt/AC demonstrates a significant 31 % decrease in the CO_{chem}/Pt while there is no significant change in CO_{chem}/Pt for the used *n*Pt@*h*C. Since neither sintering nor aggregation of Pt metals had occurred in both samples under such a mild operating condition, as determined from TEM analyses, the drop in CO_{chem}/Pt values is directly correlated to the decrease of Pt active sites. As there is no changing amount of Pt-Pt and Pt-O bonds observed in EXAFS (data not shown), absence of further development of surface platinum oxide after reaction excluded the possibility of Pt over-oxidation. Thus, the decrease of Pt surface active sites on Pt/AC could be conveniently correlated to the coverage of active sites by strongly adsorbed species. The used Pt/AC was further studied by TPD measurement by heating the samples to 500 °C in a He flow at a constant rate of 10 °C min^{-1}. The detection of considerable amount of desorbed benzyl fragments in the temperature ranged from 400–500 °C proved the chemical poisoning of Pt by these strongly adsorbed components. In comparison, there is no observation of any component desorbed at this temperature range for *n*Pt@*h*C. Although there is no direct evidence at the current stage, the suppression of deactivation in *n*Pt@*h*C should be directly related to the embedded structure of Pt nanoparticles in carbon matrix. When the poisoning species is formed on the surface of Pt nanoparticles, it is efficiently "removed" or "diffused" into the carbon matrix, leaving the Pt nanoparticles poison-free and active. In comparison, because the Pt nanoparticles are located on the surface of carbon support in Pt/AC, exposing most of the Pt surface to the reaction environment, therefore deactivation of Pt by poisoning species is much profound.

Based on the above results, the *n*Pt@*h*C exhibits higher reaction rate and higher suppression towards Pt deactivation compared with the commercial Pt/AC. Its higher reaction rate is induced by the stabilization of positively charged reaction intermediates in the

rate-determining step by the surrounded electron-rich carbon matrix. The exact mechanism of suppression of deactivation in *n*Pt@*h*C remains unclear. However, we believe it is most possibly attributed to the Pt nanoparticles' embedment in the microporous carbon matrix that provides a different Pt morphology and its microenvironment. The research in this direction is now underway.

5.2.4 Conclusion

In summary, the generally accepted oxidative dehydrogenation mechanism of Pt metal-catalyzed oxidation of alcohol is experimentally proved in this study. The mechanistic investigations using *n*Pt@*h*C catalyst shows that the reaction occurs through the formation of alcoholate, β-hydride transfer and reoxidation of Pt-hydride. β-hydride transfer is the rate-determining step before the deactivation becomes significant. Higher reaction rate in *n*Pt@*h*C is owing to the stabilization of intermediate species in the reaction rate-determining step while chemical poisoning of Pt, the main deactivation mode of Pt metal in most cases, is effectively suppressed by embedding the Pt nanoparticles in a porous carbon network. The findings revealed in this study should find use in improving the design of Pt catalyst to better fit its industrial applications in the production of aldehydes and ketones.

5.2.5 References

[1] (a) W. J. Mijs and C. R. H. de Jonge, *Organic Synthesis by Oxidation with Metal Compounds*, Plenum Press, New York, **1986**. (b) B. M. Trost and I. Fleming,

Comprehensive Organic Synthesis, Pergamon Press, Oxford, **1991**. (c) G. Cainelli and G. Cardillo, *Chromium Oxidations in Organic Chemistry*, Springer-Verlag, Berlin, **1984**.

[2] (a) T. Nishimura, Y. Maeda, T. Onoue, K. Ohe and S. Uemura, *J. Chem. Soc. Perkin Trans.*, **2000**, *1*, 4301. (b) G. J. ten Brink, I. W. C. E. Arends and R. A. Sheldon, *Science*, **2000**, *287*, 1636. (c) S. S. Stahl, *Angew. Chem. Int. Ed.*, **2004**, *43*, 3400. (d) T. Naota, H. Takaya and S. I. Murahashi, *Chem. Rev.*, **1998**, *98*, 2599. (e) J. Bozell, B. R. Hames and D. R. Dimmel, *J. Org. Chem.*, **1995**, *60*, 2398. (f) M. Beller and C. Bolm, *Building Blocks and Fine Chemicals, Wiley VCH, Weinheim*, **1998**, 350.

[3] (a) I. E. Marko, P. R. Giles, M. Tsukazaki, S. M. Brown and C. J. Urch, *Science*, **1996**, *274*, 2044. (b) D. H. R. Barton, A. E. Bartell and D. T. Sawyer, *The Activation of Dioxygen and Homogeneous Catalytic Oxidation, Plenum, New York*, **1993**, 133.

[4] (a) Y. Uozumi and R. Nakao, *Angew. Chem.*, **2003**, *42*, 194. (b) B. Z. Zhan, M. A. White, T. K. Sham, J. A. Pincock, R. J. Doucet, K. V. R. Rao, K. N. Robertson and T. S. Cameron, *J. Am. Chem. Soc.*, **2003**, *125*, 2195. (c) K. Yamaguchi and N. Mizuo, *Angew. Chem.*, **2002**, *41*, 4538. (d) A. Kockritz, M. Sebek, A. Dittmar, J. Radnik, A. Bruckner, U. Bentrup, M. M. Pohl, H. Hugl and W. Magerlein, *J. Mol. Catal. A*, **2006**, *246*, 85. (e) T. Mallat and A. Baiker, *Catal. Today*, **1994**, *19*, 247. (f) S. Biella, G. L. Castiglioni, C. Fumagalli, L. Prati and M. Rossi, *Catal. Today*, **2002**, *72*, 43.

[5] (a) H. E. van Dam, L. J. Wisse and H. van Bekkum, *Appl. Catal.*, **1990**, *61*, 187. (b) M. Besson and P. Gallezot, *Catal. Today*, **2000**, *57*, 127. (c) T. Mallat and A. Baiker, *Chem. Rev.*, **2004**, *104*, 3037.

[6] (a) Y. Schuurman, B. F. M. Kuster, K. van der Wiele and G. B. Marin, *Appl. Catal. A*, **1992**, *89*, 31. (b) F. R. Venema, J. A. Peters, H. van Bekkum, *J. Mol. Catal.* **1992**, *77*, 75. (c) J. H. J. Kluytmans, A. P. Markusse, B. F. M. Kuster, G. B. Marin and J. C. Schouten,

Catal. Today, **2000**, *57*, 143. (d) F. Alardin, B. Delmon, P. Ruiz and M. Devillers, *Catal. Today*, **2000**, *61*, 255.

[7] J. H. Vleeming, B. F. M. Kuster, G. B. Marin, F. Oudet and P. Courtine, *J. Catal.*, **1997**, *166*, 148.

[8] (a) Y. H. Ng, S. Ikeda, T. Harada, S. Higashida, T. Sakata and M. Matsumura, *Adv. Mater.*, **2007**, *19*, 597. (b) Y. H. Ng, S. Ikeda, T. Harada, S. Park, T. Sakata, H. Mori and M. Matsumura, *Chem. Mater.*, **2008**, *20*, 1154. (c) Y. H. Ng, S. Ikeda, T. Harada, T. Sakata, H. Mori, A. Takaoka and M. Matsumura, *Langmuir*, **2008**, *24*, 6307. (d) Y. H. Ng, S. Ikeda, T. Harada, Y. Morita and M. Matsumura, *Chem. Commun.*, **2008**, 3181. (e) Y. H. Ng, S. Ikeda, S. Park, Y. Morita, T. Harada and M. Matsumura, *Tops. Catal.*, **2008**, accepted for publication.

[9](a) S. Murahashi, T. Naota, K. Ito, Y. Maeda and H. Taki, *J. Org. Chem.*, **1987**, *52*, 4319. (b) S. Kanemoto, S. Matsubara, K. Takai, K. Oshima, K. Utimoto and H. Nozaki, *Bull. Chem. Soc. Jpn.*, **1988**, *61*, 3607. (c) A. Hanyu, E. Takezawa, S. Sakaguchi and Y. Ishii, *Tetrahedron Lett.*, **1998**, *39*, 5557. (d) K. Yamaguchi, K. Mori, T. Mizugaki, K. Ebitani and K. Kaneda, *J. Am. Chem. Soc.*, **2000**, *122*, 7144.

[10](a) H. Kwart and M. C. Latimore, *J. Am. Chem. Soc.*, **1971**, *93*, 3770. (b) H. Kwart and J. H. Nickle, *J. Am. Chem. Soc.*, **1973**, *95*, 3394.

[11](a) K. Yamaguchi and N. Mizuno, *Chem. Eur. J.*, **2003**, *9*, 4353. (b) A. Abad, A. Corma and H. Garcia, *Chem. Eur. J.*, **2008**, *14*, 212.

[12](a) H. H. C. M. Pinxt, B. F. M. Kuster and G. B. Marin, *Appl. Catal. A-Gen.*, **2000**, *191*, 45. (b) T. Mallat, Z. Bodnar, P. Hug and A. Baiker, *J. Catal.*, **1995**, *153*, 131. (c) P. Gallezot, *Catal. Today*, **1997**, *37*, 405. (d) A. Deffernez, S. Hermans and M. Devillers,

Appl. Catal. A-Gen., **2005**, *282*, 303. (e) C. Keresszegi, T. Mallat, J. Grunwaldt and A. Baiker, *J. Catal.*, **2004**, *225*, 138.

CHAPTER 6

General Conclusions and Research Recommendations

6.1 General Conclusions

This thesis describes the designing and nanocasting of hollow porous carbon encapsulating platinum nanoparticles (*n*Pt@*h*C) based on a TiO_2 photocatalytic reaction. Most of the work presented in this thesis has been carried out at Research Center for Solar Energy Chemistry, Osaka University. Objectives stated in Chapter 1 are generally accomplished. The *n*Pt@*h*C prepared in this study possesses unique hollow structure with the platinum nanoparticles embedded in the porous carbon shell. Fabrication of this novel nanocatalyst is aimed for exploiting a new class of carbon-supported metal catalyst equipped with unique properties, therefore leading to certain specific functions in catalytic reaction. Physical properties and catalytic activities of this nanocatalyst are studied in detail. The main findings obtained through this wok are summarized as below.

In Chapter 2, we have demonstrated the fabrication of *n*Pt@*h*C using TiO_2 nanoparticles as both the photocatalyst and the inorganic mold. The principle of the fabrication is based on the redox ability of photoirradiated TiO_2 nanoparticles to induce simultaneous photoreduction of Pt(IV) ions and photooxidative polymerization of phenol, which eventually result in Pt-loaded TiO_2 covered by a thin layer of phenolic polymer. This methodology enables loading of Pt nanoparticles and coverage of the carbon precursor on the TiO_2 template in a one-step process, and prevails the conventional multistep method. Based on the results of TG-DTA, FTIR and GC-MS spectroscopy, mechanism of the phenol polymerization on the surface of TiO_2 under this experimental condition is proposed. Subsequent carbonization of the polymer layer at 700 °C in vacuum and removal of TiO_2 using HF acid yield the *n*Pt@*h*C nanocomposites. *n*Pt@*h*C nanocomposites are found to consist of a spherical porous carbon with hollow structure containing several face-centered cubic platinum nanoparticles within

the thin carbon shell. Besides, porosity analyses of the carbon shells indicate the presence of mesopores and bimodal micropores in *n*Pt@*h*C. This composite works as an efficient catalyst for hydrogenation of various olefins.

As an extension of this finding, we found that polymerization of phenol proceeded even after the surface of TiO_2 was fully covered. This observation prompted us to study the irradiation time-dependent effect on the physical properties of thus-obtained *n*Pt@*h*C. By using short and prolong irradiation, remarkable alterations in properties of the carbon shells are observed, affecting the carbon morphology, density and porosity. Short irradiation time (< 1 h) resulted in the sheet-like *n*Pt@*h*C sample owing to the inadequate polymerization to covering the surface of TiO_2; sphere-type *n*Pt@*h*C is obtained through moderate irradiation time (2-5 h); Prolong irradiation induce a significant densification of the carbon matrix, resulting in a decrease in pore volume. Mainly due to the modulation of active surface of Pt nanoparticles in each *n*Pt@*h*C, changes in morphology and density of carbon are found to influence catalytic activity for hydrogenation of normal olefins. These results are included in Chapter 3. Due to its simplicity (by merely changing the irradiation time), this strategy can be used as a tool for tailoring properties of carbon-based materials.

After investigating the controllability of carbon density, porosity and morphology, in Chapter 4, we focus on clarifying the location of platinum nanoparticles in *n*Pt@*h*C using an electron tomography technique. From a tomogram obtained through reconstructing 121 tilted images of *n*Pt@*h*C, the platinum nanoparticles are found to be embedded in the thin carbon shell and physically separated from each other by the carbon matrix. Owing to this entrapment of platinum inside the porous carbon shell, they are kinetically locked within the

same location. In other term, it is "frozen" inside the carbon; any possible movement of platinum is minimized. Because of this unique structure, the platinum nanoparticles showed high resistance to sintering when subjected to thermal treatment at temperatures up to 800 °C. As a result, hydrogenation reactions using *n*Pt@*h*C pre-heated at various temperatures indicate that loss of catalytic activity is minimized. For comparison of sintering behavior, activated carbon-supported platinum (Pt/AC) prepared by conventional impregnation/H_2 reduction method is prepared. From TEM images obtained on Pt/AC treated at elevated temperatures, we found that platinum of Pt/AC continuing grow to a bigger agglomerate according to the temperature. The deactivation of the catalyst at high temperatures is therefore attributed to the morphological change. The remarkable property of the *n*Pt@*h*C is its physical stability at high temperatures because the platinum nano-particles are "frozen" inside the carbon shell. Owing to this property, *n*Pt@*h*C could serve as a promising candidate in other catalytic processes requiring similar rigorous conditions.

Besides the physical stabiliyty of *n*Pt@*h*C, we found that it has another advantage when used as catalyst for oxidation of alcohols. Oxidation of alcohols into corresponding aldehydes, ketones and carboxylic acid is a reaction of importance in chemical industry. We evaluate the performance of *n*Pt@*h*C in the oxidation of various alcohols using molecular oxygen as oxidant. Mechanism of alcohol oxidation on platinum is also studied. On account of the presence of well-developed pores inside the carbon shell that provides three-dimensional hydrophobic channels and spaces, efficient mass transfer and preferential adsorption of the substrate adjacent to the platinum is facilitated. These unique properties result in a high concentration of substrate in the platinum microenvironment, leading to the efficient catalytic function when compared to that of conventional Pt/AC sample. By using various catalytic

tools such as Hammett plot and kinetic isotope study, mechanism of oxidation of benzyl alcohol is verified. The mechanism pathways are found to be comprised of 3 major steps: (1) formation of alcoholate species on platinum, (2) formation of beta-hydride species followed by generation of benzaldehyde and, (3) reoxidation of platinum by oxygen. The detail of this mechanistic study is included in Chapter 5. Besides, comparing to a commercially available Pt/AC, *n*Pt@*h*C exhibits longer life-time in oxidation of alcohols where Pt/AC is deactivated rapidly under atmospheric pressure. Results of CO adsorption and XAFS analysis indicate that the platinum in *n*Pt@*h*C is suppressed to chemical poisoning compared to that of the Pt/AC catalyst.

In conclusion, we consider the methodology employed to synthesize the hollow porous carbon encapsulating platinum nanoparticles is an important achievement of this study. This technique is applicable to various kinds of noble metals. In fact, we have prepared *n*Rh@*h*C (Rh particle) and *n*Au@*h*C (Au particle) other than *n*Pt@*h*C in separate study using the same principle. The structure of *n*Pt@*h*C is advantageous for improving the activity, selectivity and deactivation resistance of certain reactions because the porous carbon has a function of filters and gas/liquid diffusion barrier. Lastly, the findings obtained in this thesis provide very competitive information to design a highly efficient carbon-based metal catalyst and could possibly improve the utilization of current carbon-based metal catalyst practically.

6.2 Research Recommendations

In order to explore further potential of this particular topic and to improve the comprehension of this material, we hereby deliver several research recommendations to the prospective researchers/ readers of this thesis.

1) To study the function of hollow spaces in *n*M@*h*C (M = metal). Understanding of the driving force to achieve high catalytic activity contributed by the hollow spaces is valuable.
2) To investigate and improve the mechanical strength of *n*M@*h*C. We expect the current *n*M@*h*C should possess low mechanical strength since it has a hollow structure. In order to improve the utility of this material in broader applications, high mechanical strength is therefore favorable. Intercalating the pores with other components might work.
3) To further improve the tunabilty of pore volume and pore size of carbon in a wider range. Up to date, the control of pore volume and pore size of porous carbon still is limited to a narrow region.
4) To expand the application of *n*M@*h*C. For instance, usage in controlled release of drugs or applied as the electrode of fuel cell.
5) To investigate the catalytic performance of metals other than platinum.

List of Publications

Peer-reviewed journals included in this thesis

1. "Fabrication of Hollow Carbon Nanospheres Encapsulating Platinum Nanoparticles Using a Photocatalytic Reaction"
   Yun Hau Ng, Shigeru Ikeda, Takashi Harada, Suguru Higashida, Takao Sakata, Hirotaro Mori and Michio Matsumura.
   Advanced Materials **2007**, *19*, 597-601.

2. "Photocatalytic Route for Synthesis of Hollow Porous Carbon/Pt Nanocomposites with Controllable Density and Porosity"
   Yun Hau Ng, Shigeru Ikeda, Takashi Harada, Sangin Park, Takao Sakata, Hirotaro Mori and Michio Matsumura.
   Chemistry of Materials **2008**, *20*, 1154-1160.

3. "High Sintering Resistance of Platinum Nanoparticles Embedded in a Microporous Hollow Carbon Shell Fabricated Through a Photocatalytic Reaction"
   Yun Hau Ng, Shigeru Ikeda, Takashi Harada, Takao Sakata, Hirotaro Mori, Akio Takaoka and Michio Matsumura.
   Langmuir **2008**, *24*, 6307-6312.

4. "An Efficient and Reusable Carbon-Supported Platinum Catalyst for Aerobic Oxidation of Alcohols in Water"
   Yun Hau Ng, Shigeru Ikeda, Takashi Harada, Yoshihiro Morita and Michio Matsumura.
   Chemical Communications **2008**, 3181-3183.

5. "Morphological Control of Carbon Carrier in Pt-Carbon Nanocomposites Derived *via* Photocatalytic Reactions on Titanium(IV) Oxide Powders"
   Yun Hau Ng, Shigeru Ikeda, Sang-in Park, Yoshihiro Morita, Takashi Harada and Michio Matsumura.
   Topics in Catalysis **2008**, *accepted for publication.*

Peer-reviewed journals not included in this thesis

1. "Surface Structure of Alkylsilylated HZSM-5 as Phase-Boundary Catalyst"
   Hadi Nur, Yun Hau Ng, Mohd. Nazlan Mohd. Muhid and Halimaton Hamdan.
   Physics Journal of Indonesian Physical Society **2004**, *A7*, 0218.

2. "Hydrophobic Fluorinated TiO_2-ZrO_2 as Catalyst in Epoxidation of 1-Octene with Aqueous Hydrogen Peroxide"
   Hadi Nur, Yun Hau Ng, Izan Izwan Misnon, Halimaton Hamdan and Mohd. Nazlan Mohd. Muhid.
   Materials Letter **2006**, *60*, 2274-2277.

3. "Biphasic Epoxidation of 1-Octene with H_2O_2 Catalyzed by Amphiphilic Fluorinated Ti-loaded Zirconia"
   Yun Hau Ng, Izan Izwan Misnon, Hadi Nur, Mohd. Nazlan Mohd. Muhid and Halimaton Hamdan.
   Journal of Fluorine Chemistry **2007**, *128*, 12-16.

4. "Selective Adsorption of Glucose-Derived Carbon Precursor on Amino-Functionalized Porous Silica for Fabrication of Hollow Carbon Spheres with Porous Walls"
   Shigeru Ikeda, Koji Tachi, Yun Hau Ng, Yoshimitsu Ikoma, Takao Sakata, Hirotaro Mori, Takashi Harada and Michio Matsumura.
   Chemistry of Materials **2007**, *19*, 4335-4340

5. "Rhodium-Nanoparticles Encapsulated in Porous Carbon Shell as Active Heterogeneous Catalyst for Aromatic Hydrogenation"
   Takashi Harada, Shigeru Ikeda, Yun Hau Ng, Takao Sakata, Hirotaro Mori and Michio Matsumura.
   Advanced Functional Materials **2008**, *18*, 2190-2196.

6. "Efficient Reductive Alkylation of Aniline with Acetone over Platinum Nanoparticles Encapsulated in Hollow Porous Carbon"
   Takashi Harada, Shigeru Ikeda, Natsumi Okamoto, Yun Hau Ng, Tsukasa Torimoto and Michio Matsumura
   Chemistry Letters **2008**, *37*, 948-949.

Acknowledgements

Someone has rightly said "Happiness lies in the joy of achievement and the thrill of creative effort". I am happy that my three and a half years of efforts have realized in the form of this thesis. Although it should be relatively simple, this part is not the easiest part of my thesis. All the work presented here would not have been possible without the help, collaboration and encouragement of many people to whom I am very grateful. Without them, the quest towards my PhD degree would be less rewarding, interesting and challenging.

My greatest appreciation goes to my supervisors, Prof. Michio Matsumura and Assoc. Prof. Shigeru Ikeda for their omnipresence in providing guidance, supervision, encouragement and faith throughout my Ph.D. project. They have been the source of continuous inspirations through which many new ideas were developed for studying the photocatalytic fabrication of hollow carbon/platinum nanocomposites.

I am equally thankful to Prof. Hirotaro Mori, Prof. Akio Takaoka and Dr. Takao Sakata from Research Center for Ultra-High Voltage Electron Microscopy, Osaka University. Completion of the project would not have been possible without their assistance in TEM and HRTEM imaging. Not forgetting Dr. Takashi Harada for many assistances and sessions of stimulating discussion. I would also like to thank Prof. Prashant Kamat from University of Notre Dame, Indiana USA for supervising me particularly on the development of titanium oxide-graphene nanocomposites for the application in solar cell and for hosting my stay at Notre Dame in 2008.

The awarding of the MONBUSHO postgraduate scholarship from the Ministry of Education, Culture, Sports, Science and Technology, Japan (MEXT) and also the oversea

internship to spend months in the University of Notre Dame, USA sponsored by the Global Center of Excellence (GCOE) of Osaka University are gratefully acknowledged.

Most importantly, I would like to thank my parents (Mr. Voon Pin NG and Mrs. Moo Moy CHAN), my sister (Miss Nyuk Ping NG), and my beloved fiancée (Miss Fong Mei SU) for their endless love and support.

Last but not least, I express my sincere gratitude to all past and present members of RCSEC for their share of friendship, laughter, joy and humor in making a drilling day more tolerable, especially Ass. Prof. Takeshi Hirai, Dr. Takahiro Osasa, Koji Tachi, Ikoma, Tsuru, Natsumi Okamoto, Sang-In Park, Sasaki, Hideyuki Kobayashi, Daiki Kato, Yoshihiro Morita, Yohsuke Maruyama, Chia-Lung Lee and Buc Duc Thuan.

Yun Hau NG

MARCH 2009